Dead Sea Pollen Reveal the Paleoenvironment of the Southern Levant during 147–89 ka from the Paleobotanical Perspective

Dissertation

zur Erlangung des Doktorgrades (Dr. rer. nat.)

der Mathematisch-Naturwissenschaftlichen Fakultät

der Rheinischen Friedrich-Wilhelms-Universität Bonn

vorgelegt von

Chunzhu Chen

aus Wenzhou, China

Bonn 2017

Angefertigt mit Genehmigung der Mathematisch-Naturwissenschaftlichen Fakultät der

Rheinischen Friedrich-Wilhelms-Universität Bonn

1. Gutachter: Prof. Dr. Thomas Litt

2. Gutachter: PD Dr. Gösta Hoffmann

Tag der Promotion: 24. November 2017

Erscheinungsjahr: 2017

Table of Contents

1 Introduction

The Levant hosts a long history of the mankind and the regional environment in the eastern Mediterranean (EM) region. Connecting Africa with the Arabian Peninsula, the southern Levant is a hotspot for investigating the dispersal of anatomically modern human (AMH) to the rest of the world since its emergence in Africa (Gibbons, 2017). Pivotal findings are the AMH remains in Israel (Skhul and Qafzeh Caves; Figure 1) dated to the time range of 130–90 thousand years ago (ka; Grün et al., 2005; Mercier et al., 1993; Shea, 2003; Valladas et al., 1988). These findings suggest the occupation of modern humans in the southern Levant during the last interglacial (LIG). This dispersal event is regarded either as an unsuccessful expansion into Eurasia (Mellars, 2006a, b; Shea and Bar-Yosef, 2005) or a part of the migration towards Arabia (Armitage et al., 2011; Breeze et al., 2016; Petraglia et al., 2011).

The present southern Levant is covered by large areas of un-inhabitable deserts, whereas in the past the desert barrier was probably turned into a migration corridor with sufficient water and food resources during climatic ameliorations (Breeze et al., 2016; Petraglia et al., 2012). In particular, the LIG was indicated to comprise at least episodes of favorable climatic conditions (Frumkin et al., 2011; Parton et al., 2015; Petraglia et al., 2010; Vaks et al., 2007). Nevertheless, inconsistences exist between regional paleoenvironmental archives regarding the timing and extent of the favorable climatic conditions (Bar-Matthews et al., 2003; Torfstein et al., 2015; Vaks et al., 2010; Waldmann et al., 2010). This calls for more paleorecords as the key to decipher the triggers of human migration into the southern Levant during the LIG.

The LIG is a period with at least as warm conditions as the present interglacial (NGRIP members, 2004). Global ice and marine records suggest the LIG optimum was characterized by remarkably strong summer insolation (Berger et al., 2007), high atmospheric CO_2 concentration (Ganopolski et al., 2016), high global temperature (Masson-Delmotte et al., 2010; NEEM community members, 2013), and higher mean sea levels than the present (Dutton et al., 2015; Rohling et al., 2007). In the context of current global warming, the LIG serves as an outstanding case for studying the interactions between the earth systems and the internal and external forcings in the absence of human influences (Govin et al., 2015).

On land, LIG conditions in the Mediterranean region are extensively investigated based on long terrestrial records from southern Europe and the Near East. These records unveil the close associations of Mediterranean climate with orbital forcings, Northern Hemisphere ice sheet, and North Atlantic circulations with respect to both long-term and abrupt climatic variabilities (see section 2.1). The EM region is predicted to be one of the most vulnerable

regions suffering water deficiency under the warming climate (Milano et al., 2012). This highlights the southern Levant as an exceptional region for studying the LIG climatic history.

The southern Levant is controlled by the Mediterranean climate in the north and the Saharo-Arabian desert climate in the south. The regional climate is thus linked to both mid-latitude and sub-tropical atmospheric-oceanic systems. The highly varied topography further modulates the regional climate, leading to a steep gradient of temperature and precipitation distribution (Enzel et al., 2008). As a result, this region is sensitive to climatic variations, which have been documented in geological archives (see section 2.2).

Nevertheless, the triggers of paleoclimatic changes remain under debate due to the paleoenvironmental inconsistences implied by records of different archives and proxies. Of the most prominent are the discrepancies between lacustrine and speleothem records (see sub-sections 2.2.2 and 2.2.3). For instance, in the arid central and southern Negev Desert, relatively active speleothem deposition during the LIG suggest wetter conditions as compared to the last glacial and the present interglacial (Vaks, 2008; Vaks et al., 2007, 2010). However, the Dead Sea lake stands during the LIG were significantly lower than during the glacials and are suggested to represent drier conditions (Waldmann et al., 2007, 2009, 2010). Controversies are focused on the relative impact of the climatic variables, i.e., precipitation, temperature, evaporation, and seasonality (Gasse et al., 2011). In this case, more paleorecords involving independent proxies are needed.

The Dead Sea is located at the lowest point on the continental earth. Based on a series of proxies such as sedimental lithology (e.g., Neugebauer et al., 2014), geochemistry (e.g., Lazar et al., 2014), and pollen assemblages (e.g., Litt et al., 2012), the Dead Sea is a remarkable archive for investigating the paleoenvironment of the southern Levant. Of the most representative are lake-level reconstructions of the Holocene Dead Sea and its Pleistocene precursors (Stein, 2014 and references therein). These studies show the sensitivity of Dead Sea sediments to changes in regional hydrology and hydroclimate (Bookman (Ken-Tor) et al., 2004; Enzel et al., 2003), as well as to fluctuations in the North Atlantic (Kushnir and Stein, 2010; Stein et al., 2010; Torfstein et al., 2013a, b). For instance, the lake level at ca. 27–24 ka was particularly high (ca. 270 m higher than the present level), resulting in the mergence of the Dead Sea and the Sea of Galilee along the Jordan Valley (Hazan et al., 2005). This high stand was followed by an abrupt drop to ca. 30 m lower-than-present level during the Bølling-Allerød interstadial (Stein et al., 2010).

Compared to the well-studied last glacial and Holocene Dead Sea sediments, the LIG conditions remain elusive due to limitations of available materials deposited in the lake margin. In 2010–2011, the Dead Sea Deep Drilling Project (DSDDP) retrieved unprecedentedly long sediment cores dated back to ca. 220 ka from the deepest part of the

basin (Figure 1; Stein et al., 2011a; Torfstein et al., 2015). The project successfully recovered the LIG sediments consisted of conspicuously thick halite deposits (Neugebauer et al., 2014). Previous analyses of chronology, lithology, and isotope composition of these sediments suggested the LIG period was characterized by low lake levels and generally dry conditions with sporadic wetness (Torfstein et al., 2015).

Despite these progresses, the paleovegetation as independent evidence for the LIG paleoenvironment in the southern Levant is nearly unknown. Pollen analysis is widely employed for reconstructing vegetation successions. Previous palynological studies in the southern Levant are mainly confined to the Holocene and late glacial period, whereas the LIG pollen records are rare, fragmentary, and poorly-dated (see subsection 2.2.1). This restricts the potential of resolving the above-mentioned inconsistences implied by existing records in the region.

This study presents a high-resolution pollen record dated to 147–89 ka based on the DSDDP cores. The main objectives are to reconstruct the paleovegetation in the southern Levant and to elucidate the response of vegetation successions to variations in regional climate. Discussions are focused on comparisons with other regional records, attempting to add information and to provide new insights into the paleoenvironmental setting of the early modern human dispersal. This work is a part of the Collaborative Research Centre 806 project “Our Way to Europe” targeting at addressing the culture-environment interactions and the human mobility during the late Quaternary.

2 Current state of research

Interglacials represent the Quaternary stratigraphical stages that were marked by globally warm or warmer climates with analogous atmospheric and oceanic circulations as those of the current interglacial (Fairbridge, 1972). The ambiguities in defining the boundaries of an interglacial always exist as it refers to the general state of the climate. As a result, regional definitions of the last interglacial have been applied, e.g., the Riss/Würm interglacial in the Alps (Penck and Brückner, 1909). Nowadays, the interglacials and glacials are increasingly expressed by the chronostratigraphic units of long sedimental records. The pervasively used Marine Isotope Stages (MIS) imply the status of global ice volume with even numbers denoting the glacials and vice versa (Martinson et al., 1987). The MIS 5 is divided into five climatostratigraphical units based on benthic oxygen isotope records, with MIS 5e representing the period encompassing the penultimate glacial/last interglacial transition, the last interglacial climatic optimum, and the subsequent glacial inception (132–115 ka; Shackleton et al., 2002).

On land, the biostratigraphical unit ‘Eemian’ is used in Europe to describe the terrestrial climatic optimum marked by major forest expansions to an extent similar as during the Holocene (Brauer et al., 2007; Harting, 1874; Kukla et al., 2002). It is important to note that the Eemian is not equivalent to MIS 5e, as demonstrated by terrestrial and marine proxies from the Iberian marine cores (Shackleton et al., 2003). Analyses of these proxies allowed direct sea-land correlation revealing the onset of the MIS 5e preceded that of the Eemian by thousands of years. The definition of interglacials, proposed by Jessen and Milthers (1928) and suggested to be still applicable to the Quaternary climate stratigraphy (Gibbard and Van Kolfschoten, 2004), is adopted in this study from the paleobotanical perspective. That is, the term ‘Interglacial’ refers to periods of climatic optima that were characterized by at least as warm conditions as the present interglacial, so that climax vegetation developed in the same region. In this sense, interstadials were intervals with ameliorated climate conditions but were either too short or too cold for the full development of the vegetation.

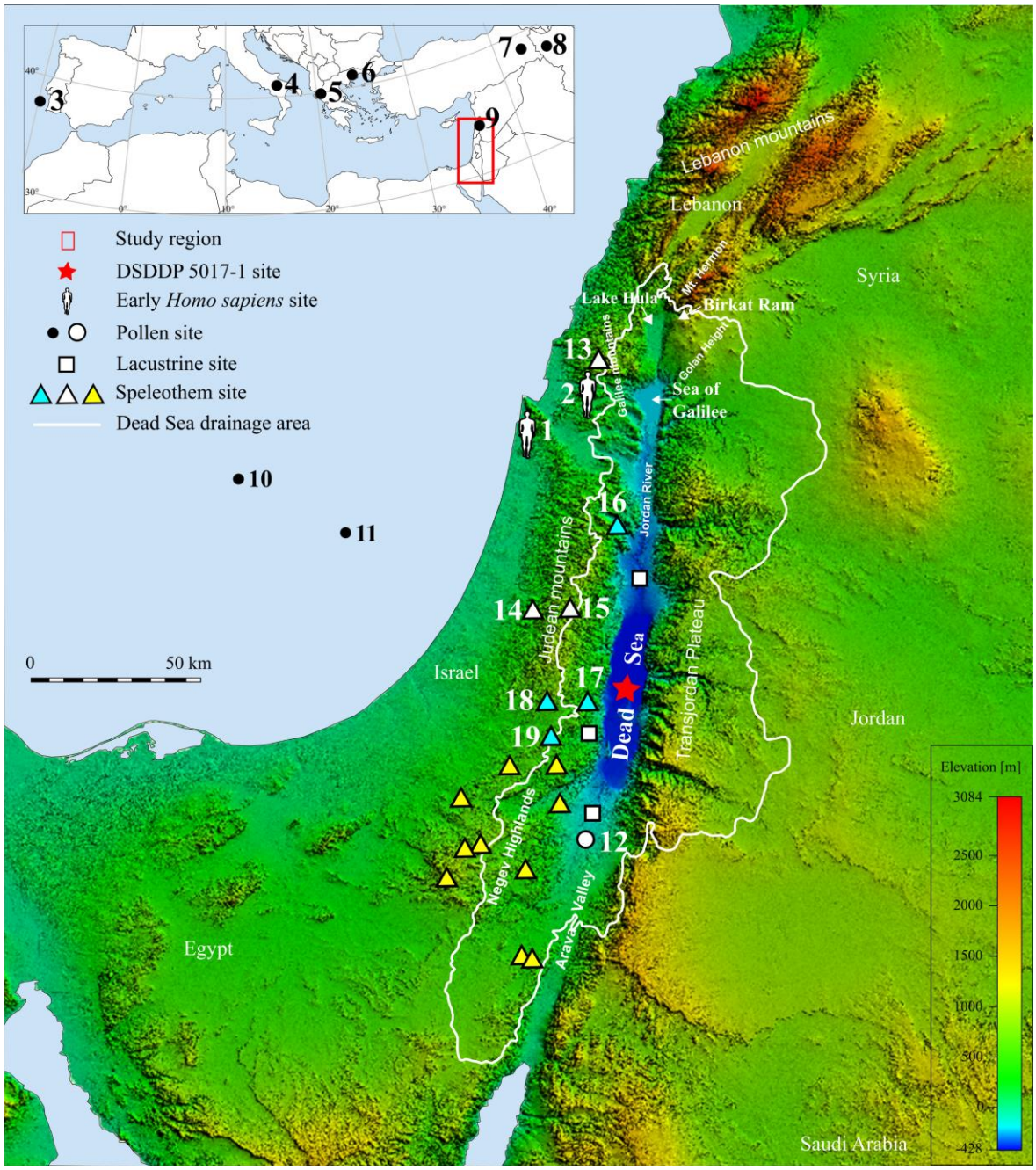

Figure 1: Previously studied sites in the Mediterranean region concerning the investigated interval in this study, marked with numbers and legends. *Red star*: DSDDP 5017-1 drilled site at the Dead Sea, this study. *Human shapes*: early modern human sites of 1=Skuhl Cave and 2=Qafzeh Cave (Shea and Bar-Yosef, 2005). *Dots*: pollen sites of 3=marine core MD95-2042 (Sánchez Goñi et al., 1999), 4=Lago Grande di Monticchio (Allen and Huntley, 2009; Brauer et al., 2007), 5=Ioannina Basin (Tzedakis, 1994b; Tzedakis et al., 2003a), 6=Tenaghi Philippon (Milner et al., 2013; Tzedakis et al., 2006), 7=Lake Van (Pickarski et al., 2015a, b), 8=Lake Urmia (Djamali et al., 2008), 9=Yammoûneh Basin (Gasse et al., 2011, 2015), 10&11=marine cores MD 84 642 and MD 84 627 (Cheddadi and Rossignol-Strick, 1995a), and 12=travertine deposits south of the Dead Sea Basin (Weinstein-Evron, 1987). *White squares*: MIS 5 Dead Sea deposits (Waldmann et al., 2009). *White triangles*: speleothem sites of 13&14=Peqi'in Cave & Soreq Cave (Bar-Matthews et al., 2003) and 15=Jerusalem Cave (Frumkin et al., 1999) in the sub-humid mountains. *Blue triangles*: speleothem sites of 16&17= Ma'ale Efrayim Cave (Vaks et al., 2003) & Kanaim Cave in the Judean Desert (Vaks, 2008) and 18&19=Ma'ale-Dragot Caves and Tzavoa Cave in the northern Negev (Vaks et al., 2006). *Yellow triangles*: speleothem sites in the central and southern Negev deserts (Vaks et al., 2007, 2010).

2.1 Pollen-based paleoenvironmental research in the Mediterranean region

Palynological investigations during the past decades have provided invaluable insights into vegetation successions and associated environmental variations in the Mediterranean region. Across southern Europe, many high-resolution pollen records encompassing the LIG period are available (Figure 1), e.g., at Ioannina Basin (Frogley and Tzedakis, 1999; Tzedakis, 1994b; Tzedakis et al., 2002a, 2003a), at Tenaghi Philippon (Milner et al., 2012, 2013, 2016; Tzedakis et al., 2003b, 2006) and at Kopais Basin (Tzedakis, 1999) in Greece, at Lake Ohrid in Albania (Lézine et al., 2010; Sadori et al., 2016), with varve-constrained chronology at Lago Grande di Monticchio in Italy (Allen et al., 1999, 2000; Allen and Huntley, 2009; Brauer et al., 2007), and from marine cores at the Iberian margin (Sánchez Goñi et al., 1999; Shackleton et al., 2002, 2003).

These archives have greatly improved our knowledge about the vegetation successions of glacial-interglacial cycles. As concluded by Tzedakis (2007), a recurrent pattern with three phases was distinct of interglacial vegetation successions in southern Europe. Firstly, the glacial-interglacial transitions were marked by a pre-temperate phase of open woodland. Secondly, the interglacials experienced a temperate phase with an early expansion of Mediterranean sclerophylls followed by a succeeding increase in other temperate and coniferous trees. Lastly, the glacial inceptions were characterized by a post-temperate phase of open woodland accompanied by an invasion of steppic elements. Magri and Tzedakis (2000) evaluate the link between independently-dated southern European pollen sequences and astronomical configurations. They unravel the prominent control of orbital signatures on vegetation successions, and thus verify the feasibility and reliability of tuning the chronology of long pollen sequences orbitally (Tzedakis et al., 2002a, 2003a, 2006).

In southern and northern Europe, the onset of Eemian was nearly simultaneous, coinciding with the culmination of sea-surface temperature (SST) of the North Atlantic at ca. 126 ka after complete deglaciation. However, southern Europe witnessed a good prevalence of tree populations until the significant ice built-up at ca. 110 ka, as compared with the counterparts in northern Europe at ca. 115 ka (Brauer et al., 2007; Lézine et al., 2010; Tzedakis, 2003 and references therein). This phenomenon is explained to be a result of warm conditions that persisted in the North Atlantic for several millennia after glacial inception (Broecker, 1998; Kukla et al., 2002). The warm sea surface provided moisture to southern Europe where the temperature was the secondary factor controlling forest development (Tzedakis, 2003). Since 110 ka, the significant contraction of European forests implied a climatic deterioration that was accompanied by millennial-scale instabilities (Brauer et al., 2007; Milner et al., 2013;

Shackleton et al., 2002; Tzedakis, 2003) associated with cooling events in the North Atlantic (Chapman et al., 2000; Kukla et al., 2002; McManus et al., 1994; Müller and Kukla, 2004).

In the Near East (Figure 1), well-dated long pollen records encompassing the LIG period are comparatively scarce. Palynological investigations have been conducted at the Black Sea (134–119 ka; Shumilovskikh et al., 2013), at Lake Urmia in Iran (Djamali et al., 2008), at Lake Van in Turkey (Litt et al., 2014; Pickarski et al., 2015a, 2015b), and at Yammoûneh Basin in Lebanon (Gasse et al., 2011, 2015). Among these archives, the deep drilling project at Lake Van provides a high-resolution pollen record that shows similar phases of LIG vegetation successions as inferred from the southern European sites. Nevertheless, the proportions of thermophilous trees in the Near East are much smaller due to the moisture deficiency (Pickarski et al., 2015a).

In the Levant, pollen sequences in Lebanon document the vegetation history in the high-altitude mountains (Gasse et al., 2011, 2015), whereas the LIG vegetation conditions in lower altitudes remain nearly unknown. In northern Africa, the scarcity of pollen records and their limits to the Holocene period exclude these records from the scope of this study (e.g., Lamb et al., 1995; Leroy, 1992).

2.2 Paleoenvironmental research in the southern Levant

2.2.1 Palynological research

The Levant refers to the historical-geographical region in the EM region. Core areas of the southern Levant encompass present political territories of Israel, Palestine, and Jordan (Steiner and Killebrew, 2014). Palynological investigation in the southern Levant was initiated at Lake Hula in 1950s (Figure 1; Picard, 1952). Since then, a number of localities have been studied palynologically and most of these sites are dated back to no later than the last glacial.

In northern Israel, long sediment cores drilled at Lake Hula are estimated to document the vegetation history since the early last glacial (Horowitz, 1971; Weinstein-Evron, 1983; Weinstein-Evron et al., 2001). Shorter sediment cores were retrieved from the same lake, and the obtained pollen spectra (Baruch and Bottema, 1991, 1999) are assumed to go back to 11.3 ka (van Zeist et al., 2009) with the help of biostratigraphical correlation (Rossignol-Strick, 1995). The vegetation history at the Sea of Galilee is investigated by Miebach et al. (2017) and Weinstein-Evron et al. (2015) for the period of early MIS 2, by Schiebel (2013) for the past 8.2 ka, and by Baruch (1986) for the past 5.3 ka. In terms of environmental archaeology, the interval 5.6–2.5 ka is investigated focusing on the history of olive cultivation (Langgut et al., 2015a, 2016). The episode at 3.25–3.1 ka is detailedly analyzed to reveal the vegetation conditions during the Late Bronze Age when a collapse of civilizations marked the Levant (Langgut et al., 2013a). On the Golan Height, Weinstein-Evron (1976) firstly presents a pollen record back to the last glacial based on sediment cores obtained from the maar lake Birkat Ram. Neumann et al. (2006) apply botanical-climatological transfer functions to quantitatively reconstruct climatic conditions since 6.5 ka based on new pollen data from Birkat Ram. Latest palynological results covering the past 30 ka from the same lake are presented by Schiebel (2013).

In the Dead Sea Basin (DSB), pollen records are available from outcrops and sediment cores along the western shore. Cores drilled south of the Dead Sea are assumed to comprise the vegetation history of past 3.5 million years (Horowitz, 1989; Weinstein-Evron and Horowitz, 1986). Fragmentary sequences of pollen assemblages from the MIS 7 and MIS 5 travertines found south of the DSB in the Arava Valley (Figure 1) are investigated by Weinstein-Evron (1987). Yet, only one sample is available for the LIG period in this pollen record, and the derived data are subject to statistical uncertainties and are insufficient for identifying vegetation changes over time. Better chronologically-constrained pollen sequences have been

available since the 1990s. Baruch (1990) studies pollen from Holocene sedimentary cores drilled in the Ein Gedi alluvial plain. Deep coring from the Dead Sea was performed in 1993 and the sediments are consisted of laminae and salt layers, enabling the analysis of vegetation and climatic conditions during the past 2.5 ka (Heim et al., 1997; Leroy, 2010). Neumann et al. (2007) investigate pollen samples collected from erosion gullies (Ein Feshkha and Ze'elim; Figure 2B) dated back to 6.8 ka. A high-resolution Holocene pollen record is realized by the cores drilled near the Ein Gedi Spa (Figure 2B) dated back to ca. 10 ka (Litt et al., 2012). In this study, pollen-based quantitative climatic reconstructions reveal the sensitive response of vegetation belts to climatic variations. Distinct human disturbances are also recognized by pollen indicators of anthropogenic activities. Late Holocene pollen sequences from the Ze'elim outcrops (Figure 2B) show clear signals of vegetation change during the late Bronze Age (Langgut et al., 2014). Palynomorphs embedded in the aragonite and detrital laminae of the Ze'elim Formation serve for assessing whether these laminae are annual deposition (López-Merino et al., 2016).

Palynologically analyzed marine cores in the southeastern Mediterranean Sea are located in the Nile Cone area (Figure 1). Cheddadi and Rossignol-Strick (1995a, b) provide pollen results with foraminiferal $\delta^{18}O$ chronology dated back to 250 ka and show that palynomorphs in the sapropel layers are particularly well preserved. More recently, core 9509 is retrieved in the vicinity of the Nile Cone cores, and pollen-based vegetation history since 86 ka are achieved (Almogi-Labin et al., 2009; Langgut, 2017; Langgut et al., 2011).

As the southern Levant has a long history of human occupation, pollen analysis has been utilized as an important approach to infer vegetation conditions not only in the region but also in the vicinity of archaeological sites along with macrofossil evidence (faunal and floral). However, the data obtained are usually fragmentary and discontinuous. The investigated sites are situated at the Gesher Benot Ya'aqov Acheulian site (800–700 ka; van Zeist and Bottema, 2009) and at Nahal Mahanayeem Outlet (65–51 ka; Aharonovich et al., 2014) in the Hula Basin, and at the middle paleolithic site Tabun Cave in the coastal area (Horowitz, 1979). Recently, fossil pollen assemblages are used to reveal the import of fruit trees and ornamentals into the ancient garden in the Jerusalem area at 2.4 ka (Langgut et al., 2013b). Blooming seasons of different pollen taxa captured in a kiln are incorporated into resolving the timing of an ancient earthquake at Tel Yavneh in central Israel (Langgut et al., 2015b). Attempts have also been paid to evaluate the influence of seismic activities on vegetation and agriculture (Leroy et al., 2010; Neumann et al., 2009).

In terms of modern pollen studies, some of them were prepared for allergic research but additionally facilitated the interpretation of fossil pollen results. A calendar of air-borne pollen is established with the help of traps set up in the DSB (López-Merino et al., 2016 and reference therein). Similar air-borne pollen observations are reported in Jordan (Al-Eisawi

and Dajani, 1987, 1988; Al-Qura'n, 2008) and in other parts of Israel (Keynan et al., 1991; Waisel et al., 1997; Weinstein-Evron, 1979). Dust samples collected in Jerusalem and Tel Aviv suggest storms bring some pollen grains from the remote desert (100–150 km away), although these elements only constitute a minor part of the pollen spectra (Horowitz, 1992; Horowitz et al., 1975).

Baruch (1993) collects 35 soil surface pollen samples from the Judean Mountains down to the Dead Sea shoreline. Major vegetation components are observed at each site and the main vegetation types in the southern Levant are covered: the Mediterranean, Irano-Turanian, and Saharo-Arabian vegetation. Similarly, Davies and Fall (2001) analyze modern pollen assemblages along an elevational transect from the Transjordan Plateau at 1700 m above mean sea level (m amsl) to the DSB at 300 m below mean sea level (m bmsl). Both studies show vegetation types can be well recognized by their respective pollen spectra. Pollen assemblages in the recent sediments are investigated at the Dead Sea (Horowitz, 1979; Rossignol-Strick, 1969), at the Sea of Galilee (Horowitz, 1969), in the Hula Basin (Horowitz, 1971), at Birkat Ram (Horowitz, 1966; Weinstein-Evron, 1976), at the Bay of Elat, and offshores of Israel (Rossignol-Strick et al., 1969).

2.2.2 Limnological and stratigraphical research

In the DSB, the paleowaterbodies deposited sediments of up to 10 km (Garfunkel, 1997), which have been extensively investigated for limnological and hydrological evolution in the DSB based on studies of stratigraphy, radiometric dating, and paleoshoreline indicators (Bartov et al., 2002; Bookman et al., 2006; Lisker et al., 2009; Migowski et al., 2006; Niemi, 1997b; Stein, 2001, 2014; Stein et al., 2010; Torfstein et al., 2009, 2013a; Waldmann et al., 2009).

During the early and middle Miocene, fluvio-lacustrine sediments covered the most of the present Israeli territory (Calvo, 2002; Shaliv, 1991) until the low-lying valleys were invaded by marine ingressions during the late Neogene (Garfunkel, 1997). The subsequently formed Sedom Lagoon extended along the Dead Sea-Kinnarot rift valley. The Sedom Formation (Fm.) is nowadays exposed in Mount Sedom (Figure 2B) as a salt diaper with ca. 2 km of sediments. The sediments are mainly composed of thick halite with intercalations of dolomite and some lacustrine-type deposits (Stein, 2014; Zak, 1967). Ca-chloride brine in the present Dead Sea was a product of the seawaters dolomitizing the Cretaceous limestone of the basinal wall rocks. The brine played a critical role on the geochemistry of the quaternary waterbodies in the DSB (Gavrieli and Stein, 2006; Starinsky and Katz, 2014; Stein et al., 2000, 2002).

The Sedom Lagoon was disconnected with the open sea ca. 3 million years ago (Torfstein et al., 2009). After that, the DSB has been occupied by Lake Amora, Lake Samra, Lake Lisan, and the Dead Sea. The lacustrine sediments were primarily comprised of evaporites (aragonite, gypsum, and halite) and detrital material delivered by perennial and ephemeral rivers (Enzel et al., 2006). Different depositional facies point to variations in lake levels and hydroclimatic conditions in the region (Stein et al., 1997).

The Amora Fm. is exposed at the section of Arubotaim Cave along the eastern flank of Mount Sedom. The formation consisted of sedimentary sequences of several glacial-interglacial cycles (MIS 18–6) and the uppermost part reached the LIG (ca. 130 ka; Torfstein et al., 2009). Primary sediments were carbonate rocks, evaporites, and clastics (Stein, 2001). The lake level of Lake Amora is estimated to average around 350 m bmsl (Waldmann et al., 2007, 2009).

Exposed sections of the Samra Fm. in the DSB (e.g., in the Perazim Valley; Figure 2B) suggest that Lake Samra existed between ca. 135 and 70 ka (Figure 1). The lake level fluctuated around 340 m bmsl, which was in average higher than the Holocene lake stand. Sequences of laminated detritus (*ld*) mainly composed of calcite and quartz were deposited. This is explained to indicate limited supply of fresh water to the lake, low lake levels, and generally arid conditions that prevailed in the drainage area (Waldmann et al., 2009).

Sediments of the Lisan Fm. were pervasive along the DSB (Figure 3B) due to the high stand of Lake Lisan during the last glacial (70–14 ka; Haase-Schramm et al., 2004). The lake level fluctuated between 370 and 160 m bmsl (Stein, 2014), and the Lisan Fm. was primarily represented by alternating aragonite and detrital laminae (*aad*). The MIS 3 sequence was composed of *ld* pointing to low lake stands during ca. 49–31 ka (Haase-Schramm et al., 2004; Machlus et al., 2000; Schramm et al., 2000). This period was also characterized by large floods as indicated by slackwater deposits in a cave in the southern Negev desert (Greenbaum et al., 2006b). At ca. 27–24 ka, Lake Lisan rose to maximal stand and merged with the Sea of Galilee into a megalake with a lake level of ca. 160 m bmsl (Bartov et al., 2002, 2003; Hazan et al., 2005).

Since the late glacial, Lake Lisan significantly shrank with a short resumption to ca. 330 m bmsl at ca. 13–11 ka. This resumption was followed by abrupt lake-level drops as indicated by massive salt deposition (Stein et al., 2010). The Holocene Dead Sea deposited sediments of the Ze'elim Fm. Sections and drilled cores of this formation were studied (Heim et al., 1997; Migowski et al., 2004, 2006; Yechieli et al., 1993). The Ein Gedi archive (Figure 2B) probably retrieved the most continuous Holocene sequences covering the past 10 ka. The sediment cores were comprised of calcitic marl laminae, as well as some aragonite and detrital laminae. The inferred lake level fluctuated between 430 and 370 m bmsl (Bookman (Ken-Tor) et al., 2004; Migowski et al., 2006).

Changes in the modern Dead Sea lake level are forced by climatic and anthropogenic impacts. It is observed that the unstable regional climate causes high-amplitude annual and decadal variability in the lake levels (Anati, 1997). Since the early 1960s, anthropogenic diversions of the upstream (the upper Jordan River and the Yarmouk River) led to a significant lowering of the lake level, from 395 m bmsl in 1960 to 429 m bmsl in 2015 (Greenbaum et al., 2006a). The lake-level drop and shrinkage of the surface area have induced significant changes in the lake's morphology, hydrography, geochemistry, and surrounding biological communities (Aloni et al., 1997; Niemi, 1997a).

2.2.3 Speleological research

Whereas lacustrine sediments deposited prior to the last glacial are confined to limited localities, cave sediments in the carbonate rock terrain of the southern Levant provide the longest paleoenvironmental records with well-defined chronology. The steep precipitation gradient from north to south leads to a division of the speleothem sites into three geographic clusters: the sub-humid northern and central Israel, the rain-shadow semi-desert and northern Negev, and the arid central and southern Negev desert (marked as colored triangles in Figure 1).

2.2.3.1 Speleothem deposition

Speleothem formation in the southern Levant is mainly controlled by the availability of moisture in the unsaturated zone, especially in drier areas (Vaks et al., 2003, 2006, 2007, 2010). The amount of water reaching the unsaturated zone is determined by the effective precipitation (precipitation-(evaporation+runoff); Ford and Williams, 2007).

In northern and central Israel, the sub-humid Mediterranean climate (>400 mm mean annual precipitation (MAP)) prevails in the mountains and the Mediterranean biome covers the landscape. Almost continuous deposition of speleothem since ca. 185 ka and 240 ka is indicated by the Soreq and Peqi'in cave stalagmites, respectively (Bar-Matthews et al., 1997; 2000, 2003; Grant et al., 2012). Situated close to the Soreq cave, the Jerusalem cave provides records spanning the past ca. 220 ka (Frumkin et al., 1999, 2000; Frumkin and Stein, 2004).

In turn, proxies from these sub-humid caves are considered to be less sensitive to environmental changes as compared to the more arid sites, where discontinuous speleothem deposition are directly diagnostic of the effective precipitation (Frumkin et al., 2011). In the

southern Levant, no modern speleothem deposition is observed in the semi-arid and arid areas because the precipitation is too low to trigger cave dripping (MAP <300 mm). Latest speleothem deposition in these areas occurred in the Ma'ale Dragot Cave at 3.8 ka. As current MAP of this cave area is 280–300 mm, a minimum MAP of 300–350 mm is suggested as the prerequisite for speleothem deposition during past interglacials (Vaks et al., 2006), given analogously warm conditions to the Holocene (Emeis et al., 2003; McGarry et al., 2004). The glacials, estimated with temperatures of 5–10°C lower than the present (Emeis et al., 2003; McGarry et al., 2004), benefited from less water loss caused by evaporation and runoff, and thus required a lower MAP (200–275 mm) for speleothem deposition (Vaks et al., 2010 and references therein).

In the semi-arid areas, the landscape is covered either by the Irano-Turanian steppe or transitions to the steppe with a mix of herbs and scattered trees and shrubs. In the rain-shadow semi-desert on the eastern flank of the Judean mountains, speleological studies are mainly from the Ma'ale Efrayim cave (ca. 354–12 ka) with intervals of speleothem deposition centering at the last and penultimate glacials (Lisker et al., 2010; McGarry et al., 2004; Vaks, 2008; Vaks et al., 2003). The northern Negev speleothems are represented by the Tzavoa cave, where speleothems were primarily deposited during the glacials at 190–150 ka, 76–25 ka, and 23–13 ka, with minor deposition occurring during the interglacials at 200–190 ka, 137–123 ka, and 84–77 ka (Vaks et al., 2006).

In the even drier central Negev desert (150–50 mm MAP) and hyper-arid southern Negev desert (50–25 mm MAP), a series of karst caves were discovered. These caves were episodically active. Late-Quaternary uranium-thorium (U-Th) ages of the speleothems are clustered at 350–290 ka, 220–190 ka, and 142–109 ka. These intervals are termed as the 'Negev Humid Periods' (NHPs), mostly coinciding with interglacials (Vaks, 2008; Vaks et al., 2007, 2010).

The growth rate of speleothems is directly indicative of effective precipitation, although it can hardly be calculated on a regional basis because it requires a high density of dated points (Frumkin et al., 2011). Instead, proxies like numbers and thickness of laminae are used as indicators of local dripping rates in the caves (Bar-Matthews et al., 1997; Vaks, 2008). Besides, relative age frequencies based on dates from speleothems of multiple caves can provide insights into regional climatic fluctuations (Frumkin et al., 2011). For example, during the late Quaternary, the highest age frequency of the speleothems in the central and southern Negev occurs during the last interglacial (142–109 ka) along with relatively thick and abundant laminae, indicating relatively intense speleothem deposition and thus a moister-than-present climate in this area (>300 mm MAP; Vaks, 2008).

2.2.3.2 Stable isotopes

Stable isotopes from speleothems are widely used as paleoclimatic indicators (McDermott, 2004). For the low-altitude southern Levantine caves, the changes in speleothem oxygen isotope on glacial-interglacial timescales are attributed to the "source effect" of the EM seawater on the composition of oxygen isotope of the rainfall above the cave (Bar-Matthews et al., 2017). This conclusion is based on the close coupling of $\delta^{18}O$ records between the Israeli speleothems and EM Sea over a long time scale (Almogi-Labin et al., 2009; Bar-Matthews et al., 2003; Frumkin et al., 1999; Vaks et al., 2010).

In northern and central Israel, the speleothem hydrogen isotope record shows that the EM Sea is the constant rainfall source of this area over time (McGarry et al., 2004). In semi-arid areas, the general trend of speleothem $\delta^{18}O$ variations resembles the counterparts in the sub-humid northern and central Israel, implying a similar EM moisture source (Vaks et al., 2003, 2006). In the arid central and southern Negev desert, it is suggested that rainfall during the NHPs was most probably brought by the mid-latitude Atlantic-Mediterranean cyclones. This argument is supported by the remarkable decreasing trend of speleothem depositional frequency from north to south in the central and southern Negev desert. The trend is accompanied by a southward thinning of coeval speleothem laminae, pointing to the fade-out of Mediterranean rains (Vaks et al., 2010). In addition to the EM Sea as the dominant rainfall source, the arid areas benefit from southern tropical rain-generating systems (e.g., the Red Sea Trough) presently, and presumably also during past wet episodes (Waldmann et al., 2010).

The climatic implications of speleothem calcite $\delta^{13}C$ are more perplexing. In the southern Levant, it mainly reflects changes in CO_2 of the soils above the cave, which is in turn controlled by vegetation types and soil-water interactions (Bar-Matthews et al., 1997, 2003; Frumkin et al., 1999, 2000). Under closed system conditions, speleothem $\delta^{13}C$ values show a range between -13‰ and -9‰ for C3-dominated plant communities (Calvin photosynthesis cycle) and higher values for C4-dominated plant communities (Hatch-Slack cycle). The C4 plants are relatively more photosynthetically efficient under stressed conditions such as water deficit (Vaks, 2008).

In central and northern Israel, speleothem $\delta^{13}C$ records indicate the general predominance of C3 plants in the cave area during interglacials and increases of C4 plants in the vegetation under drier conditions during glacials (Bar-Matthews et al., 1997, 1999, 2000, 2003). Exceptional periods coinciding with the EM Sea sapropel events at 9–7 ka and 128–120 ka were characterized by remarkably high $\delta^{13}C$ and low $\delta^{18}O$ values of speleothem calcite. These periods are interpreted as deluge episodes of 20%–70% higher-than-present MAP. The

notably high $\delta^{13}C$ values are pointed to the fast infiltration of rainwater to karst caves almost without equilibrium with soil CO_2, based on the evidence of enhanced host-rock weathering and the present-day analog (Bar-Matthews et al., 2000, 2003 and references therein). Frumkin et al. (2000) suggest these intervals of high speleothem $\delta^{13}C$ values were marked by extremely low vegetation and soil cover. As concluded by Bar-Matthews et al. (2017), the enhanced precipitation during peak interglacials was consistent with the coeval vegetation loss in the presently sub-humid cave areas. That is, the rainfall was extreme and unstable, leading to intense flash-floods stripping the poorly vegetated soils, which in turn facilitated flooding and erosion.

In the rain-shadow areas, the similarities of speleothem $\delta^{13}C$ values with the sub-humid caves indicate these two areas were covered by similar vegetation types during the glacials. During periods of speleothem deposition in the northern Negev, higher speleothem $\delta^{13}C$ values imply the vegetation was of a similar mixed C3-C4 plant type as the present-day (Bar-Matthews et al., 2017). In the central and southern Negev desert, high speleothem $\delta^{13}C$ values during the NHPs are explained to reflect the low vegetation cover and the significant influence of host rock CO_2 (Vaks, 2008).

Strontium isotopes from speleothem calcite are analyzed for tracing aeolian dust transport and for reflecting the amount of dust originating from the Sahara (Frumkin and Stein, 2004). Recently, a new approach is developed to resolve the seasonal or sub-annual climatic variability based on high-resolution geochemical analysis of the Soreq Cave stalagmites (Orland et al., 2009, 2012, 2014).

3 Dead Sea and its setting

3.1 Dead Sea and its drainage area

The Dead Sea is a hypersaline lake bordered by Israel and the Palestine territory to the west and Jordan to the east (Figure 2A). It is situated at the lowest point on the continental earth and occupies the Dead Sea Basin (DSB) in the Dead Sea Transform (DST; Garfunkel and Ben-Avraham, 1996). The lake is 76 km long and up to 17 km wide and has a surface area of ca. 760 km^2 (Figure 2B). The DSB comprises two sub-basins separated by a sill at ca. 402 m bmsl (Figure 2C; Neev and Emery, 1967). The bathymetric measurements show that the northern sub-basin is flat-bottom shaped, and the slopes in the west and east are steep (Hall, 1997). The northern sub-basin is deep with a bottom depth at 730 m bmsl (Neev and Hall, 1979). It is occupied by the present Dead Sea with a water depth of ca. 300 m, whereas the southern sub-basin is shallow (411 m bmsl at the bottom) and currently serves as evaporation ponds for potash production (Bookman et al., 2006). The Dead Sea water has a salinity of ca. 27.5% (340 g/l), and the brine is composed of unique Ca-chloride that plays a key role in the formation of evaporites in the lake (Gavrieli and Stein, 2006).

The Dead Sea is a terminal lake in the dryland. Its lake level is determined by the balance of incoming water and surface evaporation. The Dead Sea drainage area (Figure 2A) is ca. 42,200 km^2, extending from Mount Hermon in the north to the vicinity of the Gulf of Aqaba in the south (Greenbaum et al., 2006a). The drainage area primarily encompasses the mountains in the west and highlands in the east, the Jordan Valley, and the northern Arava Valley (Bentor, 1961). The Jordan River is the most important inflow of the Dead Sea. It drains the northern sub-humid areas to the arid DSB in the south, covering 17,670 km^2 of the whole drainage area and delivering ca. $1{,}100\times10^6$ m^3 water to the Dead Sea. The ephemeral Nahal Arava originates from the arid south and feeds the Dead Sea with limited volumes of water (ca. 5×10^6 m^3), although the drainage area is large (ca. 13,250 km^2; Greenbaum et al., 2006a). The west and east of the Dead Sea are bordered by steep rocky escarpments, which yield perennial and ephemeral flows delivering water and sediments to the Dead Sea (Bartov et al., 2003). Despite the small fraction of water volume the semi-arid and arid tributaries supply to the Dead Sea, they are characterized by large rainstorm-induced flash floods (Greenbaum et al., 2006a). These floods lead to intensive erosion in poorly vegetated areas and carry large volumes of coarse clastic sediments to the Dead Sea and its surroundings (Weinstein-Evron and Horowitz, 1986). Groundwater such as springs marginally contributes to the Dead Sea (Greenbaum et al., 2006a; Yechieli, 2006).

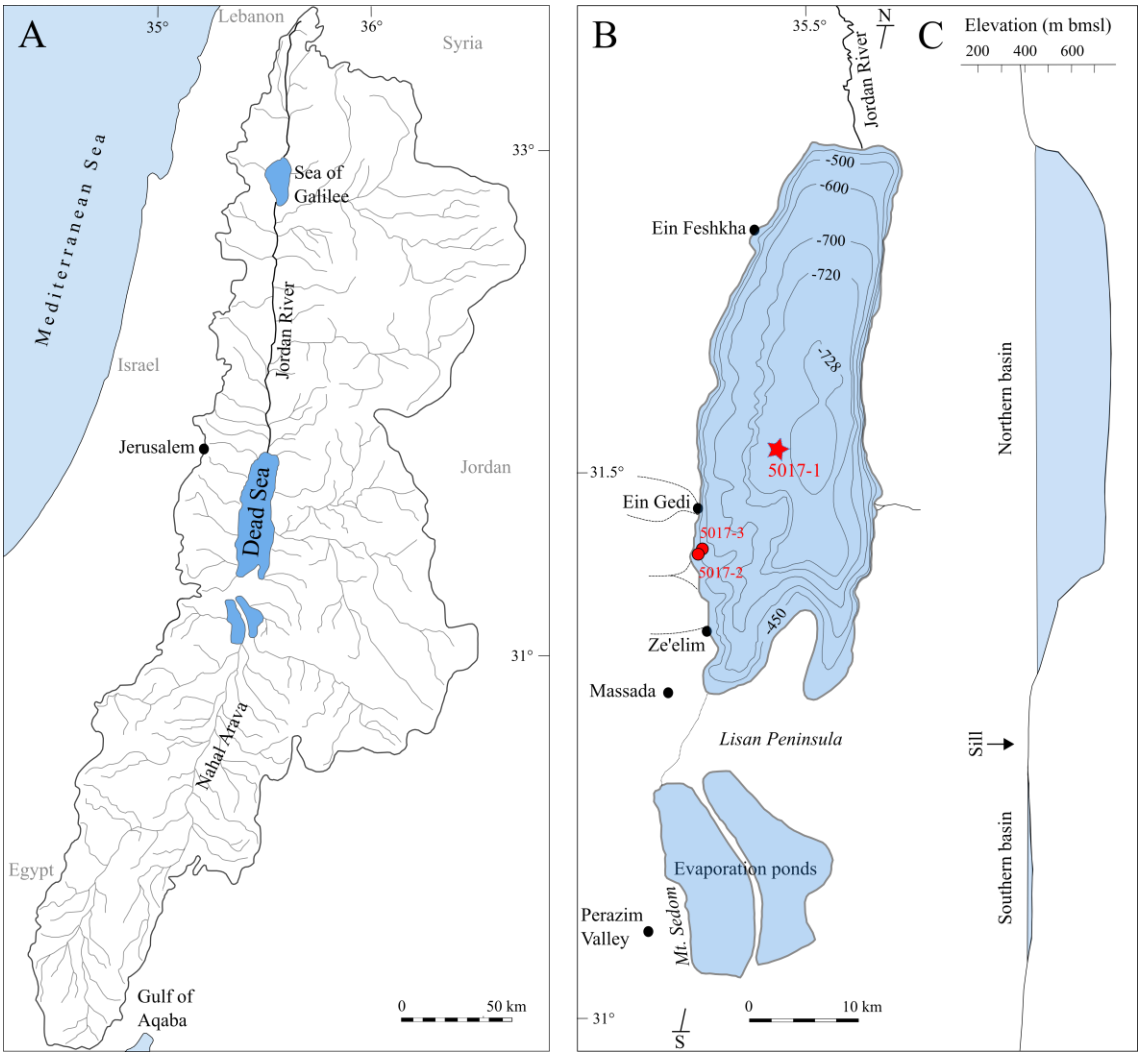

Figure 2: A) The Dead Sea drainage area, after Bentor (1961); B) Bathymetric map of the Dead Sea, after Neev and Hall (1979). Locations of the Dead Sea Deep Drilling Project (DSDDP) sites are marked in red. The red star denotes the investigated site 5017-1 in this study and the red dots indicate the shallow-water sites 5017-2 and 5017-3 (described in section 4.1). The black dots mark locations of previously studied cores and exposures of Dead Sea sediments. C) North-south cross section of the Dead Sea Basin, after Bookman (Ken-Tor) et al. (2004). The sill at 402 m bmsl separates the northern and southern sub-basins.

The evaporation rate of the Dead Sea water is estimated to be over 1,000 kg/m^2/year. The strong evaporation is largely controlled by temperature changes affecting both lake and air conditions. In addition, water input and evaporation influence salinity dynamics of the lake surface, which indirectly cause changes in evaporation because saline water has a lower evaporative loss than fresh water under similar settings (Steinhorn, 1997).

Aquatic lives such as plants and animals are scarce in the Dead Sea due to its high salinity. Common organisms are microscopic, including archaea, bacteria, and eukarya (Oren, 1997). Underwater springs near the shore of the Dead Sea nourish numerous bacteria and archaea

(Ionescu et al., 2012; Oren et al., 2008). During periods of low salinity caused by flooding, the green alga *Dunaliella* flourished with reddish halobacteria in the diluted upper water column (Oren and Ben-Yosef, 1997). In recent sediments on the lake bottom, Elazari-Volcani (1940a, 1940b) found green algae (e.g., species of *Scenedesmus* and *Pediastrum*) and diatoms (e.g., genera *Melosira*, *Navicula* and *Gomphonema*). Diatoms were present in late Pleistocene Dead Sea sediments as well (Begin et al., 1974; Thomas, 2015).

3.2 Geology

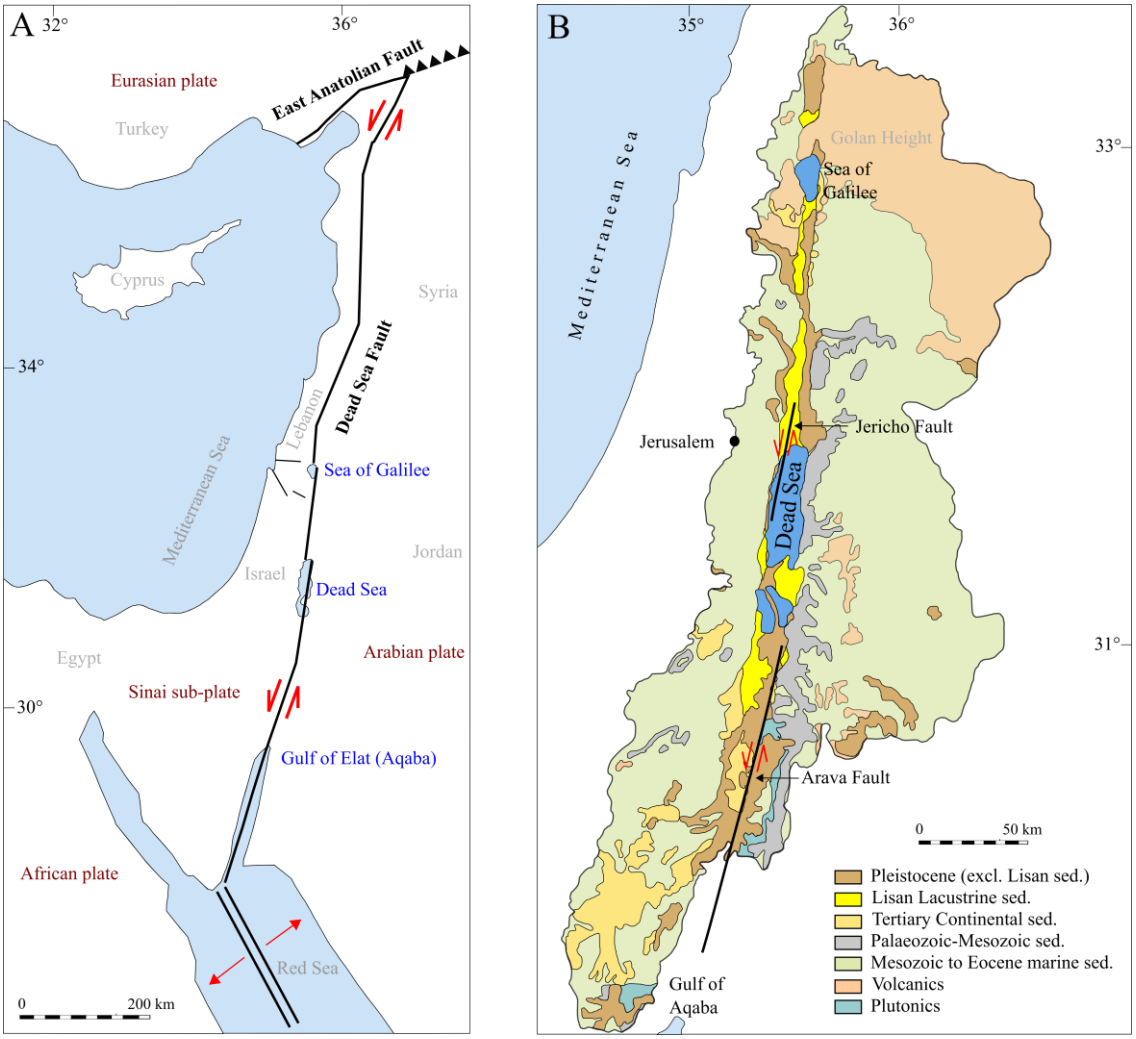

Figure 3: A) Tectonic setting of the Dead Sea Transform and the waterbodies occupying the pull-apart basins (labeled in blue). Red arrows denote regional tectonic plate movement, after Ben-Avraham (2014); B) Exposed geological units in the Dead Sea drainage area, after Bentor (1961).

The DST is a transform fault ca. 1,000 km long ranging from the Red Sea in the south to the East Anatolian Fault in the north (Figure 3A). The DST has developed during the early Miocene as a result of the breakup between the African and Arabian plates, accompanied by the formation of narrow valleys and uplifting of its shoulders at the plate boundary (Garfunkel, 1997). Regional-scale igneous activities occurred primarily in the east of the DST, e.g., on the Golan Height. Seismic activities were intense along the DST, as revealed by geological archives and instrumental records (Agnon, 2014; Hofstetter et al., 2014; Migowski et al., 2004).

The formation of DST is dominated by left-lateral motion. In the southern segment of the DST, this motion is associated with the occurrence of elongated and deep depressions whose structure is dominated by pull-apart basins (Ben-Avraham, 2014). These basins are occupied by waterbodies: the Gulf of Elat (Aqaba), the Dead Sea, and the Sea of Galilee as well as the small Lake Hula to the north (Ben-Avraham, 2014). The origin and geometry of these pull-aparts are related to their location between two master strike-slip faults (Figure 4A). The depression originates when divergence occurs in the position where the master faults overstep. As the lateral motion continues, the pull-apart basin grows in length and depth while the width of the basin is theoretically limited to the distance between the faults and the length of the overlap. In the case of the DSB, its structure is embedded in a transform valley delimited by normal faults on both sides (Figure 4B; Garfunkel, 1997).

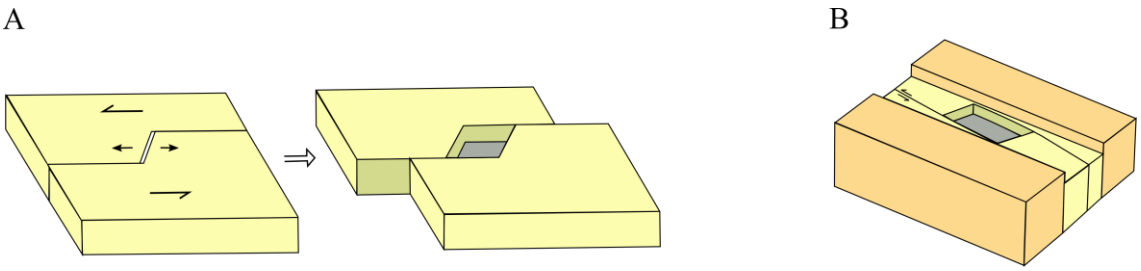

Figure 4: A) A simplified model showing the formation of a pull-apart basin (Garfunkel, 1997); B) The structural setting of the Dead Sea Basin: the pull-apart occupied by the basin and the master strike-slip faults are embedded in a valley delimited by normal faults (Garfunkel, 1997).

The DSB is the lowest (bottom depth at 730 m bmsl) and one of the largest pull-apart basins on the earth. It is about 150 km long and 15–17 km wide, encompassing the area between the Arava Fault and Jericho Fault (Figure 3B). In the Dead Sea drainage area, Precambrian plutonics of granites and siliceous volcanics are occasionally found in the south (Bentor, 1961). Paleozoic-Mesozoic sandstones cover the eastern escarpments of the lower Jordan Valley and northern Arava Valley (Gardosh et al., 1997). Mesozoic to Eocene marine sediments are the most prevailing exposed rock units, mainly composed of limestones and dolomites (Bentor, 1961). The northern Negev and Arava is characterized by Tertiary sediments of lacustrine and continental shales and sandstones (Bentor, 1961). Pliocene to Quaternary volcanic eruptions along the DST have resulted in the thick accumulation of alkali basalts on the Golan Height and the Lower Galilee (Weinstein and Garfunkel, 2014).

In the rift valley, especially in the DSB, sustaining subsidence of the basin and existence of the waterbodies have yielded up to 10 km of sediments since the early Miocene. The sediments mainly comprise three divisions: the Miocene siliciclastics (Hazeva Fm.), the

Pliocene halite (the Sedom Fm.), and the post-Sedom-Fm. lacustrine and fluvial deposits (Gardosh et al., 1997; Garfunkel, 1997). The active subsidence of the basin and the physiography of the steep basin margin, as well as recent anthropogenic lake-level drops, led to the incised streams cutting into the sediments and consequently to the exposure of these sediments (Bartov et al., 2006; Bowman, 1997; Moshe et al., 2008; Niemi, 1997a). The most prominent exposures are of the Quaternary lacustrine stratigraphy that is found along the Jordan Valley, the Dead Sea, and the northern Arava Valley (Niemi, 1997b). The Quaternary sediments are mainly comprised of evaporites (aragonite, gypsum, and halite), sand, gravel, conglomerates, and aeolian detritus consisted of quartz and calcite grains of different sizes (Enzel et al., 2006; Haliva-Cohen et al., 2012; Stein, 2001).

3.3 Climate

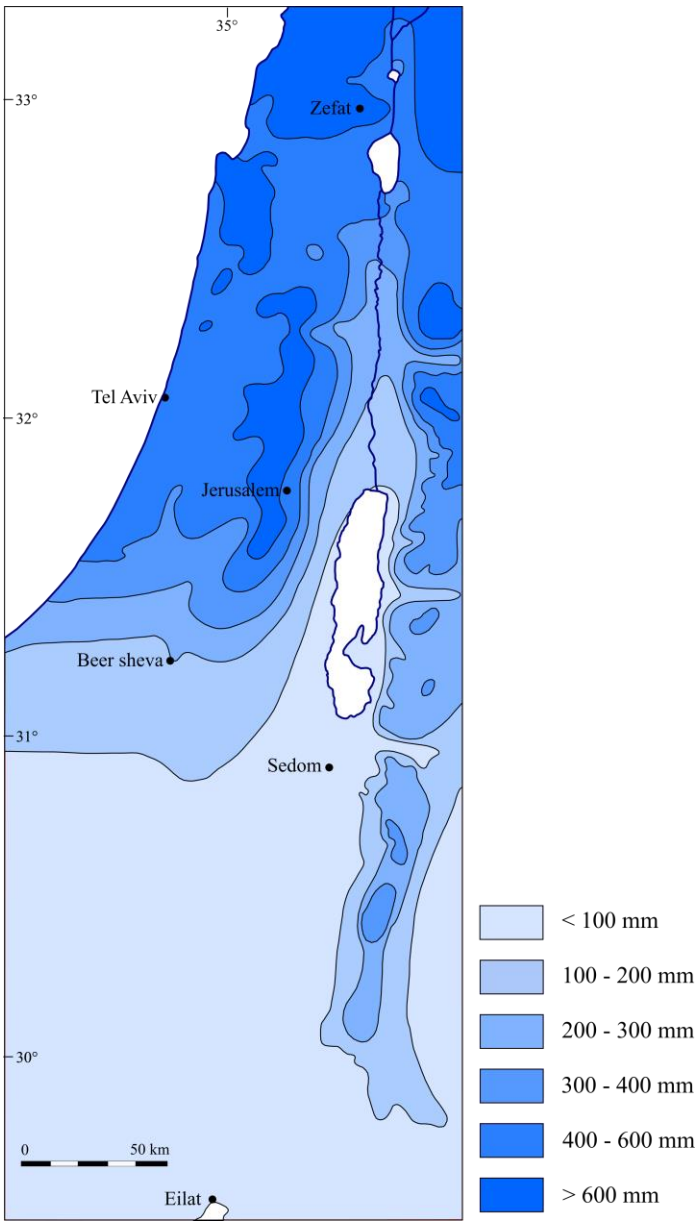

Figure 5: Distribution of mean annual precipitation (mm) in the southern Levant, after Zohary (1962). Black dots mark the meteorological stations listed in Table 1 (source: Israel Meteorological Service).

Due to its transitional location between the Mediterranean and Saharo-Arabian climate zones as well as the varied topography, the southern Levant is characterized by hot-dry summers and cold-wet winters in the north, while the southern part and the lowlands undergo semi-arid to arid conditions. As a result, the precipitation gradient is prominent in the region (Figure 5; Table 1).

Table 1: Meteorological data from the Israel Meteorological Service (img.gov.il), including temperature and rainfall data for the period 1981-2000 and 1970/1971-1999/2000, respectively. Meteorological stations are shown in Figure 5 and 6.

Station	Altitude (m amsl)	Mean max. temperatue (°C)		Mean min. temperatue (°C)		Mean rainfall (mm)	
		January	July	January	July	January	July
Zefat	934	9.4	29.8	4.5	18.8	158.8	n.a.
Tel Aviv	4	17.5	29.4	9.6	23	126.9	n.a.
Jerusalem	815	11.8	29	6.4	19.4	133.2	n.a.
Beer Sheva	195	16.7	32.7	7.5	20.5	49.6	n.a.
Sedom	-390	20.5	39.7	12.7	29.6	7.8	n.a.
Elat	12	20.8	39.9	9.6	25.9	3.5	n.a.

The mountainous areas are largely influenced by the sub-humid Mediterranean climate, whereas the low-lying areas, especially the rift valley and the DSB, become hot rain-shadow deserts due to the interception of rain by the N-S oriented mountain ridge (Horowitz, 1979). For instance, the Dead Sea itself receives a mean annual precipitation (MAP) of 50–100 mm/year and has a mean annual temperature (MAT) of 25°C (Greenbaum 2006). Jerusalem, situated in the Judean Mountains (815 m amsl), has a MAP of 400–600 mm/year and a MAT of 18°C. Snowfall occasionally occurs in the mountains and highlands from December to January and accounts for a minor part of the annual precipitation. In the further north, snowfall is more common and caps the summit of Mount Hermon forming the headwaters of the Jordan River (Horowitz, 1979).

The majority of moisture originates from the Mediterranean Sea during the winter, when the mid-latitude westerly jet systems move eastwards and drive the cold airmass over the warm Mediterranean Sea. Consequently, a series of active cyclones are developed, e.g., over Cyprus (the Cyprus Low) and the Aegean Sea (Alpert et al., 1990; Goldreich, 2003). The air masses are saturated with moisture that is subsequently released over the Levant, and most of the precipitation occurs between December and February (Dayan and Morin, 2006).

During the summer, the North African tropical high-pressure systems occupy the southern Levant. The stable and hot subsiding airmass induces significant dryness (Rohling et al., 2009). During the autumn, the southern arid/semi-arid areas are subject to convectional rainstorms caused by active low-pressure systems. For instance, the Red Sea Trough, as an extension of the African monsoon, is developed in tropical eastern Africa and penetrates northward along the Rea Sea, bringing moisture to the southern Dead Sea drainage area (Dayan and Morin, 2006). The rainfall regime associated with the Red Sea Trough is characterized by localized intensive (up to 60 mm/hr) but short-lived rainstorms that generate large flash floods (Greenbaum et al., 2006a; Sharon and Kutiel, 1986). A third synoptic system is the upper tropospheric jet, which originates in tropical Africa and intensifies the cyclogenesis over the EM region (Dayan and Morin, 2006; Ziv et al., 2006).

Western and northwestern winds prevail in the southern Levant (Weinstein-Evron, 1983). During the spring, dust storms associated with the Sharav cyclone developed in North Africa move east- and north-ward to the southern Levant (Alpert and Ziv, 1989; Goudie and Middleton, 2001). Strong easterly winds in the winter and early spring bring dust from Arabia as well (Saaroni et al., 1998). These regional winds mainly influence the mountains and highlands, while the coastal plain and valleys are subject to local winds. Coastal currents breeze westwards in the daytime and eastwards at night. Northern and southern winds blow along the Jordan and Arava Valley with diurnal directional changes (Bitan, 1974; Horowitz, 1979; Weinstein-Evron, 1983).

3.4 Vegetation

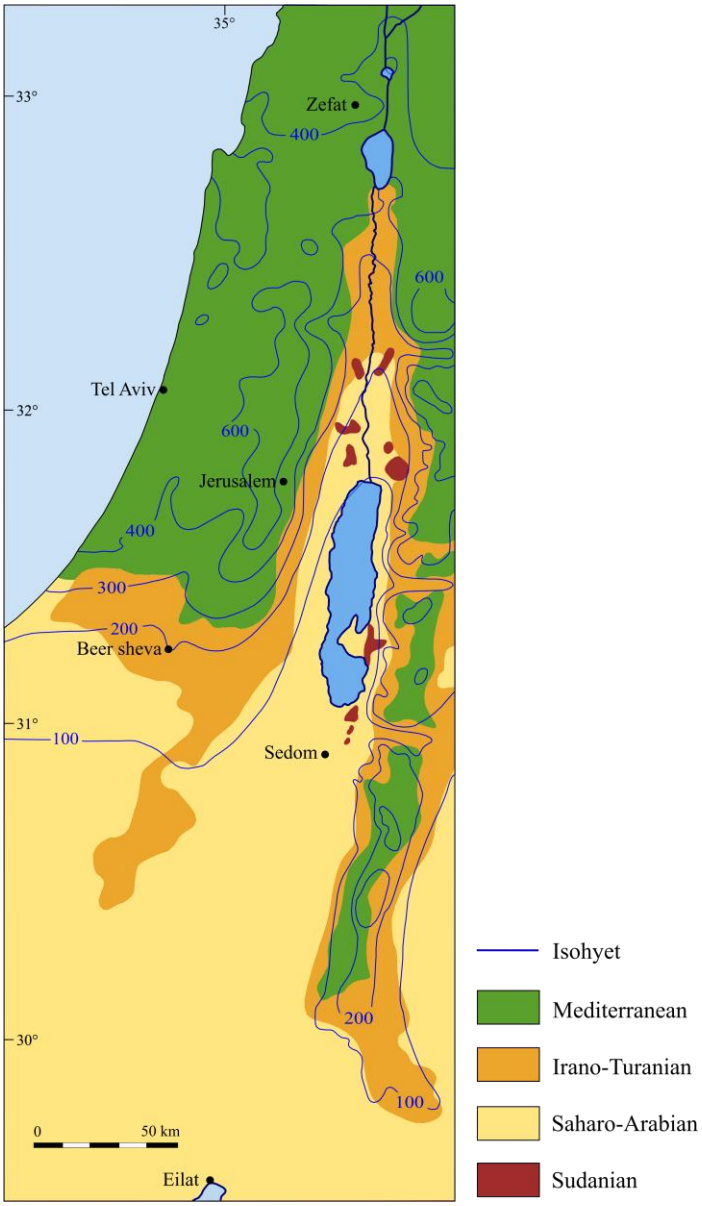

Figure 6: Vegetation territories and precipitation isohyet of the southern Levant, after Zohary (1962). The black dots mark the meteorological stations listed in Table 1.

As illustrated in Figure 6, the varied precipitation and topography pattern primarily determine present vegetation distribution in the southern Levant. Three phytogeographical territories converge here: the Mediterranean, the Irano-Turanian, and the Saharo-Arabian territory. Other factors influencing the vegetation are mainly soil types, anthropogenic impacts (deforestation/afforestation, grazing, and agriculture) during the past thousands of years, as

well as introduction of exotic plants such as *Eucalyptus*, *Casuarina*, and *Washingtonia* (Horowitz, 1979). The results of previous vegetation investigations (e.g., Danin, 1992; Danin and Plitmann, 1987; Eig et al., 1931; Zohary, 1962) are summarized below.

The Mediterranean territory

The Mediterranean vegetation is primarily found in the coastal plains, the Galilee and Judean Mountains, the Golan Height, and the Transjordan Plateau (Figure 6; Danin, 1992). Typical soil types are red terra rossa and white-grayish rendizina derived from carbonate rocks, basaltic soil, and sandy soil (Zohary, 1962). Different successional levels of the Mediterranean maquis are the most characteristic of the Mediterranean vegetation with a MAP of >400 mm (Danin and Plitmann, 1987). Under favorable ecological conditions, the maquis reach climax with the predominance of evergreen sclerophyllous trees and shrubs represented by evergreen oaks (*Quercus calliprinos*), pistachio (*Pistacia lentiscus*), olive trees (*Olea europaea*), carob trees (*Ceratonia siliqua*), *Phillyrea media*, *Arbutus andrachne*, *Laurus nobilis*, and *Rhamnus alaternus*. Major deciduous trees are oaks (*Quercus ithaburensis* and *Q. boissieri*), *Pistacia palaestina*, and *Styrax officinalis*. *Q. boissieri* is found in higher elevations (>400 m amsl) accompanied by deciduous rosaceous trees, while *Q. ithaburensis* is the main constituent of park forests in lower elevations (Zohary, 1962). The most common coniferous tree is Aleppo pine (*Pinus halepensis*), the only native pine species that occurs in the southern Levant. Other conifers are less common and are mainly from the Cupressaceae family (e.g., *Juniperus phoenicea*, *J. oxycedrus*, and *Cupressus sempervirens*). Nowadays, *J. phoenicea* grows in the mountains of southern Jordan (Edom; Al-Eisawi, 1996; Atkinson and Beaumont, 1971). In between the trees and shrubs, herbaceous communities dominated by grasses and wild cereals such as wheat (*Triticum dicoccoides*), barley (*Hordeum spontaneum*), and oat (*Avena sterilis*) are common (Danin, 1992). The southern end of the Mediterranean woodland is located in southwestern Jordan and is represented by *Quercus calliprinos* and *Pistacia palestina* (Davies and Fall, 2001).

The transitional areas between the Mediterranean and Irano-Turanian territory are characterized by batha (scrub and low bushes) and garigue (tall shrubs) interspersed by scattered trees of *Pistacia atlantica*, *Crataegus azarolus*, and *Amygdalus communis*. The semi-steppe batha covers the areas of 250–400 mm MAP (Danin and Plitmann, 1987), where climatic and edaphic conditions are harsh for maquis development. Instead, dwarf evergreen shrubs are distributed. Besides, anthropogenic disturbances lead to the penetration of ruderal elements into the vegetation. The plant communities are mainly composed of *Sarcopoterium spinosum*, rockroses (e.g., *Cistus salvifolius* and *C. creticus*), *Euphorbia thamnoides*,

Anchusa strigosa, *Salvia triloba*, *Thymbra spicata*, and *Teucrium creticum* (Danin, 1992; Zohary, 1962).

Oro-Mediterranean vegetation (Danin and Plitmann, 1987) ins found in Mount Hermon and southern Lebanon Mountains. Characteristic trees are relics of *Cedrus libani* forests tolerant of coldness and strong winds, accompanied by some deciduous oaks (e.g., *Quercus libani* and *Q. boissieri*) and junipers (*Juniperus drupacea*; Danin, 1992; Weinstein-Evron, 1983).

The Irano-Turanian territory

The Irano-Turanian vegetation is a dwarf-shrub steppe commonly found in the vast interior of Asia from the Anatolia to the Gobi Desert (van Zeist and Bottema, 1991). In the southern Levant, this vegetation type covers the upper part of the lower Jordan Valley as well as the lower elevations of the mountains and the Transjordan Plateau. In these areas, the climate is more continental and the precipitation (MAP of 70–250 mm) is lower than those of the Mediterranean territory (Figure 6; Danin and Plitmann, 1987). The principle soil types are gray steppe soil and loess soil. The landscape is vegetated by herbaceous and dwarf-shrub communities dominated by white wormwood (*Artemisia herba-alba*; Danin and Plitmann, 1987). Other common elements are grasses (including wild cereals such as *Hordeum spontaneum*), *Thymelaea hirsute*, *Ephedra aphylla*, *Noea mucronata*, *Haloxylon articulatum*, *Salsola vermiculata*, *Pistacia atlantica*, *Ziziphus lotus*, *Salvia lanigera*, *Marrubium alysson*, and *Achillea santolina* (Danin, 1992; Danin and Plitmann, 1987; Zohary, 1962).

The Saharo-Arabian territory

The Saharo-Arabian vegetation dominates the southern Negev Desert, the Judean Desert, and the Syrian Desert (Figure 6). Typical desert climate (MAP <100 mm) is characteristic of this floristic territory. The deserts undergo short rainy seasons and long hot-dry summers, as well as extreme diurnal and annual temperature changes. The barren land is covered by hammadas, sands, and salines. The vegetation cover is extremely low and the landscape is interspersed with low-diversified plant species. Relatively dense communities are found in small patches and confined to moisture-favorable localities such as depressions and wadis. Halophytic dwarf shrubs of various goosefoot species (Chenopodiaceae) such as *Suaeda* spp., *Salsola* spp., and *Atriplex* spp., as well as tamarisk (e.g., *Tamarix nilotica*) are common (Al-Eisawi, 1996). Other important plants are *Retama raetam*, *Zygophyllum dumosum*, *Calligonum*

comosum, *Anabasis articulate*, *Suaeda asphaltica*, *S. vermiculata*, *Salsola tetrandra*, *S. rosmarinus*, *Haloxylon persicum*, *H. salicornicum*, *Chenolea arabica*, *Traganum nudatum*, *Fagonia mollies*, *Nitraria retusa*, *Convolvulus lanatus*, and *Stipagrostis scoparia* (Danin, 1992; Danin and Plitmann, 1987; Zohary, 1962).

Localized plant communities

The Sudanian plant communities in the southern Levant are northern penetrations of the African Sudanian flora. Dominating plants are tropical Savannah elements represented by *Acacia* spp. (Danin and Plitmann, 1987). The penetrations developed along the streams in the lower Jordan Valley as well as the outlet areas of the Dead Sea and the northern Arava Valley. These areas are hot and hyper-arid but the plants are able to make use of the high water table in the lowlands. Main components of the plant communities are trees and shrubs, e.g., *Acacia tortilis*, *A. raddiana*, date palm (*Phoenix dactylifera*), *Tamarix aphylla*, *Maerua crassifolia*, *Moringa aptera*, *Salvadora persica*, *Balanites aegyptiaca*, and *Ziziphus spina-christi* (Al-Eisawi, 1996; Danin, 1992; Zohary, 1962).

The Dead Sea is located in the desert. In its vicinity, halophytes of Chenopodiaceae (e.g., *Atriplex halimus*) and Tamarisk (*Tamarix aphylla*) are common constituents of the flooded saline and marsh areas (Weinstein-Evron, 1983, 1987). These elements are also pioneer inhabitants of the newly exposed shoreline due to lake-level drops (Aloni et al., 1997). Other plants around the Dead Sea are grasses (e.g., *Stipa tortillis* and *Bromus aulerosus*), species of Zygophyllaceae, Asteraceae, Brassicaceae, and Plumbaginaceae, as well as *Capparis cartilaginea*, *Cleome* spp., *Thymelea hirsute*, *Haplophyllum* spp., *Ephedra* spp., *Centaurea* spp., and *Asphodelus* spp. (Weinstein-Evron, 1979). Fresh and brackish springs along the Dead Sea area create oases (e.g., Ein Gedi and Ein Feshkha) that are covered by green patches of *Tamarix* spp., *Phragmites australis*, and *Typha australis*. Hydrophilous trees and shrubs are also found along the river banks, represented by *Salix acmophylla*, *Tamarix jordanis*, *Populus euphratica*, *Platanus orientalis*, *Fraxinus syriaca*, *Ulmus* spp., and *Nerium oleander*. They are accompanied by tall perennial reed thickets of *Phragmites australis* and *Arundo donax* (Danin, 1992; Nadel et al., 2006; Weinstein-Evron, 1983; Zohary, 1962).

4 Material and methods

4.1 Drilling campaign

Between November 2010 and March 2011, the Dead Sea Deep Drilling Project (DSDDP) was conducted under the framework of the International Continental Scientific Drilling Program (ICDP), supported by the ICDP and other funding agencies in Israel, Germany, and the United States etc. The drilling was operated by DOSECC (Drilling, Observation and Sampling of the Earth's Continental Crust) with the Deep Lake Drilling System (DLDS) in the northern DSB (Stein et al., 2011a, b).

The operation was carried out with the drilling rig 'Atlas Copco T3WDH', and two types of drilling tools were applied considering different lithological characters. The rotating extended core bit was mainly used for penetrating and retrieving thick consolidate salt sequences, while hydraulic piston core tool was designed for softer lake sediments (Neugebauer et al., 2014).

Three locations were chosen for the drilling campaign (Figure 2B). The site 5017-1 was close to the deepest part of the basin and the other two localities 5017-2 and 5017-3 were situated in the shallower water near the Ein Gedi Spa. All the sites together yielded a total of 722.65 m sediments with a drilling length of 922.44 m and an average recovery rate of 78.34% (Neugebauer et al., 2014).

The site 5017-1 was most free of turbidites and was subjected to slightest disturbances during the sedimentation process in the past. The top depth of the borehole 5017-1A (31°30′28.98″ N, 35°28′15.60″ E) was at 297.46 m below lake level in 2010. Total drilled length of this borehole was 455.34 m, retrieving 405.83 m sediments with a recovery rate of 89.13%. Five shorter parallel cores close to the borehole 5017-1A were drilled and serve for deriving the top 80 m composite profile of site 5017-1 by correlating marker layers and the boundaries of sedimentary facies (for details see Neugebauer et al., 2014).

All the sediment cores were transported to Germany and firstly kept in the GFZ Potsdam cold storage at 4°C. The sediment cores were split into the working and archive halves. Preliminary investigations of the sediments are visual description and non-destructive analyses including optical line scanning, magnetic susceptibility analyses and µXRF element scanning (Neugebauer et al., 2014). After the initial sampling campaign, the sediment cores were transferred to the IODP (International Ocean Discovery Program) Bremen Core Repository for conservation and further sampling.

4.2 Stratigraphy and lithology

The composite sediment profile of the site 5017-1 comprises four major sediment units that can be ascribed to the Amora Fm. (455–320 m blf (meters below lake floor)), Samra Fm. (320–200 m blf), Lisan Fm. (200–88 m blf), and Ze'elim Fm. (88–0 m blf), respectively. Detailed descriptions of the stratigraphy and lithology are provided by Neugebauer et al. (2014). In this study, the investigated sediments are deposited at the depth between 340.6 and 199.22 m blf, covering the whole Samra Fm. and upper part of the Amora Fm. (Figure 7). Therefore, only the 5017-1A sediment cores are involved in this study. Major sedimentary facies of these cores are summarized below.

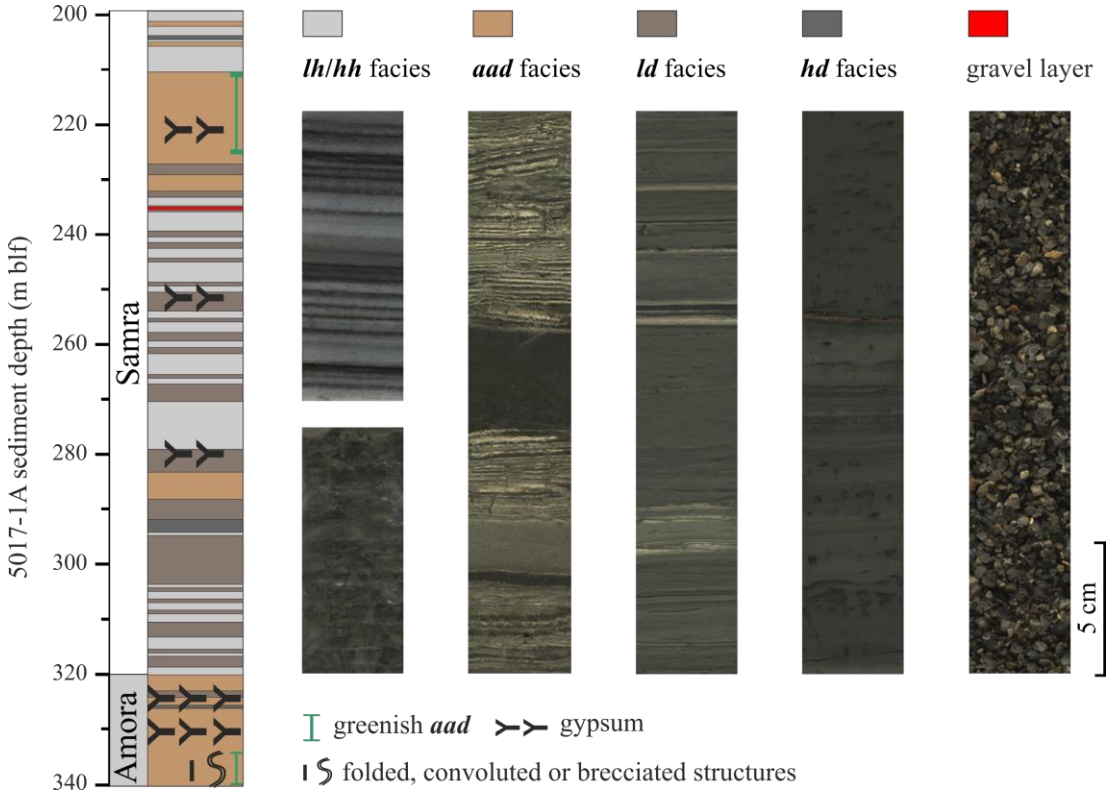

Figure 7: Sediment profile of the Dead Sea Deep Drilling Project (DSDDP) core 5017-1A at the depth between 340.6 and 199.2 meters below lake floor (m blf), encompassing the Samra Fm. and upper part of the Amora Fm., after Neugebauer et al. (2014). Also shown are figures of representative sedimentary facies: *lh*=layered halite, *hh*=homogeneous halite, *aad*=alternating aragonite and detritus, *ld*=laminated detritus, *hd*=halite and detrital marl.

The marl facies include alternating aragonite and detritus (*aad*), laminated detritus (*ld*), and gypsum and detritus. The *aad* deposit is composed of thin white aragonite laminae and clay to silt-sized marl laminae. The *ld* deposit is made up of homogeneous marl layers with intercalation

of aragonite and gypsum laminae. The gypsum and detritus facies is characterized by massive gypsum layers within marl.

The halite facies, on the other hand, are featured by layered halite (*lh*), homogeneous halite (*hh*), and halite and detrital marl (*hd*). The *lh* deposit is formed by alternations of fine-grained halite layers, crystal halite layers, and/or marl laminae. In comparison, halite crystals enveloped in marl matrix is characteristic of *hh* deposits, while halite crystals in *hd* deposits are larger and scattered in marl detritus.

Other sedimentary facies are less distinctive. For example, the mass transported deposits, which compose a significant part of the Lisan Fm., mainly include homogenous clay-silt sized marl and sometimes incorporate coarse base with fining-upwards structures. Coarse clastic detritus has gravel beds made up of limestone, dolomite, and halite crystals and the gravels are enveloped in marl. One remarkable exception occurs at ca. 235 m blf, where a 35 cm gravel layer absent of marl is found (Figure 7).

The Amora and Lisan Fm., coming into existence during the glacials, mainly preserved sedimentary sequences of marl facies and mass transported deposits. The Samra and Ze'elim Fm., formed during the interglacials, were primarily consisted of *lh*/*hh*, *ld*, and some sequences of *aad* deposits. A detailed description of the 5017-1A core sediments concerned in this study is provided in Table 2.

Table 2: Sediment profile of the Dead Sea core 5017-1A at the depth between 340.6 and 199.22 meters below lake floor (m blf). The lithological descriptions are provided by Ina Neugebauer.

Depth (m blf)	Formation	Sedimentary facies	Further components
199.22–210.46	Lisan/Samra	Layered or homogeneous halite and alternating aragonite and detritus (***lh***/***hh*** and ***aad***)	*aad*-mud-gypsum Packages intercalated; no recovery between 205.76 and 210.46 m
210.46–233.21	Samra	Alternating aragonite and detritus (***aad***)	Gypsum at 220.88 m; some salt in basal part
233.21–236.35	Samra	Layered or homogeneous halite and laminated detritus (***lh***/***hh*** and ***ld***)	Gravel layer at 234.86–235.21
236.35–239.24	Samra	Layered or homogeneous halite (***lh***/***hh***)	-
239.24–279.11	Samra	Layered or homogeneous halite and laminated detritus (***lh***/***hh*** and ***ld***)	Frequent gypsum layers

Table 2: continued from previous page

Depth (m blf)	Formation	Sedimentary facies	Further components
279.11–288.85	Samra	Laminated detritus and alternating aragonite and detritus (***ld*** and ***aad***)	Gypsum in upper 1.5 m
288.85–291.89	Samra	Laminated detritus (***ld***)	-
291.89–294.95	Samra	Halite and detrital marl (***hd***)	-
294.95–303.66	Samra	Laminated detritus (***ld***)	-
303.66–315.46	Samra	Layered or homogeneous halite and laminated detritus (***lh***/***hh*** and ***ld***)	-
315.46–318.70	Samra/Amora	Laminated detritus (***ld***)	-
318.70–320.11	Samra/Amora	Layered or homogeneous halite and laminated detritus (***lh***/***hh*** and ***ld***)	-
320.11–330.89	Amora	Alternating aragonite and detritus (***aad***)	Gypsum triplet
330.89–334.58	Amora	Alternating aragonite and detritus (***aad***)	Some gypsum layers
334.58–340.60	Amora	Alternating aragonite and detritus (***aad***)	Some folding in upper part

4.3 Chronology

For the upper 150 m sediments of the 5017-1 composite cores, the chronological framework was based on ^{14}C dates and U-Th dates covering the past 50 ka (Kitagawa et al., 2017; Torfstein et al., 2015). For older sediments, only U-Th dating was applied, and several samples of primary aragonites at the same horizon were dated (Torfstein et al., 2015). The acquired ages were corrected due to the existence of detrital Th and U and hydrogenous Th in the aragonites. Subsequently, the average single sample U-Th age was calculated for each horizon. The initial age-depth model of 5017-1 composite cores was established by combining these radiometric dates with anchor ages (Torfstein et al., 2015). The anchor ages were obtained by comparing the $\delta^{18}O$ values of 5017-1 aragonites with the $\delta^{18}O$ profile of the marine isotope stack LR04 (Lisiecki and Raymo, 2005) and the Soreq Cave speleothem records (Bar-Matthews et al., 2003; Grant et al., 2012), as well as by correlating stratigraphic units to well-dated counterparts on the exposed DSB margins.

In this study, the chronology was adapted by integrating the concerned U-Th dates and anchor ages (Table 3). The average single sample U-Th age of 102.091 ka at 220.03 m blf was based on a recalculation of the original U-Th data for the following reasons. Firstly, the isochron age of 95.446 ka at this horizon proposed by Torfstein et al. (2015) involved an additional U-Th date at 222.91 m blf and was liable to confusion. Secondly, as proposed by Torfstein et al. (2009), the selection of isochron age instead of average single sample age should follow the criterion that the difference between these two ages is less than 5%, which cannot be fulfilled in this case. Lastly, the sediments between 193.58 and 220.03 m blf were mainly composed of *aad* deposits, which were characterized by relatively low sedimentation accumulation rate and did not agree with the proposed isochron age. The anchor ages at 286.1 and 328 m blf were involved in the chronology due to the absence of reliable U-Th ages in between 241.07–347.23 m blf. This interval was characterized by prominent lithological changes (Figure 8) and a fluctuating sediment accumulation rate was thus probable.

Besides, three dates were excluded from the chronology (Table 3). The anchor ages at 234.6 m blf and 235 m blf, which indicated a depositional hiatus coincident with the occurrence of the gravel layer (Figure 8), were both extrapolated and their reliability is questioned (see discussion in sub-section 6.1.1.3). The U-Th date at 283.17 m blf was rejected because it was obviously too young. Finally, the age-depth model for this study was established based on interpolations of the selected dates (Figure 8). It suggests that the investigated section of core 5017-1A in this study encompasses the interval of 147.3–89.1 ka.

Table 3: Chronological data of the Dead Sea core 5017-1A at the depth between 360 and 180 meters below lake floor (m blf).

Sediment depth (m blf)	Age (ka, ± 2δ standard error)	Remarks
193.58	85.557 ± 8.176	U-Th average single sample age
220.03	102.091 ± 8.625	U-Th average single sample age; recalculated based on original data
234.60	109.99 ± 5.2	Extrapolated age; excluded from the age-depth model
235.00	116.65 ± 3	Extrapolated age; excluded from the age-depth model
241.07	117.401 ± 2.637	U-Th average single sample age
283.17	94.347 ± 6.481	U-Th age; excluded from the age-depth model
286.10	123 ± 1	Anchor age; correlated with LR04 record
328.00	135 ± 1	Anchor age; correlated with LR04 record
347.23	153.837 ± 0.981	U-Th average single sample age

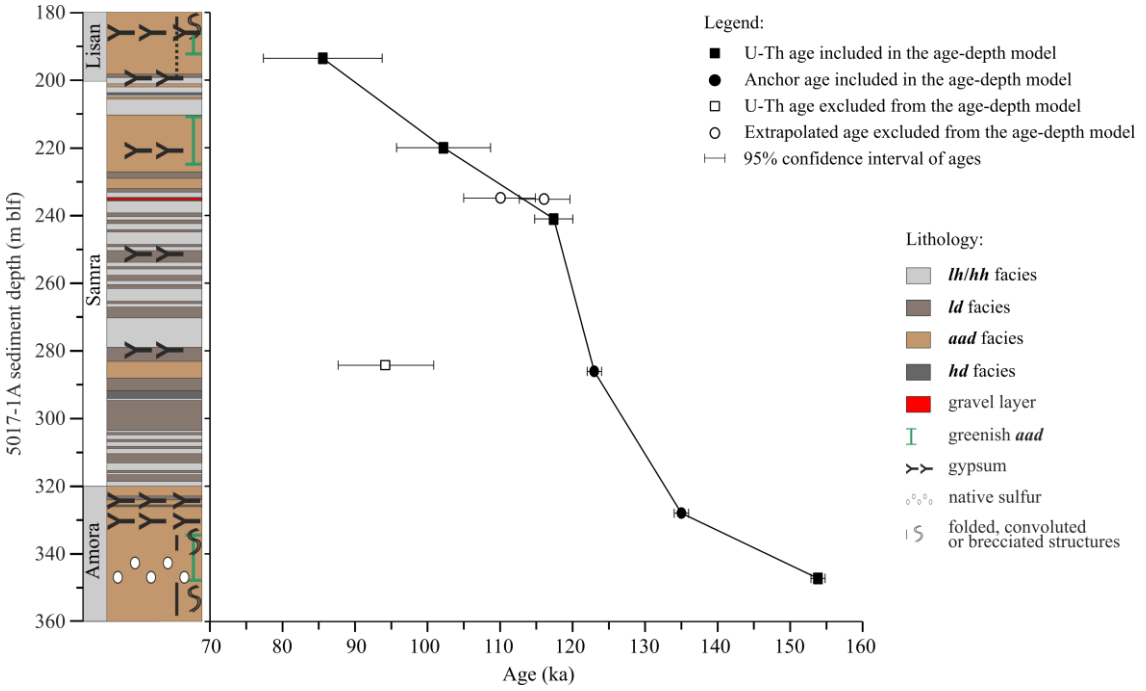

Figure 8: Age-depth model for the Dead Sea core 5017-1A at the depth between 360 and 180 meters below lake floor (m blf). In the lithological profile: *lh*=layered halite, *hh*=homogeneous halite, *ld*=laminated detritus, *aad*=alternating aragonite and detritus, *hd*=halite and detrital marl (Neugebauer et al., 2014).

4.4 Palynology

4.4.1 Palynomorph extraction and counting

For the sediment depth 340.6–199.22 m blf of the core 5017-1A, a total of 219 subsamples were taken from 110 core sections at an average interval of 65 cm (Tabel A.1 in Appendix). According to the current age-depth model, the time resolution of palynomorph analysis averages 266 years for the whole investigated period (147.3–89.1 ka) and 97 years for the LIG period (290.2–238.4 m blf; 124.2–115.5 ka; see sub-section 6.1.1.2).

Soft laminated samples were taken with a scoop, while hard halite samples were obtained using a saw. For chemical preparation, ca. 4 cm^3 volume of the laminated samples and ca. 20 cm^3 volume of the halite samples were used. Before the chemical treatment, *Lycopodium clavatum* tablets, Batch No. 3862 with 9666 spores/tablet or Batch No. 177745 with 18584 spores/tablet, were added to each sample for calculating pollen concentrations (Stockmarr, 1971). Halite samples were dissolved in distilled water first. Afterwards, all the samples followed the standard protocol of chemical treatment described by Faegri and Iversen (1989), based on the high resistance of palynomorphs to chemical destructions.

The treatment involved hot hydrochloric acid (10% HCl) to remove carbonates, hot potassium hydroxide (10% KOH) to remove humic acids, sieving of organic and inorganic materials >200 µm, cold hydrofluoric acid (40% HF) to remove silicates, hot HCl (10%) to break up siliceous colloidal clumps that formed during the silica reaction, cold glacial acetic acid ($C_2H_4O_2$) to remove water, hot acetolysis mixture (9 parts of acetic anhydride ($C_4H_6O_3$) and 1 part of sulfuric acid (H_2SO_4)) to remove cellulose, cold $C_2H_4O_2$ to remove acetolysis liquid, and finally ultrasonic sieving to remove fine particles <10 µm. The obtained residues were preserved in glycerol, stained with safranin, and mounted for counting.

Palynomorphs were identified and counted using the transmitted-light microscope Zeiss Axio Lab.A1 at ×400 magnification. The identification was assisted using palynomorph keys (Beug, 2004; Horowitz and Baum, 1967; Jankovská and Komárek, 2000; Punt, 1976-1991) and atlases (Reille, 1995, 1998, 1999), as well as recent pollen collection from Israel (stored in the Steinmann Institute at University of Bonn). Pollen and spore nomenclature referred to Beug (2004). Criteria used for distinguishing Cerealia type pollen from Poaceae pollen were in accordance with those described by Beug (2004). The Cerealia type pollen was distinctive by its big pore (>2.7 µm in diameter), protuberant and thick annulus (>2.0 µm in thickness and >2.7 µm in width), and large grain size (>40 µm).

At least 500 terrestrial pollen grains were counted for each sample. Pollen percentages were calculated to show the relative frequencies of pollen taxa based on terrestrial pollen sum (100%). Degraded/corroded, broken, crumpled, concealed, and unknown pollen were grouped (Berglund and Ralska-Jasiewiczowa, 1986) and were excluded from the pollen sum. Microscopic charcoal particles were counted simultaneously with palynomorphs and were classified into two groups according to their length: 0–100 µm and >100 µm. The abundance of pollen from the marsh and aquatic plants (mainly Cyperaceae), non-pollen-palynomorphs (NPPs) such as spores and algae, as well as microscopic charcoal were all presented in concentrations (e.g., specimens/cm^3).

Pollen diagram was plotted by using the software Tilia (version 2.0.41, © 1991–2015, Eric C. Grimm) and a 5-fold exaggeration was applied to those taxa in low abundances. CONISS was utilized for stratigraphically constrained cluster analysis (Grimm, 1987) involving taxa whose percentages were >2%.

4.4.2 Principles of palynological investigation

Pollen grains are characterized by good dispersal ability, a close link with the parental plants, and good resistance to degradation. On this basis, fossil pollen grains in sedimentary archives (e.g., lakes) are outstanding proxies for reconstructing vegetation in the past (Birks and Birks, 1980; Faegri and Iversen, 1989). Pollen concentration and influx in sediments are indicative of the general vegetation cover. The abundance of a specific plant in the communities can be reflected by its proportions in respective pollen assemblages (Davis, 1963). With the aid of an age-depth model, it is possible to infer vegetation changes through time. Assuming the ecological significance of the plants has not changed, which holds true for the late Quaternary, variations in pollen assemblages can indicate past environmental conditions. In Europe, particularly, extensive pollen data have contributed to the establishment and development of the European Pollen Database (Brewer et al., 2016; Davis et al., 2013) and to the mapping of large-scale biome distribution at a certain time in the past (Allen et al., 2010; Prentice et al., 1996).

The presence/absence of indicator taxa relying on narrow ecological amplitude can be precisely diagnostic of environmental conditions (Iversen, 1944). Pollen ratios such as the *Artemisia*/Chenopodiaceae ratio has been utilized to semi-quantitatively reconstruct moisture availability given differentiated drought-tolerance of relevant plants in the drylands (El-Moslimany, 1990). Botanical-climatological transfer functions have been developed to quantitatively reconstruct climatic parameters such as temperature and precipitation rates.

These functions are based on prerequisites assuming the relation between modern pollen data and climatic parameters remained constant through time (e.g., Davis et al., 2003; Guiot et al., 1989; Kühl et al., 2002; Overpeck et al., 1985; Seppä et al., 2004).

Despite these progresses in palynology, presentations of pollen data are more conventionally expressed as pollen percentages of the terrestrial pollen sum, which are dependent on the relative frequencies of all the taxa involved in calculation. This would lead to the "Fagerlind effect" showing a simple linear relationship between pollen percentages and their respective shares in the vegetation do not exist (Fagerlind, 1952). Investigations in this aspect suggest pollen grains preserved in sediments are the remainder that either has intrinsic differences among themselves or has gone through different processes (Prentice, 1985).

Firstly, pollen production varies among plants. Even for the same plant, pollen production of each stamen, flower, and inflorescence is different from one another, let alone the inter-annual variability (Donders et al., 2014). This hampers estimates of absolute pollen production. Instead, relative productivity among the common taxa are assessed (Andersen, 1970; Bunting et al., 2005). Secondly, pollen dispersal is not only associated with the shape and structure of pollen grains, but also with conditions of transport media. Prevailing wind directions can determine the major pollen source area, although wind velocity can be highly variable in forests and open areas within short distances (Andersen, 1974). Insect-pollinated species generally have weak dispersion, and the contribution of waterflows to the delivery of pollen grains should not be neglected (Horowitz, 1992). Thirdly, preferential pollen deposition in lakes is observed and linked with water circulation and pollen morphology (Davis and Brubaker, 1973). Lastly, pollen preservation in sediments is affected by oxidation, mechanical and chemical destruction (Campbell, 1991, 1999; Campbell and Campbell, 1994), pollen and sediment types (Cushing, 1967; Havinga, 1964, 1984), as well as organismal activities (insects, bacteria, and fungi).

For instance, the bisaccate *Pinus* pollen are well-known for their ability to travel even kilometers by winds. *Pinus* pollen are characterized by high production and good resistance to degradation, leading to extreme over-representation in pollen assemblages, especially in open landscapes. A misinterpretation of high *Pinus* pollen percentages would exaggerate the share of pine trees in the vegetation (Davis, 1963). On the contrary, pistachio pollen (e.g., *Pistacia atlantica*) are commonly under-represented and their low abundance in pollen records can point to greater distribution of pistachio trees in the vegetation (van Zeist and Bottema, 1977). In sediments with poorly preserved pollen spectra, Liguliflorae pollen would have magnified contents due to their thick exine and identifiable fenestrate structure, while other pollen taxa become indeterminable (Lebreton et al., 2010).

These discrepancies can be solved by modern pollen studies, which aim at revealing the relationships between pollen assemblages and vegetation based on analysis of pollen traps (e.g., Giesecke et al., 2010), surface soils (e.g., Baruch, 1993; Davies and Fall, 2001), and recent sediments (e.g., Weinstein-Evron, 1979). These analyses demonstrate that pollen percentages of a taxon in sediments tend to show a decreasing trend with increasing distance from the respective parental plants. In addition, it is widely agreed that larger lakes with larger surface area generally have greater pollen source area (Prentice, 1985; Sugita, 1993). In the case of the Dead Sea, fossil pollen in this large lake probably have originated from a wide region. Hence, the lake acts as a huge natural pollen trap in the rift valley.

In addition to climatic impacts, human activities are important factors influencing Holocene vegetation changes. For instance, in the Levant, an increasingly important human impact can be inferred from anthropogenic indicators. Cultivation can be directly reflected by fast increasing pollen frequencies of fruit trees such as olives (*Olea europaea*), walnuts (*Juglans regia*), and grapevines (*Vitis vinifera*; Baruch, 1990; Behre, 1990; Bottema and Woldring, 1990). Forest clearings are notable by the abrupt decline of arboreal pollen from trees such as deciduous and evergreen oaks (Litt et al., 2012; van Zeist et al., 2009). Findings of abundant Cerealia type pollen are usually connected with ancient agriculture. In the case of the Levant, however, this indication is limited because Cerealia type pollen can also be attributed to wild cereals or grasses (Beug, 2004). Secondary anthropogenic indicators refer to those elements indirectly related to human activities. For example, ruderal plants such as *Sarcopoterium spinosum*, *Plantago lanceolata*, and some Asteraceae species might have invaded the newly opened areas in favor of deforestation, burning, grazing, or abandonment of groves (Baruch, 1986; Behre, 1990).

Current limitations of palynology are associated with the identification of pollen taxa. In most cases, pollen grains can only be identified to genus/family level, whereas plants from the same genus/family may grow in habitats of a large ecological range. For instance, fossil Poaceae pollen could originate from swamps, semi-arid grass steppes or the understories of humid/sub-humid woodlands (van Zeist et al., 2009).

5 Results

As shown in Figure 9 (section 5.1), major pollen taxa found in the investigated sediments are illustrated in percentages of the total terrestrial pollen sum (100%). This simplified pollen diagram also shows the total arboreal (AP) and non-arboreal pollen (NAP) percentages, as well as concentrations of Cyperaceae and total terrestrial pollen (grains/cm^3). Given the long time span of the DSDDP 5017-1 cores, the pollen diagram was first divided into pollen assemblage superzones (PASs), according to the hierarchical biostratigraphical classification proposed by Tzedakis (1994a). The PASs zonation numbers were assigned consecutively following the existing pollen result of the DSDDP 5017-1 cores (Miebach, 2017). The PASs were further subdivided into 9 pollen assemblage zones (PAZs). Divisions of these biozones were made in accordance with CONISS calculation, as well as by visual inspection of the changes in AP/NAP ratios and in the relative abundances of major pollen taxa. The zonation boundaries were defined on the basis of the characteristics of each biozone and are described in Table 4.

In this study, due to <40–50% *Artemisia*+Chenopodiaceae pollen at some horizons (Figure 9), the *Artemisia*/Chenopodiaceae pollen ratio is not necessarily an indicator of moisture availability and is thus not calculated (Zhao et al., 2012). Pollen-based botanical-climatological transfer functions are used to quantitatively reconstruct precipitation and temperature rates. The methods and results are presented by Stolzenberger (2017).

Concentrations of selected NPPs and charcoal particles are presented separately in Figure 10 (section 5.2). The complete palynomorph and charcoal diagrams are attached in the Appendix (Figure A.1). Additionally, comparisons of pollen grains from representative deposit types were made to evaluate the potential impact of depositional shifts on the pollen results (section 5.3).

5.1 Pollen zonation

In the entire pollen record, AP percentages range between 3% and 40%. Most important AP taxa are *Quercus ithaburensis* type, *Q. calliprinos* type, *Pistacia*, *Olea*, *Phillyrea*, *Juniperus* type, *Pinus*, and *Cedrus*. Minor AP such as riparian tree pollen (e.g., *Salix*, *Tamarix*, and *Platanus*) occurred sporadically and were thus excluded from the simplified pollen diagram. NAP taxa account for 60–97% of the pollen sum and are represented by *Artemisia*, *Poaceae*, Cerealia type, Chenopodiaceae, as well as some *Plantago*, *Rumex*, non-*Artemisia* Asteraceae (Tubuliflorae, Liguliflorae, and *Centaurea*), Brassicaceae, Scrophulariaceae, Apiaceae and *Euphorbia* type. Terrestrial pollen concentrations fluctuate in the range between 217 and 106,858 grains/cm^3.

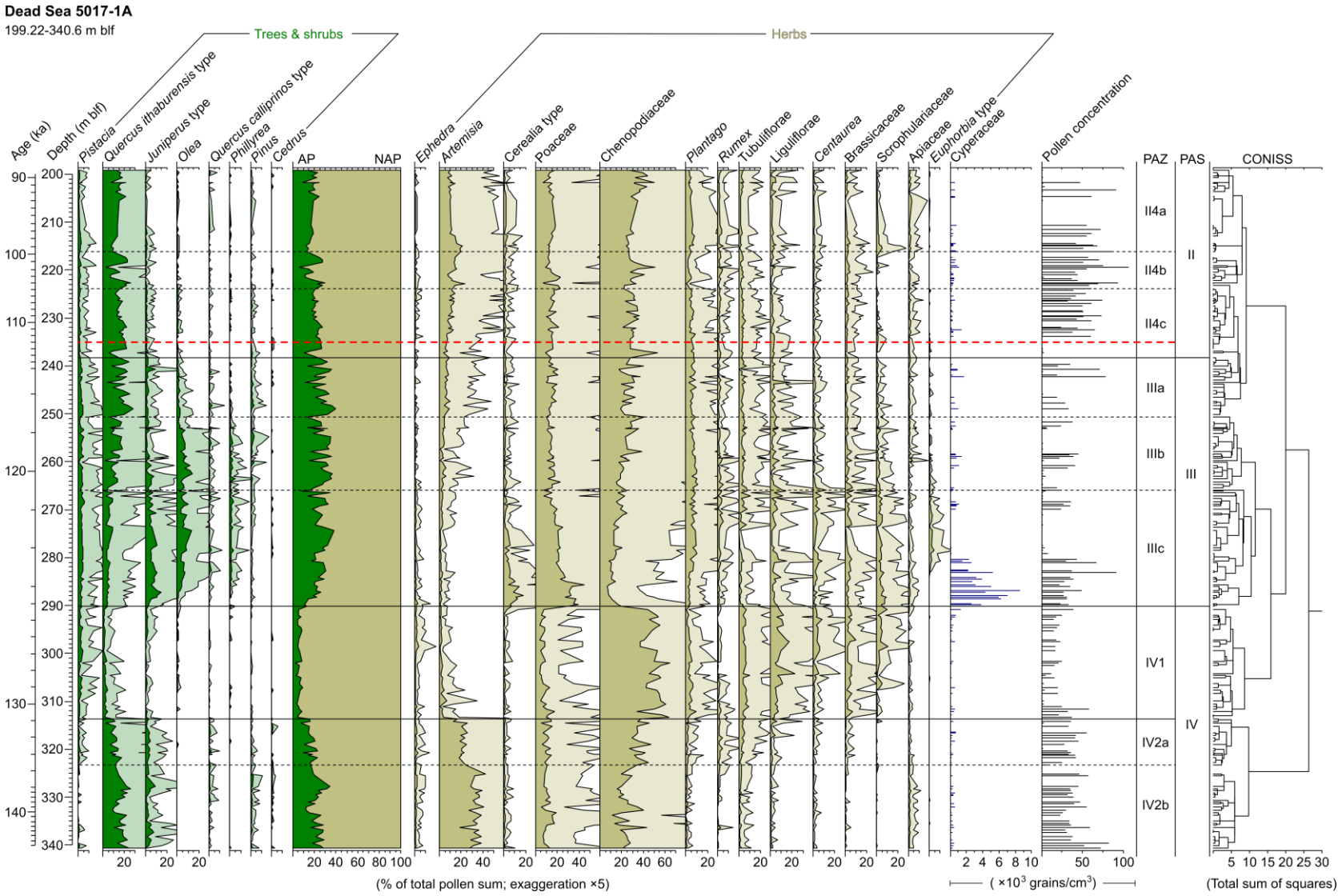

Figure 9: Simplified pollen diagram of the Dead Sea core 5017-1A at the depth between 199.22 and 340.6 meters below lake (m blf). The chronology is based on interpolations of the dates listed in Table 3. AP=arboreal pollen, NAP=non-arboreal pollen, PAZ=pollen assemblage zone, PAS=pollen assemblage superzone. The red dashed line denotes the gravel layer at ca. 235 m blf (Torfstein et al., 2015).

PAZ IV2 (340.6–313.7 m blf; 147.3–130.9 ka) is characterized by the predominance of *Quercus ithaburensis* type, *Artemisia*, and Chenopodiaceae pollen. In subzone PAZ IV2b (340.6–232.3 m blf; 147.3–133.7 ka), the AP is composed of moderate percentages of *Q. ithaburensis* type (mean of 17%) and *Juniperus* type (<10%) pollen, as well as small amounts of *Pinus* (<2%) and *Cedrus* (<1%) pollen. The NAP is dominated by *Artemisia*, Chenopodiaceae, and Poaceae pollen. In PAZ IV2a (323.3–313.7 m blf; 133.7–130.9 ka), pollen grains of *Q. ithaburensis* type decrease gradually (mean of 11%) together with those of conifers. On the contrary, *Pistacia* pollen slightly increase to mean values of 1%. The total NAP correspondingly show a progressive increase and are marked by a proportion of *Artemisia* pollen substituted by Chenopodiaceae pollen. Other herbaceous elements such as *Plantago*, *Rumex*, and non-*Artemisia* Asteraceae exhibit a concomitant increase. Most pollen samples in PAZ IV2 are laminated and the pollen concentrations average at 36,430 grains/cm^3.

PAZ IV1 (313.7–290.2 m blf; 130.9–124.2 ka) is marked by minimum AP contents of the whole record (mean of 6%). Compared to PAZ IV2, *Q. ithaburensis* type pollen decrease to mean values of 2%, whereas *Pistacia* pollen increase to ca. 2%. Among the herbaceous components, *Artemisia* pollen percentages drop to notably low values (mean of 2%) along with a slight decrease in Poaceae pollen. Notably high Chenopodiaceae pollen contents (mean of 50%) form the plateau of 'Chenopodiaceae phase' accompanied by abundant non-*Artemisia* Asteraceae (mean of 17%), *Plantago* (mean of 4%), Brassicaceae (mean of 4%), and Scrophulariaceae pollen (mean of 3%). The majority of pollen samples are laminated, with intercalation of some halite samples. Mean pollen concentrations are lower than PAZ IV2 (19,214 grains/cm^3) and vary between 2,067 and 57,854 grains/cm^3.

PAZ III (290.2–238.4 m blf; 124.2–115.5 ka) has the most abundant AP of up to 40%. This pollen zone can be subdivided into 3 subzones due to changes in the AP ingredients.

In PAZ IIIc (290.2–265.9 m blf; 124.2–120.5 ka), *Pistacia* pollen continue to increase slightly since the last phase and the percentages maximize in this subzone (up to 6%). *Q. ithaburensis* type pollen increase slightly and gradually (up to 10%). *Juniperus* type pollen contents rise abruptly, culminate at 287.2 m blf (15%) and decline subsequently. Shortly after the peak percentage of *Juniperus* type pollen, sclerophyllous pollen (*Olea*, *Phillyrea*, and *Q. calliprinos* type) quickly reach high values (up to 16%). Among the NAP, of the most characteristic at the onset of this subzone is the abrupt significant rise of Poaceae (up to 45%) and Cerealia type (up to 15%) pollen contents at the expense of Chenopodiaceae pollen (down to 7%). Cyperaceae pollen concentrations also show synchronous high values (mean of 2,053 grains/cm^3). This event is accompanied by the decline of non-*Artemisia* Asteraceae and Brassicaceae pollen, whereas *Plantago*, *Rumex*, and Apiaceae pollen start to increase slightly and Scrophulariaceae pollen percentages reach highest values (up to 9%). Following this

event, Poaceae and Cerealia type pollen decrease progressively and Chenopodiaceae pollen simultaneously increase. Meanwhile, *Euphorbia* type pollen abruptly increase and show highest percentages of the record (up to 5%). All pollen samples in the lower part of this subzone (290.2–279.2 m blf) are laminated and the mean pollen concentration is 36,125 grains/cm^3. In the upper part, most samples are halite and the pollen concentrations are generally low (down to 259 grains/cm^3).

PAZ IIIb (265.9–250.6 m blf; 120.5–118.6 ka) displays relatively higher values of *Q. ithaburensis* type pollen (mean of 12%) and the increase in *Pinus* pollen (<4%). Sclerophyllous elements remain abundant (up to 17%) but show a decreasing trend towards the end of this subzone, which is also observed in *Pistacia* percentages. The gradual increase in Chenopodiaceae pollen (mean of 25%) is accompanied by the same changes in *Artemisia* pollen (mean of 4%), while Poaceae pollen contents maintain nearly constant (mean of 15%). Pollen samples are either halite or laminated, and pollen concentrations fluctuate between 287 and 45,181 grains/cm^3.

PAZ IIIa (250.6–238.4 m blf; 118.6–115.5 ka) is characterized by the predominance and fluctuations of *Q. ithaburensis* type pollen (5–28%). *Olea* and *Phillyrea* pollen have low percentages (<3% and <1%, respectively) and are evidently decreasing. *Pistacia* pollen decline from 5% to 2%, whereas percentages of *Pinus* pollen stay relatively stable (<3%). NAP constituents do not exhibit obvious changes except the fluctuations of Chenopodiaceae pollen content (17–40%). Pollen samples are either halite or laminated, and pollen concentrations range between 217 and 78,532 grains/cm^3.

In **PAZ II** (238.4–199.2 m blf; 115.5–89.1 ka), AP percentages are generally low (mean of 20%) and NAP accounts more (mean of 81%) compared to PAZ III. PAZ II can be subdivided into PAZ II4c (238.4–223.9 m blf; 115.5–104.9 ka), PAZ II4b (223.9–216.1 m blf; 104.9–99.6 ka), and PAZ II4a (216.1–199.2 m blf; 99.6–89.1 ka), due to the changes in AP contents, which is controlled by the frequencies of *Q. ithaburensis* type pollen. *Q. ithaburensis* type pollen gradually decrease from 22% to 12% towards the end of PAZ II4c, resume in relative abundance with remarkable fluctuations in PAZ II4b (3–26%), and maintain stable values of ca. 14% in PAZ II4a. All other AP taxa have very low amounts in PAZ II. Among them, *Pistacia* is the most important AP (mean of 2%). *Artemisia* pollen in PAZ II (mean of 12%) show an opposite trend of variations to those of *Q. ithaburensis* type. Chenopodiaceae pollen contents firstly fluctuate around 32% in PAZ IIc and IIb and later increase towards the upper limit of this record (up to 50%). Most samples in PAZ II are from the *aad* depositional phase and have high pollen concentrations (mean of 55,703 grains/cm^3). In contrast, halite samples in the upper and lower part of PAZ II have low pollen concentrations (mean of 1,573 grains/cm^3).

Table 4: Pollen zonation of the Dead Sea core 5017-1A at the depth between 199.22 and 340.6 m blf. PAS=pollen assemblage superzone, PAZ=pollen assemblage zone, AP=arboreal pollen, NAP=non-arboreal pollen, LB=lower boundary.

PAS	PAZ	Top depth (m blf)	Top age (ka)	Characteristics
II	II4a	199.2	89.1	**AP**: relatively low values of *Q. ithaburensis* type (mean of 14%), decreased percentages of *Pistacia* to mean of 1% **NAP**: increasing Chenopodiaceae (up to 50%), decreasing trend of Poaceae and *Artemisia*, increase of Apiaceae **LB**: increase of Chenopodiaceae
	II4b	216.1	99.6	**AP**: flucutations dominated by *Q. ithaburensis* type (3–26%) **NAP**: slight increase of Chenopodiaceae and *Artemisa*, slight decrease of *Artemisia*, Poaceae, and non-*Artemisia* Asteraceae **LB**: resumption of AP values up to 30%
	II4c	223.9	104.9	**AP**: decreasing *Q. ithaburensis* type (from 22% to 12%), some *Pistacia* (mean of 2%), *Juniperus* type (<2%), and *Pinus* (<2%) **NAP**: stable values of Chenopodiaceae (mean of 31%) and Poaceae (mean of 15%), increase of *Artemisia* (mean of 10%) **LB**: decrease of *Q. ithaburensis* type
III	IIIa	238.4	115.5	**AP**: predominance and fluctuations of *Q. ithaburensis* type (5–28%), decrease of *Olea* (down to 0.2%) and *Pistacia* (down to 2%), some *Juniperus* type (mean of 2%) and *Pinus* (<3%) **NAP**: increasing trend of Chenopodiaceae and *Artemisia* **LB**: high values of *Q. ithaburensis* type
	IIIb	250.6	118.6	**AP**: increase of *Q. ithaburensis* type (up to 19%) and *Pinus* (<4%), abundant values of *Olea* (up to 14%) and *Phillyrea* (up to 5%), decrease of *Juniperus* type (mean of 3%) **NAP**: decrease of Poaceae, increasing trend of Chenopodiaceae and *Artemisia*, abundance of *Plantago*, decrease of Scrophulariaceae and *Euphorbia* type **LB**: increase of *Q. ithaburensis* type
	IIIc	265.9	120.5	**AP**: remarkable increase of *Juniperus* type (up to 15%), *Olea* (up to 13%), *Pistacia* (up to 6%), and *Phillyrea* (up to 4%), increasing trend of *Q. ithaburensis* type (<10%) **NAP**: abrupt peak values of Poaceae (45%) and Cerealia type (15%), minimum values of Chenopodiaceae (7%) and *Artemisia*, decrease of non-*Artemisia* Asteraceae, increase of Scrophulariaceae and *Euphorbia* type **LB:** remarkable increase of AP amounts

Table 4: continued from previous page

IV	IV1	290.2	124.2	**AP**: minimum amounts of *Q. ithaburensis* type (mean of 2%), increase of *Pistacia* (mean of 2%) **NAP**: plateau of Chenopodiaceae (mean of 50%), high abundance of Tubuliflorae and Liguliflorae (up to 27% in total), low values of Poaceae and *Artemisia*, increase of *Ephedra*, *Centaurea*, *Plantago*, Brassicaeae, and Scrophulariaceae **LB**: minimum values of AP (mean of 6%)
	IV2a	313.7	130.9	**AP**: decrease of *Q. ithaburensis* type (mean of 11%) and *Pinus* (mean of 0.4%), slight increase of *Pistacia* (mean of 1%) **NAP**: decrease of *Artemisa*, increase of Chenopodiaceae, non-*Artemisia* Asteraceae (Tubuliflorae, Liguliflorae, and *Centaurea*), *Plantago*, and *Rumex* **LB**: decrease of *Q. ithaburensis* type
	IV2b	323.3	133.7	**AP**: predominance of *Q. ithaburensis type* (mean of 17%) and *Juniperus* type (<10%), some *Pinus* (<2%) and *Cedrus* (<1%) **NAP**: high values of *Artemisia* (mean of 33%) and Chenopodiaceae (24%), some Poaceae **LB**: not defined (end of this record)

5.2 Non-pollen-palynomorphs and microscopic charcoal

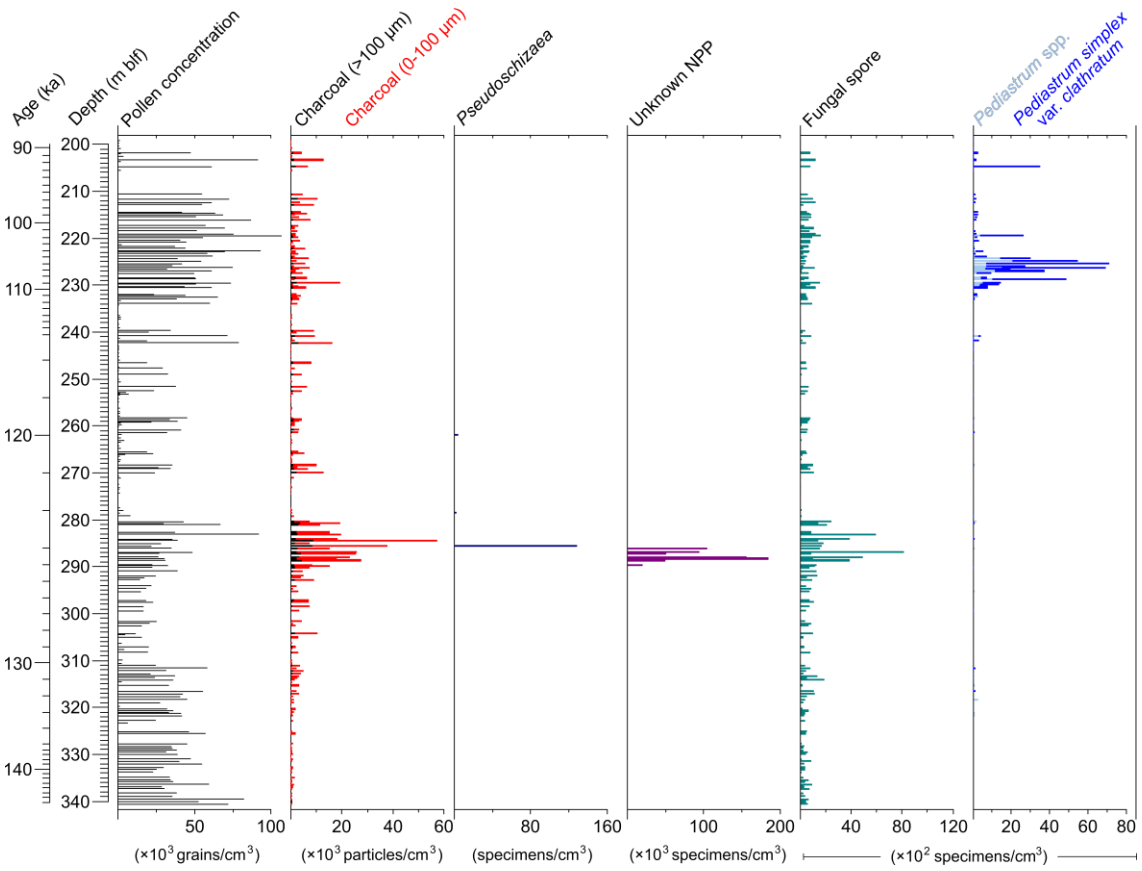

Figure 10: Concentrations of selected non-pollen-palynomorphs (NPPs) and charcoal particles in the Dead Sea core 5017-1A at the depth between 199.22 and 340.6 meters below lake floor (m blf). The terrestrial pollen concentration is given for reference.

As shown in Figure 10, common NPPs in the Dead Sea sediments are fungal spores, algae (mainly *Pediastrum simplex* var. *clathratum*), the acritarch *Pseudoschizaea* (possibly a type of algae spore), and an unknown NPP type. Microscopic charcoal particles are primarily in the range of 0–100 µm. The consecutive presence of NPPs and charcoal particles mainly occur at two intervals: ca. 290–280 m blf and ca. 230–200 m blf. The former is characterized by peak concentrations of charcoal (up to 57,153 particles/cm^3 in total), fungal spores (up to 8,108 specimens/cm^3), *Pseudoschizaea* (128 specimens/cm^3) and the unknown NPP (up to 184,411 specimens/cm^3). At ca. 230–200 m blf, these components either disappear or have relatively low concentrations, whereas total *Pediastrum* concentration reaches maximum (7,124 specimens/cm^3). Additionally, other organic objects such as trichomes of oak and olive trees (hairs of the leaves) and sponge are encountered sporadically during palynomorph counting.

5.3 Comparisons of pollen grains in representative deposit types

The investigated Dead Sea 5017-1A pollen samples are represented by laminated sediments (*aad* and *ld* deposits) and halite (*lh* and *hh* deposits). It is necessary to elucidate the relationship between pollen grains and the deposit types and to clarify whether deposit types are influencing factors that bias interpretations of the pollen results in this study. Here, the preliminary analysis is focused on comparing the pollen concentrations and percentages of the deposit types.

As shown in section 5.1, it is obvious that pollen concentrations in these two deposit types are considerably different. Halite samples have very low pollen concentrations (mean of 1,511 grains/cm^3) due to a fast accumulation of salt crystals, while laminated samples hold a much higher pollen concentration of 39,910 grains/cm^3 on average (Table 5). Both deposit types are composed of evaporites (salt layer/aragonite laminae) and detritus, which is best expressed by the *lh* and *aad* deposits. By subdividing deposit layers of the *lh* and *aad* deposits, pollen concentration of each layer can be calculated. For this purpose, one representative sample of each deposit type was selected. The result shows that pollen concentration in the salt layer constitutes 2% of total pollen concentration in the *lh* sample and that in the aragonite laminae takes up 10% of total pollen concentration in the *aad* sample (Table 5). Therefore, a simple conclusion can be reached that pollen grains incorporated in detritus are the most important components of pollen assemblages in Dead Sea sediments, no matter which type of deposits is analyzed.

Table 5: Mean pollen concentrations of representative deposit types, as well as the pollen concentration of each deposit layer. The latter is shown as the percentage of the total pollen concentration of a deposit type and is calculated on the basis of a selected sample for each deposit type.

Deposit type	Pollen concentration (grains/cm^3)	Deposit layer	Percentage of pollen concentration (%)
Halite (*lh* & *hh*)	1,511	Salt layer	2
		Detrital layer	98
Laminated (*aad* & *ld*)	39,910	Aragonite laminae	10
		Detrital laminae	90

In terms of pollen percentages in the deposit types, *Quercus ithaburensis* type and Chenopodiaceae are selected to represent major changes in pollen spectra because they

dominate the AP and NAP, respectively. Involving all the investigated pollen samples, the mean shares of *Q. ithaburensis* type/Chenopodiaceae pollen are nearly identical in the halite (12%/29%) and laminated samples (11%/30%). Additional analysis in the aspect of pollen percentages is performed on two selected sample sets. Each set is composed of several pollen samples and is characterized by rapid shifts of deposit types between samples within a short-term deposition (Table 6). In the first set, *Q. ithaburensis* type pollen have higher amounts in the laminated sample, whereas they account more in the halite deposits of the second sample set. For Chenopodiaceae pollen, no direct correspondence exists between the deposit types and pollen percentages as well. Besides, in both sets, no explicit tendency can be observed between the lower two samples.

Table 6: Pollen percentages of *Quercus ithaburensis* type and Chenopodiaceae of two selected samples sets. Set 1 (202–201.7 m blf) and Set 2 (253.4–252.9 m blf) are both characterized by rapid shifts of deposit types between samples within a short-term deposition.

	Deposit type	Depth (m blf)	*Quercus ithaburensis* type (%)	Chenopodiaceae (%)
Set 1	Halite	201.738	7.7	50.1
	Laminae	201.810	21.0	31.6
	Halite	201.978	16.9	31.8
Set 2	Laminae	252.930	6.9	29.0
	Halite	253.102	18.9	23.6
	Laminae	253.167	8.9	35.8
	Halite	253.400	10.8	33.5

These preliminary observations indicate that shifts in deposit types are not directly related to changes in pollen assemblages, although both variations might have been triggered by changes in the regional environment. Hence, depositional shifts between halite and laminated deposits are not considered as factors influencing the Dead Sea pollen spectra in the following discussions.

6 Discussions

This study focuses on addressing the issues elucidated in the Introduction. In this chapter, section 6.1 reconstructs the paleovegetation and paleoenvironment of the southern Levant based on pollen, NPPs, and charcoal data. Further discussions of the southern Levantine paleoenvironment are undertaken by comparisons with records from regional archives (e.g., lacustrine sediments and speleothems). On this basis, potential paleoenvironmental scenarios are proposed concerning the inferred inconsistencies of environmental conditions by different records. Section 6.2 relates to the link between early modern human dispersal and environmental conditions along the potential migrational route. Section 6.3 correlates EM palynological records and attempts to provide insights into possible mechanisms triggering the variations of vegetation across the EM region.

6.1 Paleovegetation and paleoenvironment of the southern Levant

6.1.1 Paleovegetation and inferred paleoenvironmental conditions

Major botanical components of the vegetation territories are well represented by respective pollen taxa in the Dead Sea 5017-1A core sediments. As proved by previous palynological studies on Holocene Dead Sea sediments, changes in relative frequencies of principle pollen taxa can reflect regional biome shifts in response to climatic variations (Litt et al., 2012). Pollen concentration is commonly used for estimating vegetation cover. In this study, the fluctuations of pollen concentrations mainly point to the shifts of deposit types (see section 5.3). The charcoal concentrations, conventionally applied as an indicator for fire activities, are probably also biased by the deposit types. In this case, the ratio of charcoal to terrestrial pollen counts (C/T ratio; Figure 11, 12 & 13) is more appropriate for representing fire activities (MacDonald et al., 1991; Swain, 1973). Additionally, the NPPs and other biotic remains are valuable markers for limnological and hydrological conditions.

This study reconstructs the vegetation of the southern Levant between 147.3 and 89.1 ka, covering the late penultimate glacial (147.3–130.9 ka), the initial warming (130.9–124.2 ka), the LIG optimum (124.2–115.5 ka), and the early last glacial (115.5–89.1 ka). These intervals are discussed separately with an emphasis and elaboration on the periods of initial warming

and LIG optimum, which are relatively well biostratigraphically and chronologically constraint.

6.1.1.1 Late penultimate glacial

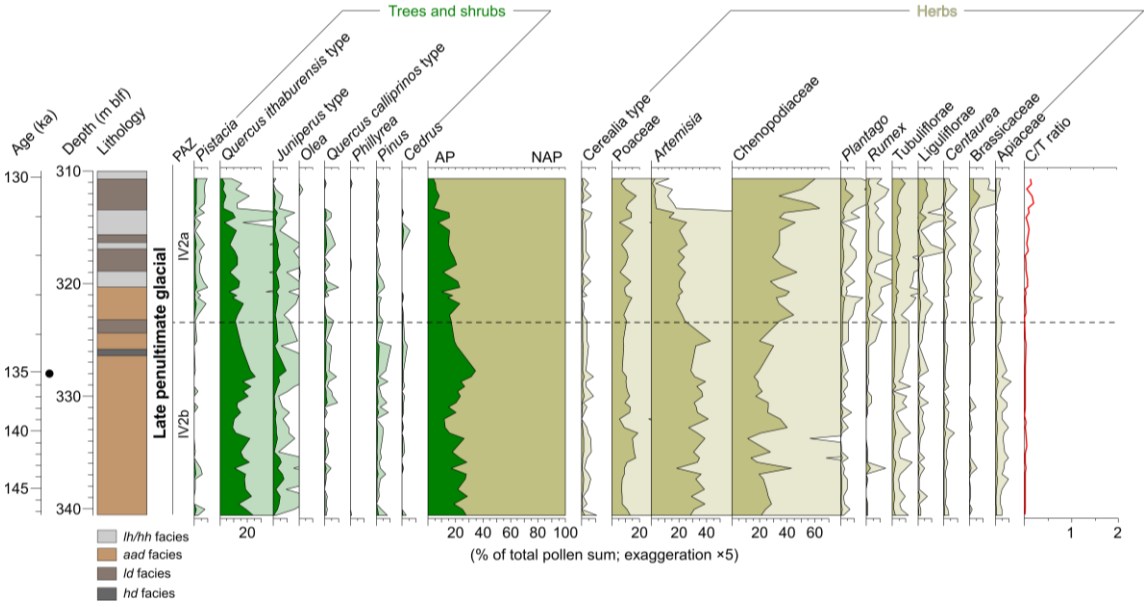

Figure 11: Simplified pollen diagram of Dead Sea core 5017-1A for the period of late penultimate glacial. PAZ=pollen assemblage zone, AP=arboreal pollen, NAP=non-arboreal pollen, C/T ratio=charcoal to pollen ratio. In the lithological profile, *lh*=layered halite, *hh*=homogeneous halite, *aad*=alternating aragonite and detritus, *ld*=laminated detritus, *hd*=halite and detrital marl (Neugebauer et al., 2014). The black dot indicates the position of the anchor age.

The late penultimate glacial is represented by PAZ IV2 (340.6–313.7 m blf; 147.3–130.9 ka; Figure 11) and can be corresponded with MIS 6 (Lisiecki and Raymo, 2005). The vegetation was dominated by wormwood (*Artemisia*), the goosefoot family (Chenopodiaceae), and grasses (Poaceae and Cerealia type). Trees and shrubs were of moderate amounts and were characterized by the predominance of deciduous oaks (*Quercus ithaburensis* type) and some conifers such as juniper and/or cupressus (*Juniperus* type), pine (*Pinus*), and cedar (*Cedrus*). Since 133.7 ka, all the arboreal elements declined except for pistachio (*Pistacia*), whose relative frequency slightly increased together with goosefoots and a variety of non-*Artemisia* Asteraceae plants.

The occurrence of sporadic pine and cedar pollen in the Dead Sea was a result of long-distance transport (van Zeist et al., 2009). Cedars, in particular, are currently found in the northern cool conifer forests in Mount Hermon and Lebanon (van Zeist and Bottema, 2009).

Therefore, the continuous presence of low contents of pine and cedar pollen in the Dead Sea points to an expansion or a migration of conifers to lower elevations in the remote mountains (Weinstein-Evron, 1983). Nevertheless, in the warmer southern Levant, the rareness of conifers suggested that the temperature was not significantly reduced during the late penultimate glacial. Moreover, the moderate distribution of deciduous oaks (*Quercus ithaburensis* type) implies that the reduced temperature still reached the thermal demand of temperate trees, especially given the low-latitude setting of the southern Levant.

The reduced temperature, on the contrary, probably led to low evaporation rates and contributed to the effective moisture, which was sufficient to maintain the growth of deciduous oaks that require at least 400 mm MAP (Neumann et al., 2007). This suggests the main source areas of deciduous oak pollen in the Dead Sea, probably the Judean and Galilee Mountains, were under sub-humid conditions during the late penultimate glacial. Subsequent gradual contraction and thinning of oak woodlands thus indicate a trend of progressive aridification.

During the late penultimate glacial, the predominance of steppe and desert components in the vegetation suggest semi-arid to arid conditions prevailed in the low altitudes. As the major herbaceous plants, both wormwood and goosefoot grow in open fields, but the latter is tolerant of less moisture availability (El-Moslimany, 1990). The increasing proportions of Chenopodiaceae pollen at the expense of decreasing *Artemisia* pollen thus point to a drying trend towards the end of the penultimate glacial. As a result of the generally cool conditions, fire activities were restricted in the southern Levant as indicated by low C/T ratios (Figure 11).

6.1.1.2 Initial warming and last interglacial optimum

The LIG is a period with as warm or warmer-than-present global conditions. From the paleobotanical perspective, the LIG was characterized by a climatic optimum that allowed the development of climax vegetation (Jessen and Milthers, 1928). In the case of the Dead Sea pollen record, the transition into the LIG is expressed as a phase of initial warming (PAZ IV1; 313.7–290.2 m blf; 130.9–124.2 ka). The interval of the LIG optimum is constraint between ca. 124.2 ka and ca. 115.5 ka (PAZ IIIa–c; 290.2–238.4 m blf) by the persistent relative abundance of tree and shrub pollen (Figure 12).

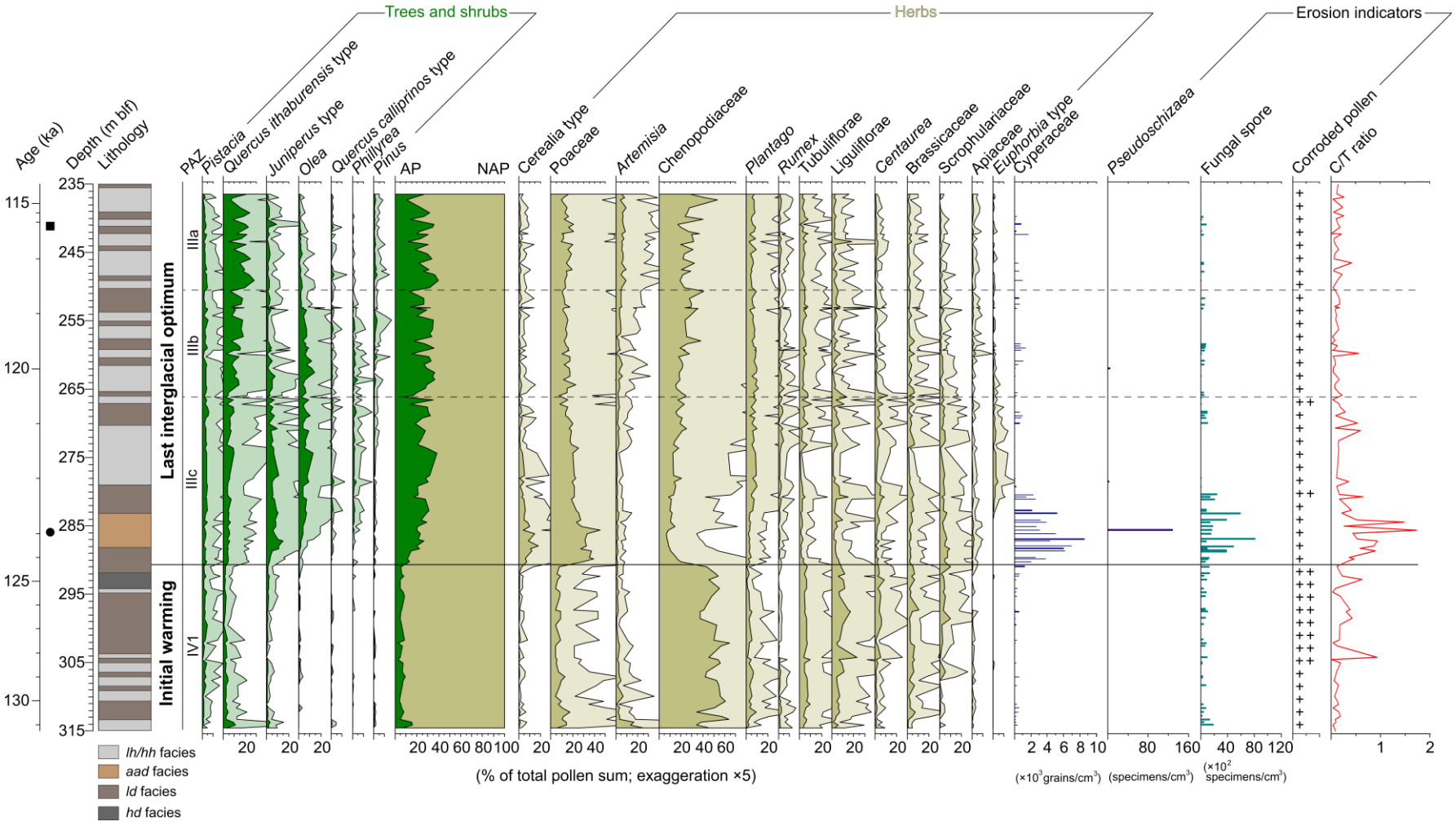

Figure 12: Simplified pollen diagram of Dead Sea core 5017-1A for the periods of initial warming (313.7–290.2 m blf) and last interglacial optimum (290.2–238.4 m blf). PAZ=pollen assemblage zone, AP=arboreal pollen, NAP=non-arboreal pollen, C/T ratio=charcoal to pollen ratio. In the lithological profile, *lh*=layered halite, *hh*=homogeneous halite, *aad*=alternating aragonite and detritus, *ld*=laminated detritus, *hd*=halite and detrital marl (Neugebauer et al., 2014). The black square and black dot indicate the positions of the U-Th age and anchor age, respectively.

Initial warming

The onset of the initial warming is marked by a small but notable pistachio pollen increase at 130.9 ka (313.7 m blf), which can be correlated with the start of MIS 5e (Lisiecki and Raymo, 2005). The growth of pistachio trees demands frost-free winters, thus changes in their pollen are indicative of thermal conditions (Rossignol-Strick, 1995). Moreover, even a low abundance of pistachio pollen can point to a wide distribution of pistachio trees in the vegetation due to their under-representation in pollen assemblages (van Zeist and Bottema, 1977).

In contrast to the remarkable increase of pistachio trees, all other arboreal plants were minimized. Since the favorable thermal conditions underline humidity as the limiting factor for tree growth, it can be indicated that severe aridity occurred not only in the low altitudes but also in the mountains. The prevailing aridity possibly led to the virtual absence of the Mediterranean biome in the mountains surrounding the Dead Sea.

As the most common pollen taxon during the initial warming, Chenopodiaceae pollen contents reach highest values forming a 'Chenopodiaceae phase'. The goosefoot family is characteristic of dry and saline habitats of open landscapes in the southern Levant (Weinstein-Evron, 1983). They occur at the Mediterranean coasts, in the desert interior of <100 mm MAP, and in the salt flats exposed following the lake-level drops (Rossignol-Strick, 1995). Due to the mountain barrier east of the Mediterranean coast, the deserts and salt flats are the main sources of goosefoot pollen in the Dead Sea. On one hand, modern observations show that halophytes of goosefoot family such as *Atriplex halimus* and *Anabasis setifera* are pioneer colonizers of the temporarily exposed Dead Sea shoreline. After a few years, the climax communities consisted of *Zygophyllum dumosum* and spp. take over the shoreline as the soil salinity is further reduced (Aloni et al., 1997). Therefore, a part of the Chenopodiaceae pollen in the Dead Sea can be ascribed to the local pioneers. On the other hand, assuming most goosefoot pollen came from the salt flats, such a long 'Chenopodiaceae phase' would be impossible because it calls for continuous lake-level drops of several millennia, which is unlikely according to coeval lake-level estimates (Torfstein et al., 2015). Instead, since most goosefoot pollen are anemophilous, the open landscape and the windiness can largely facilitate the transport of goosefoot pollen from the vast deserts to the Dead Sea, which would reduce the relative contribution of pollen from the local salt flats (Horowitz, 1992; Neumann et al., 2007).

Hence, the predominance of goosefoot pollen during the initial warming suggests the desert vegetation belt expanded eastward and northward, driven by the regional-scale drought. This dry condition is also proved by the low pollen percentages of steppic elements (*Artemisia* and

Poaceae). Insect-pollinated Brassicaceae and non-*Artemisia* Asteraceae, which are important components of the desert plant communities in the lake vicinity (Weinstein-Evron, 1983), were common during the initial warming. The relatively high abundance of non-*Artemisia* Asteraceae pollen (especially Liguliflorae) might also be a combined effect of differential pollen preservation and identifiability caused by strong erosion in the drainage area, as implied by the coeval increase of corroded pollen grains (Figure 12).

A notable increase in the C/T ratios started at ca. 128 ka, suggesting that fire hazards gradually intensified in the context of warm and dry conditions. The progressively enhanced seasonal drought, as indicated by the increase of pistachio trees (Rossignol-Strick, 1995), possibly also contributed to the ignitions (Turner et al., 2010). However, the low vegetation cover during the initial warming resulted in inadequate biomass fuel and to an extent limited fire frequency and intensity.

Last interglacial optimum

The onset of LIG optimum in the southern Levant was characterized by an abrupt increase of grasses followed by fast expansion of trees and shrubs in the mountains, which showed distinct phases of arboreal successions. At 124.2 ka, deciduous oaks started to increase in small amounts. In this context, junipers and/or cupressus first spread into the open lands and were subsequently replaced by the establishment of evergreen sclerophyllous communities. The sclerophylls were represented by olive trees (*Olea*), green olive trees (*Phillyrea*), and evergreen oaks (*Quercus calliprinos* type). Since 120.5 ka, the increase of deciduous oaks became more evident and was accompanied by a slight decrease of sclerophylls, as well as the increase of pines in the remote northern mountains. Between 118.5 ka and 115.5 ka, deciduous oaks reached maximum quantitatively and dominated the woodlands in the southern Levant, whereas pistachio trees gradually decreased and sclerophylls significantly diminished.

Grasses occur in diverse biotopes of the regional and local vegetation (van Zeist et al., 1975). They are common components of steppes, understories of woodlands (van Zeist et al., 2009), and surroundings of wetlands or lakes (Weinstein-Evron, 1983). Grass pollen in the Dead Sea 5017-1A core sediments are separated into Poaceae and Cerealia type (Figure 12). In the Near East, Poaceae pollen are produced by wild grasses, while Cerealia type pollen predating the early cultivation originate from both wild grasses and wild cereals (e.g., emmer and barley) in dry habitats (van Zeist and Bottema, 2009). Although it is impossible to define the relative contribution of Poaceae pollen from varied habitats, the synchronous peak amounts of

Cerealia type pollen confirm that grass pollen from localized marshland were not the most important ingredients. Therefore, the high contents of grass pollen in the Dead Sea were more likely indicative of the presence of a semi-arid grass-dominated steppe or the flourish of grasses in the woodlands (van Zeist and Bottema, 2009).

Nevertheless, it should not be precluded that a part of the grass pollen originated from reeds (e.g., *Phragmites australis*) in the local marshland, taking into consideration of the simultaneous presence of abundant sedge pollen (Cyperaceae; Figure 12). The emergence of marshes is a result of lentic shallow-water habitats existing on the lakeshore over time. The expansion of marshland surrounding the Dead Sea, as indicated by peak values of Cyperaceae pollen concentration, might be caused by slightly increased freshwater input (e.g., springs) to the lake.

The growth of grasses requires a moderate MAP of ca. 300 mm (El-Moslimany, 1990; Rossignol-Strick, 1995). Thus, the initial stage of the LIG optimum was characterized by a certain moisture availability that triggered the increase of grasses to replace the desert elements, yet the moisture was still insufficient for a remarkable spread of trees and shrubs. The short-lived delay of arboreal expansion following the grass dispersal might also be explained by the observation that grass is a strong competitor prohibiting trees from seeding, e.g., in the Galilee Mountains and on the Golan Height (Danin, 1992).

The landscape remained rather open for centuries until the transient take-over of pioneer junipers. Since 123.5 ka, the heat- and drought-adapted Mediterranean sclerophylls expanded, pointing to the heating and aridification of the Levantine summers (Rossignol-Strick, 1995). In contrast, the winters were mild and probably became wetter to sustain trees and shrubs. Under such a climatic regime along with increased combustible biomass, most frequent and intensive fire activities took place in the southern Levant, as inferred from the remarkably high C/T ratios between 124 and 122 ka (Figure 12). Similarly, during the early Holocene at Lake Hula, microscopic charcoal data suggest that a warm and overall wet climate characterized by seasonal drought accounted for active fires (Turner et al., 2010). In light of biomass, the rich annuals predominated by grasses and wild cereals between 124 and 122 ka, especially those grew in the interspaces of woodlands (Danin, 1992), probably accumulated abundant fuel for subsequent dry-season burning. This assumption is supported by the common presence of charred epidermal grass fragments (Limaye et al., 2007) in Dead Sea sediments. Additionally, the interval of active fires was marked by the occurrence of *Pseudoschizaea* (Mudie et al., 2011) and high concentrations of fungal spores (Figure 12), which indicated intensified soil erosions related to flash-flood events (López-Merino et al., 2016).

In the Near East, not only the rainfall but also its seasonal pattern shape the peculiar vegetation presently and in the past (El-Moslimany, 1990). During the LIG optimum, this feature was reflected by the relative frequencies of deciduous oak and sclerophyllous pollen. Deciduous oaks, in contrast to sclerophylls, can survive winter frosts but are intolerant to summer drought (Rossignol-Strick, 1995).

During the first phase of LIG optimum (PAZ IIIc), sclerophylls quickly expanded while the increase of deciduous oaks was slow, suggesting an elevated MAP with strong seasonal moisture deficit. In the second phase (PAZ IIIb), deciduous oak increased to a certain proportion in the woody communities and exceeded that of the sclerophylls, whereas total tree and shrub showed no significant changes in amounts. This possibly mirrors similar MAP as the first phase and a reduced summer heat and drought. The third phase (PAZ IIIa) identified optimal conditions for deciduous oak development in the southern Levant, whereas sclerophylls were significantly reduced. Nevertheless, trees and shrubs as a whole commenced declining slightly, pointing to the fact that the high abundance of deciduous oaks was not caused by increased MAP. The sclerophyllous reduction might be alternatively explained by the cooling of winters. However, pistachio trees remained relatively abundant coevally and thus implied the winter temperature was probably equivalent to that of the initial warming period.

6.1.1.3 Early last glacial

The early last glacial initiated at ca. 115 ka when the ice sheets started to build up gradually, before full glacial conditions were reached (NEEM community members, 2013). In this study, the early last glacial is partly covered, encompassing the interval between 115.5 and 89.1 ka (PAZ II; 238.4–199.2 m blf; Figure 13). The lower boundary of the early last glacial is defined by the decreased percentages of pistachio pollen, which are lower than those of the initial warming and LIG optimum period and thus indicate a cooling trend.

Trees and shrubs in the mountains were dominated by deciduous oaks and continued to contract slightly since the late LIG optimum. The increasingly opened landscape was occupied by light-demanding herbs such as goosefoots and wormwood. The gradual decreasing trend of deciduous oaks was terminated by a slight resumption between 105 and 100 ka (PAZ II4b). This resumption was interrupted by a 2 ka break marked by peak amounts of goosefoots. Since 100 ka, pistachio trees were further diminished and the woodlands were sparsely distributed in the mountains surrounding the Dead Sea, whereas desertification took place progressively in the low altitudes.

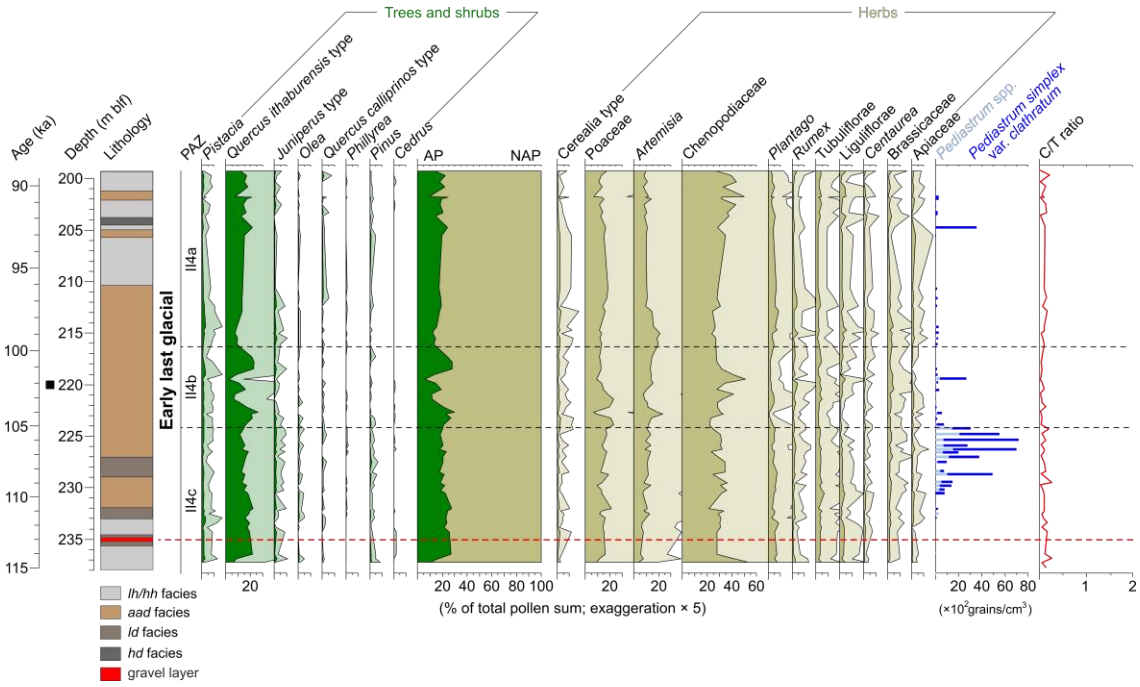

Figure 13: Simplified pollen diagram of Dead Sea core 5017-1A for the early last glacial period. PAZ=pollen assemblage zone, AP=arboreal pollen, NAP=non-arboreal pollen, C/T ratio=charcoal to pollen ratio. In the lithological profile, *lh*=layered halite, *hh*=homogeneous halite, *aad*=alternating aragonite and detritus, *ld*=laminated detritus, *hd*=halite and detrital marl (Neugebauer et al., 2014). The red dashed line denotes the gravel layer at ca. 235 m blf (Torfstein et al., 2015). The black square indicates the position of the U-Th age.

The early last glacial vegetation shares similarities with that of the late penultimate glacial, despite minor inconsistencies. In trees and shrubs, the differences lie in slightly more pistachio trees and fewer pines and cedars during the early last glacial. This suggests that the winter temperatures were not substantially reduced since the LIG optimum so that a certain number of pistachio trees can still survive. With respect to herbs, less wormwood, more grasses, and more ruderal herbs (e.g., *Plantago*, non-*Artemisia* Asteraceae, and Brassicaceae) are observed for the early last glacial. It indicates that the low-altitude areas were characterized by marginally warmer conditions or slightly higher moisture availability (Cheddadi and Rossignol-Strick, 1995a).

The tendency of steppe and desert expansion since the early last glacial indicates a long-term drying trend. The short-term resumption of deciduous oaks between 105 and 100 ka possibly points to the presence of an interstadial, which is defined as an interval of temporary climatic amelioration within a glacial phase (Jessen and Milthers, 1928). Compared to the LIG optimum, this interstadial-like interval was either too short or not sufficiently humid to permit significant woodland expansion in the same region.

Another characteristic during the early last glacial is two episodes of abundant *Pediastrum* algae (Figure 13). *Pediastrum* is a green alga normally living in lentic freshwater habitats (van Zeist et al., 2009). Since no clear associations with changes in terrestrial pollen assemblages are observed, the *Pediastrum* might not serve as a bioclimatic indicator. Such high amounts of *Pediastrum* colonies deposited in the deep lake center are also unlikely to be brought by the Jordan River from the Sea of Galilee. Instead, it is most probable to be related to changes in Dead Sea limnological properties such as water temperature, lake level, salinity, and nutriture. Indeed, both episodes coincide with the deposition of *aad* sequence right after halite deposits, which suggests lake-level rises and lake freshening. Moreover, the predominance of the species *P. simplex* var. *clathratum* is indicative of relatively warm habitats with a certain trophic level (Jankovská and Komárek, 2000).

In the lithological profile, a 35 cm gravel layer at ca. 235 m blf on top of the massive halite deposits is the most prominent (Figure 13). Torfstein et al. (2015) suggested that this gravel layer resembled beach deposits and the Dead Sea dried out after long-term desiccation. However, further analyses indicate that the gravel layer was not in-situ deposits. It is well-sorted containing salt crystals but is nearly absent of fine-grained materials. As the gravel layer has uniform petrographic features as the base of the mass-waste deposits 6 m above it, the gravels were most likely the residues of the mass-waste deposits that were washed out during the drilling process (Neugebauer et al., 2016). Moreover, investigations of the Dead Sea 5017-1 core halite deposits demonstrate that significant dissolution never occurred and the water depth was always over 100 m during the past 220 ka (Kiro et al., 2015). In terms of palynological analysis, almost no changes are observed in the pollen spectra above and below the gravel layer (Figure 13). The percentages of indeterminable pollen also exhibit no distinct increase. According to Campbell (1999), these facts are not in line with the presence of a depositional hiatus, which was supposed to occur at the Dead Sea between 116 and 110 ka. Therefore, these two dates, extrapolated from the anchor ages above and below, respectively (Torfstein et al., 2015), should be taken with caution and were discarded in this study.

6.1.1.4 Vegetation gradient of the southern Levant

The large surface of the Dead Sea is able to capture pollen grains from a wide region via winds (Prentice, 1985; Sugita, 1993). Runoffs in the drainage area of the Dead Sea also bring a number of pollen grains. Therefore, fossil pollen in the Dead Sea can record changes in all the vegetation territories of the southern Levant. However, it is currently impossible to define the relative pollen contribution of different source areas to the Dead Sea, due to the absence of a systematic modern pollen analysis.

Empirical investigations demonstrate that pollen percentages of a taxon in the sediments tend to show a decreasing trend with an increasing distance from the respective parental plants (e.g., Baruch, 1993; Davies and Fall, 2001; Weinstein-Evron, 1979). This conclusion is supported by the predominance of steppe and desert pollen in the entire Dead Sea 5017-1 record in this study, which is caused by the persistent proximity of respective vegetation to the Dead Sea. On the same principle, trees and shrubs in the adjacent Judean Mountains should have contributed more arboreal pollen to the Dead Sea, as compared to those produced in the Galilee Mountains or Golan Height. However, it should be taken into consideration that a decreasing arboreal density from north to south is evident within the Mediterranean biome, due to a fade-out effect of the Mediterranean rains (Zohary and Feinbrun-Dothan, 1966). It is thus difficult to reconstruct the paleovegetation of a region marked by strong vegetation gradient, provided only a single pollen record covering the concerned period is available.

The strong vegetation gradient during the present interglacial is well reflected by the recent and Holocene sediments collected from the Dead Sea, the Sea of Galilee, and Lake Hula, exhibiting notably lower content of arboreal pollen in the Dead Sea (Langgut et al., 2016; Litt et al., 2012; Schiebel, 2013; van Zeist et al., 2009). Information regarding glacial vegetation gradient of the southern Levant is scarce. Recently, a comparison of the MIS 2 pollen spectra from the Dead Sea and the Sea of Galilee shows similar contents of tree and shrub pollen (mean of 20%), suggesting the vegetation gradient was reduced (Miebach, 2017).

In this study, although trees and shrubs were most widespread during the LIG optimum, close-forest conditions were never reached in the mountains surrounding the Dead Sea due to arboreal pollen percentages of <60% (van Zeist and Bottema, 2009). Instead, open forests (termed as ‘woodland’ in this study) were distributed in sub-humid areas such as the Judean Mountains. Nevertheless, in northern wetter areas such as surroundings of the Lake Hula, Sea of Galilee and Birkat Ram, where forests established during the Holocene (Schiebel, 2013; van Zeist et al., 2009), the LIG arboreal density remains unclear due to a lack of vegetation records. Palynological sequences from the Nile Cone marine cores provide a vegetation history dated back to MIS 7, but terrestrial pollen in these cores originate from the vast borderlands of the Levantine Basin and represent a mixed EM vegetation signal (Cheddadi and Rossignol-Strick, 1995a).

During the penultimate glacial and early last glacial, tree and shrub pollen averaged 14.8% and 19.6% of the Dead Sea 5017-1A pollen spectra, respectively, as compared to a mean value of 25.9% during the LIG optimum. The inferred glacial-interglacial arboreal changes seem to be low-amplitude. This is probably caused by the high abundance of herbaceous pollen over the whole investigated period, which leads to an underestimation of the actual extent of arboreal changes in the mountains. A higher amplitude of vegetation variations is

possible provided a counterpart pollen record further north in the southern Levant, where trees and shrubs have a higher impact on the pollen spectra. Indeed, pollen records from the Sea of Galilee show that tree and shrub pollen account for ca. 45% since the mid-Holocene (Schiebel, 2013), as compared to ca. 20% during MIS 2 (Miebach et al., 2017).

6.1.2 Regional comparisons

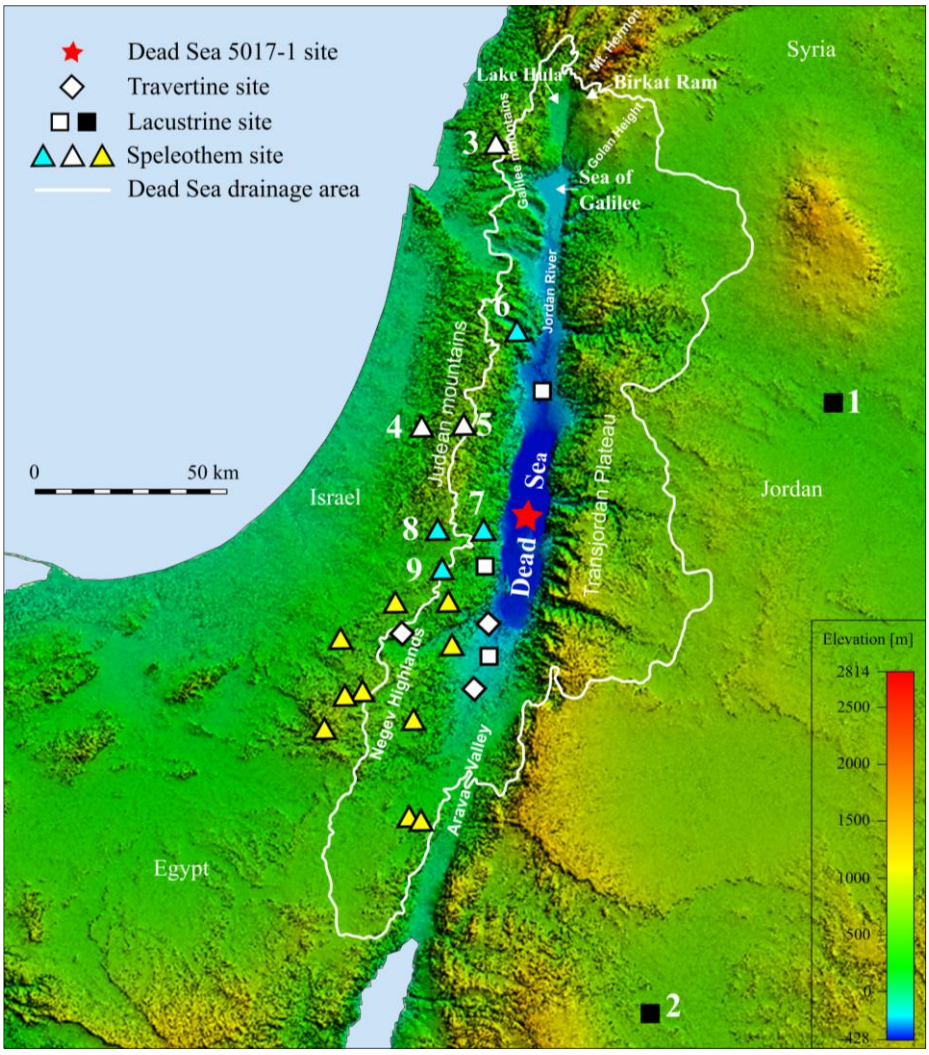

Figure 14: Previously studied sites in the southern Levant concerning the investigated interval in this study, marked with numbers and legends. *Diamonds*: travertine sites in the Arava Valley (Livnat and Kronfeld, 1985; Waldmann et al., 2010) and in the Negev Desert (Schwarcz et al., 1979). *White squares*: MIS 5 Dead Sea deposits (Waldmann et al., 2009). *Black squares*: lacustrine sites of 1=paleolake Azraq (Cordova et al., 2013) and 2=paleolake Mudawwara (Petit-Maire et al., 2010) in Jordan. *White triangles*: speleothem sites of 3&4=Peqi'in Cave & Soreq Cave (Bar-Matthews et al., 2003) and 5=Jerusalem Cave (Frumkin et al., 1999) in the sub-humid mountains. *Blue triangles*: speleothem sites of 6&7= Ma'ale Efrayim Cave (Vaks et al., 2003) & Kanaim Cave in the Judean Desert (Vaks, 2008) and 8&9=Ma'ale-Dragot Caves and Tzavoa Cave in the northern Negev (Vaks et al., 2006). *Yellow triangles*: speleothem sites in the central and southern Negev deserts (Vaks et al., 2007, 2010).

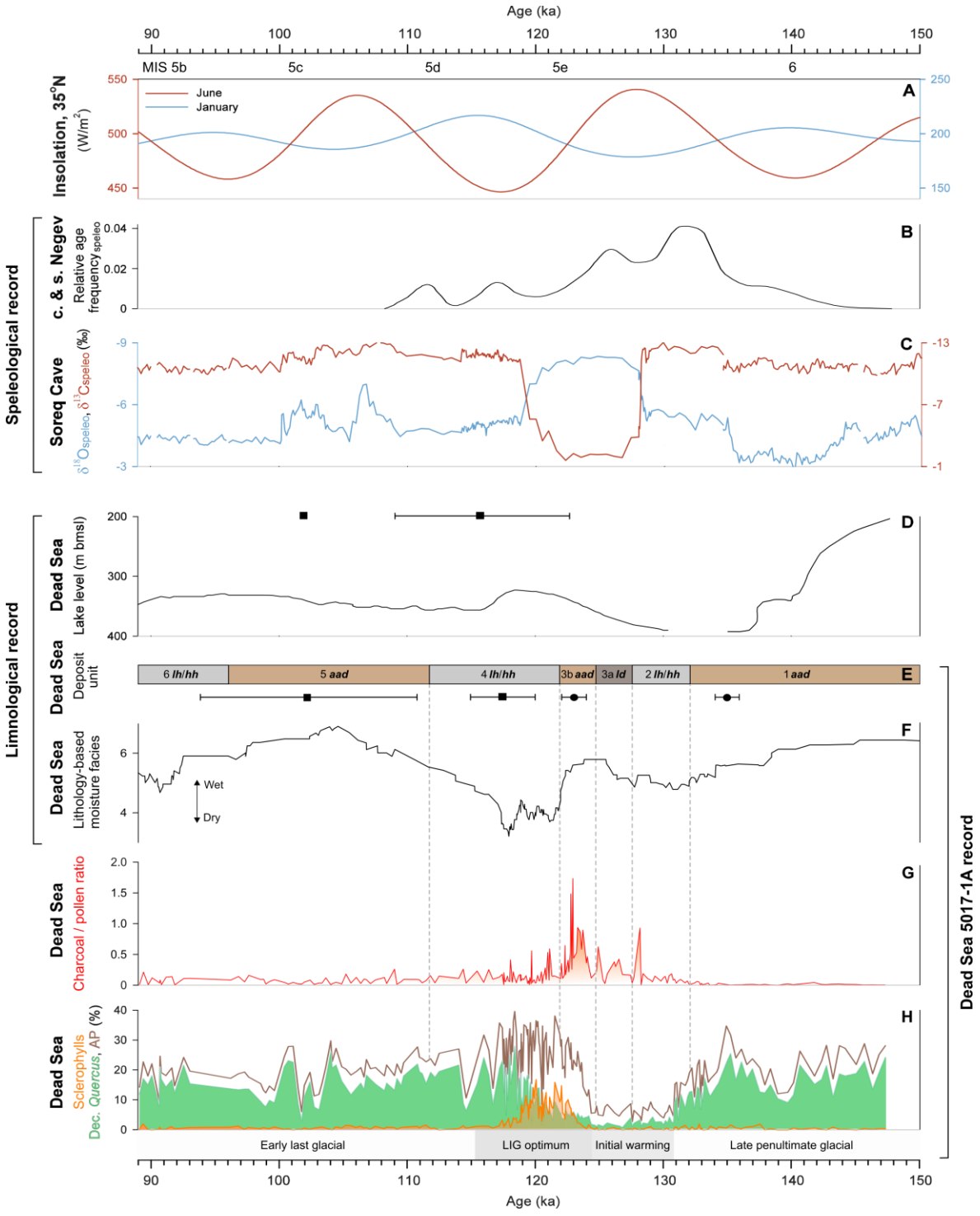

Figure 15: Comparisons of selected paleorecords in the southern Levant. Marine Isotope Stages (MIS) and Substages are after Lisiecki and Raymo (2005). A) June and January insolation at 35°N (Laskar et al., 2004); B) Relative age frequency of speleothems in central and southern Negev (Vaks et al., 2007); C) $\delta^{18}O$ and $\delta^{13}C$ record of the Soreq Cave speleothems (Bar-Matthews et al., 2003); D) Composite lake-level curve of the Dead Sea (Waldmann et al., 2010); E) Deposit units and dated points of Dead Sea 5017-1A record, adapted after Torfstein et al. (2015). Of the deposit types, *lh*=layered halite, *hh*=homogeneous halite, *aad*=alternating aragonite and detritus, *ld*=laminated detritus, *hd*=halite and detrital marl (Neugebauer et al., 2014); F) Lithology-based moisture facies of Dead Sea 5017-1A record (Torfstein et al., 2015); G) Charcoal/pollen ratio of the Dead Sea 5017-1A record, this study; H) Pollen percentages of sclerophylls (*Olea*, *Phillyrea*, and evergreen *Quercus*), deciduous *Quercus*, and arboreal taxa (AP) of the Dead Sea 5017-1A record, this study.

In the southern Levant, comparable paleorecords with the Dead Sea 5017-1A pollen record are available from travertine, lacustrine, and speleothem archives (Figure 14 and 15). For the Dead Sea 5017-1A core sediments, the magnetic susceptibility and µXRF data are not involved in paleoenvironmental comparisons. The magnetic susceptibility is determined by concentrations of magnetic minerals in the sediments and can indicate the amount of detrital material brought into the lake. However, the magnetic carrier minerals in the Dead Sea sediments are either autochthonous or allochthonous. In this case, the magnetic susceptibility cannot be used as a uniform proxy for paleoenvironmental conditions (Neugebauer et al., 2014). The µXRF element scanner data serve for a first estimation of the mineralogical compositions of the Dead Sea sediments, which ultimately reflect the shifts in deposit facies (Neugebauer et al., 2014) that can be explicitly shown by the lithological profile (Figure 15E). The deposit facies point to different lake levels and are indicative of water input to the Dead Sea. These facies were assigned with values to estimate relative lake-level changes and were suggested to represent moisture facies (Figure 15F; Torfstein et al., 2015).

This subsection aims to reveal the similarities and discrepancies concerning paleoenvironmental conditions in the southern Levant as indicated by different proxies and archives. It should be noted that the present age control of the Dead Sea 5017-1A cores is inadequate and a precise correlation with other records is currently impossible.

6.1.2.1 Initial warming and last interglacial optimum

Comparisons with limnological records

Three representative deposit facies are identified from the Dead Sea 5017-1A cores for the investigated periods (Figure 15E). The *aad* deposits comprise couplets of primary aragonite and fine-grained detritus of 8–10 µm (Haliva-Cohen et al., 2012). According to Stein et al. (1997), bicarbonates delivered by regular freshwater are essential for the formation of aragonite in the Dead Sea surface water. The presence of *aad* deposits is thus indicative of high lake stands and meromictic conditions with a layer of less saline water column overlying the denser water column at the bottom (Gavrieli and Stein, 2006).

Unlike *aad* deposits, the *ld* deposits lack regular aragonite and are characterized by coarser detritus (50–60 µm) with intercalations of aragonite or gypsum laminae. These detrital materials are mainly brought by sporadic rainstorm-generated floods from the surface cover (e.g. soils, settled dust, and loess) to the relatively low-stand lake (Haliva-Cohen et al., 2012; Stein, 2001, 2014).

Long sequences of halite deposits (*lh*/*hh*) are interspersed by *ld* deposits. Halite precipitates when the lake stand is declined to a certain level (below 401 m bmsl; Kiro et al., 2015). The freshwater input is substantially decreased, resulting in a significantly reduced density difference between the upper and lower water column (Stein, 2001). Consequently, the lake stratification is destroyed.

The period of initial warming and LIG optimum, as indicated by the Dead Sea 5017-1A pollen record, is covered by three deposit units (unit 4–2, Figure 15E). The lithology-based changes in moisture facies show prominent inconsistencies with those inferred from vegetation conditions (Figure 15F, H). It is argued that an arid climate generally prevailed as indicated by the halite deposits in unit 4 (122–112 ka) and unit 2 (132–128 ka). The prolonged aridity was interrupted by a humid interval at ca. 128–122 ka (deposit unit 3), as well as relatively moist episodes represented by *ld* intercalations in unit 4 (Torfstein et al., 2015). In contrast, from the botanical perspective, an enhanced and persistent wetness at 124–115 ka is indicated by increased trees and shrubs, while intensive drought characterized the period at 131–124 ka. The apparent discrepancy requires a closer examination.

Firstly, coarse detritus of the sub-unit 3a *ld* deposits were brought by extreme but ephemeral runoffs, which were closely connected with the intense showers caused by penetration of southern sub-tropical systems such as the Red Sea Trough (Greenbaum et al., 2006a). The occurrence of *ld* deposits thus points to slightly increased moisture availability in the southern Dead Sea drainage area, which was probably not the case in the north. Indeed, coeval desert expansion suggests regional-scale aridity prevailed. This implies that the sub-tropical synoptic systems played a limited role in vegetation development, especially in the survival of moisture-demanding trees in the north. In the southern drainage area, instead of contributing moisture to the adjacent plants or to water storage within the basin, the quick drainage of large floods induced soil erosion (Dayan and Morin, 2006) that resulted in the poor preservation of palynomorphs in the Dead Sea.

Secondly, unlike sub-unit 3a, the major part of sub-unit 3b is composed of *aad* deposits. Although both sub-units mirror increased water input to the lake, the aragonite laminae of unit 3b are explained to be indicative of enhanced Mediterranean precipitation that is regular and contributes to the majority of lake water (Greenbaum et al., 2006a). Therefore, the formation of these two subunits was triggered by different climate regimes, which is also reflected by the botanical shift from desert to grass steppe. Nevertheless, taking into consideration of the remaining high proportions of *ld* deposits in sub-unit 3b (Figure 12), the influence of Mediterranean rain on Dead Sea sediments during this short interval was likely not as strong as supposed by Torfstein et al. (2015). Instead, semi-arid conditions are inferred by the occurrence of abundant grasses and junipers. Modern observations provide an alternative interpretation for the temporal presence of *aad* deposits, that winter flooding

events are responsible for the formation of aragonite laminae in the Dead Sea (Barkan et al., 2001; Gat, 1984), especially given the most negative excursions of the $\delta^{18}O$ values in sub-unit 3b (Torfstein et al., 2009, 2015). This interpretation is consistent with the NPPs increase in Dead Sea sediments that suggests an enhanced erosion (Figure 12).

Lastly, the deposition of thick halite sequences in unit 4 implies extremely low lake stands (Kiro et al., 2015, 2017; Torfstein et al., 2015), while the concurrent woodland expansion points to the full revival of the Mediterranean rains. The formation of the thick *ld*-intercalated halite unit was a long process of recurrent alternating deposition of halite and laminated detritus (Figure 12). During relatively pluvial intervals, detrital materials were delivered to the lake along with dissolved salt, which served together with the Dead Sea brine for subsequent halite deposition during low lake stands (Kiro et al., 2015). Therefore, the unit 4 halite layers suggest periodic saturation of brine respective to halite as a result of lake lowering, but might not directly represent arid intervals. Nevertheless, the connection between the nearly synchronous long-term low lake stand and woodland expansion is to be deciphered. For this purpose, paleoenvironmental scenarios of the southern Levant are proposed (sub-section 6.1.3.) after comprehensive regional comparisons.

In addition to the Dead Sea 5017-1A cores, the DSB marginal areas (Figure 14) retain some sequences of exposed LIG deposits (Waldmann et al., 2009), which show different characters from deep-drilled lacustrine sediments. Firstly, lacustrine deposits in the marginal areas are principally made up of calcitic marls (*ld* deposit) but free of halite. The reason might be that the outcrops are situated above the upper lake-level limit for salt deposition (401 m bmsl; Kiro et al., 2015), or that halite has been deposited but dissolved by runoffs subsequently. Secondly, *aad* deposits are absent in the outcrops, which is elusive due to the faster formation of aragonite in the nearshore areas than in the deep basin (Kiro et al., 2015, 2017). These factors restrict precise correlation of sedimentary facies between the lake margins and deep lake center. Moreover, in the marginal areas, lake-level reconstructions are based on shoreline indicators from the outcrops. In the lake-level estimates derived from the lake margins and Dead Sea 5017-1A cores, a major discrepancy arises around 120 ka (Figure 15D, F). That is, lacustrine sediments were deposited in the Perazim Valley (elevation of 322 m bmsl), whereas coeval thick halite deposition in lake center suggests that the lake level dropped to ca. 490 m bmsl (Kiro et al., 2017). On one hand, the discrepancy might be related to inadequate age control in the lake margins. On the other hand, it calls for reevaluating the implications of deposit facies in varied localities.

Comparisons with speleological records

As shown in Figure 14, speleological records in the southern Levant are categorized according to their locations and the MAP rates these sites receive: 1) the sub-humid northern and central Israel (the Soreq, Peqi'in, and Jerusalem Cave); 2) the semi-arid rain-shadow Judean Desert (e.g., Ma'ale Efrayim cave) and northern Negev (e.g., Tzavoa Cave); 3) the arid central and southern Negev Desert. Speleothems in the sub-humid areas were deposited continuously since 240 ka. In the semi-arid areas, speleothem deposition was discontinuous, occurring mainly during glacials with some minor deposition during interglacials. In the arid areas, speleothem deposition was episodic, taking place during the NHPs that mainly encompass interglacials.

In central and northern Israel, the Soreq Cave speleothem $\delta^{13}C$ record (Figure 15C) suggests that most of the MIS 5 were characterized by the predominance of C3 plants in the vegetation and wetter conditions, as compared to the increase of C4 plants during MIS 6 and MIS 4–2 (Bar-Matthews et al., 2003). In the arid central and southern Negev Desert, the most frequent speleothem deposition occurred during 142–109 ka (NHP 1, Figure 15B) with relatively thick and abundant laminae, suggesting a wetter-than-present climate of >300 mm MAP (Vaks, 2008; Vaks et al., 2006).

According to the Soreq Cave $\delta^{13}C$ record, the peak interglacial within MIS 5e, dated to 128–120 ka, was characterized by a severe loss of vegetation and soil (Frumkin et al., 2000) under the pluvial conditions of ca. 70% higher MAP than present-day (Bar-Matthews et al., 2003). This interval is explained to be highly unstable and marked by deluge-generated floods (Bar-Matthews et al., 2017). The intervening episodes between deluges are inferred to be warm and dry leading to the devastation of vegetation by wildfires, and the deluge-induced erosions probably aggravated the loss of soil and vegetation.

The overall vegetation changes reflected by the Soreq Cave speleothem $\delta^{13}C$ record display a similar trend with that inferred from the Dead Sea 5017-1A pollen record, regardless of the time inconsistencies caused by potential age uncertainties in the latter. Between 128 and 122 ka, the increased fire activities indicated by high C/T ratios of the Dead Sea record (Figure 15G) are in line with the interpretations of the Soreq Cave $\delta^{13}C$ records at 128–120 ka (Bar-Matthews et al., 2017). Meanwhile, both the Dead Sea and Soreq Cave records suggest an increased flooding and soil erosion in the southern Levant. After the unstable interval, the trend of deciduous oak dispersal and C3 plant increase in the vegetation based on pollen and speleothem records, respectively, possibly imply that the climate became more stable and the precipitation was more evenly distributed.

Moisture source

The present-day southern Levantine climate is under the joint control of mid-latitude and tropical atmospheric-oceanic systems in the north and south, respectively. The majority of precipitation originates from the Mediterranean cyclones in the winter, and a small part of rainfall is related to the Red Sea Trough or tropical plumes from the south (Dayan and Morin, 2006). In light of this, discussions of moisture source are essential for investigating the paleoclimatic patterns.

In the sub-humid and semi-arid southern Levant, the close $\delta^{18}O$ alignment of speleothem records with EM marine records suggests these areas were constantly controlled by the Mediterranean precipitation during the past 240 ka (Bar-Matthews et al., 2003). In the arid central and southern Negev, the EM Sea water played a key role on speleothem deposition during MIS 5. This is supported by the decreasing trend of speleothem thickness from north to south, which points to a subdued influence of the Mediterranean cyclones due to the southeastern Mediterranean physiography (Vaks et al., 2010). In botanical terms, during the LIG optimum, the remarkably increased sclerophyllous pollen indicate the thriving of woody taxa tolerant of hot and dry summers, which underlines the Mediterranean rains as the dominant moisture source for tree growth.

During MIS 5e, the contribution of moisture brought by southern atmospheric systems is controversial. The *ld* deposits in the Dead Sea 5017-1A cores are explained to be a result of the intrusions of southern moisture associated with the northern migration of the African Monsoon (Torfstein et al., 2015). However, the extension of the African Monsoon as far as to the Levant is concluded to be unlikely, because no evidence of increased summer moisture is available (Tzedakis, 2007). Moreover, climate modeling result suggests that summer drought in the EM region was exacerbated by the intensification of the Indian Monsoon (Rodwell and Hoskins, 1996).

The episodic deposition of travertine in the Arava Valley and Negev Desert (Figure 14) during the MIS 5 points to temporal fluvial conditions and periodically increased moisture availability (Livnat and Kronfeld, 1985; Schwarcz et al., 1979; Waldmann et al., 2010). The moisture is explained to be brought by rainstorms that were associated with tropical autumn/spring low-pressure systems (the Red Sea Trough; Waldmann et al., 2010) and/or winter moisture plumes from the Inter-Tropical Convergence Zone (ITCZ) across north Africa (Enzel et al., 2012). In particular, the enhanced effect of the Red Sea Trough is also mirrored by sporadic but intensive floods in the southern Dead Sea drainage area. The floods loaded and delivered numerous detritus to the Dead Sea, although the increase of lake level was minor (Greenbaum et al., 2006b; Haliva-Cohen et al., 2012; Waldmann et al., 2009).

6.1.2.2 Glacials

Late penultimate glacial

In the central and southern Negev Desert, speleothem deposition was limited under generally drier conditions during the late penultimate glacial, as compared to the MIS 5e (Figure 15B; Vaks et al., 2007). The Dead Sea 5017-1A pollen record suggests that the central and northern mountains of the southern Levant were vegetated by moderate amounts of deciduous oaks and sub-humid conditions were confined to these areas. This is consistent with the speleothem $\delta^{13}C$ records that indicate C3 plants were important components of the vegetation in the same areas (Figure 15C; Bar-Matthews et al., 2003). These relatively favorable conditions probably led to the abundance of specific ungulates and micromammals inhabiting the sparse Mediterranean woodlands of the Judean Mountains (Marder et al., 2011).

The Dead Sea 5017-1A pollen record indicates that the southern Levant was generally cool during the late penultimate glacial. The reduced evaporation and correspondingly increased moisture availability possibly accounted for the speleothem deposition in the present rain-shadow Judean Desert (Vaks, 2008; Vaks et al., 2003). At the same time, the Dead Sea was at high stands (Figure 15D; Torfstein et al., 2009; Waldmann et al., 2010), depositing long sequences of *aad* deposits (Figure 15E). The paleolake Azraq and Mudawarra occurred coevally in the present deserts of northeastern and southeastern Jordan, respectively (Figure 14; Cordova et al., 2013; Petit-Maire et al., 2002, 2010).

Early last glacial

The late penultimate glacial and early last glacial share analogous paleoenvironmental conditions in terms of paleovegetation and lacustrine settings in the southern Levant (Figure 15F, H). Nevertheless, the Dead Sea 5017-1A pollen record shows marginally warmer conditions during the early last glacial due to the existence of more pistachio trees and fewer conifers. The comparatively higher temperatures probably led to a lower effective moisture and the absence of speleothem formation in the low-altitude semi-arid areas (Vaks et al., 2006; Vaks et al., 2003). As a result, speleothem depositions were restricted to the present sub-humid mountains (Bar-Matthews et al., 2003; Frumkin et al., 2000). The Soreq Cave $\delta^{13}C$ record indicates that C4 plants gradually increased in the vegetation, implying a long-term drying trend that is also proved by the concomitant desert expansion inferred from the Dead Sea 5017-1A pollen record.

The temporarily ameliorated conditions, marked by a short-term resumption of deciduous oaks between 105 and 100 ka, are observed from the Soreq Cave $\delta^{13}C$ record as well (Bar-Matthews et al., 2003) showing a slight increase of C3 plants in the vegetation. This wet pulse was interrupted by a ca. 3 ka dry event that likely coincided with the abruptly increased Soreq Cave $\delta^{18}O$ values between 107 and 104 ka, which was possibly indicative of the dominant control of the Mediterranean rains on vegetation changes.

6.1.3 Potential paleoenvironmental scenarios

Different proxies from the same sedimentary archive might record the paleoenvironmental changes from different perspectives. For instance, pollen grains and lithological properties of the Dead Sea sediments document botanical and hydrological responses, respectively, to changes in the regional climate systems. Pollen assemblages in the Dead Sea have a large source area and can reveal vegetation changes of a regional scale. Dead Sea lithological shifts are indicative of lake-level variations and can reflect hydrological conditions in the drainage area. With independent multi-proxies, it is possible to comprehensively reconstruct the paleoenvironment of the southern Levant.

Vegetation changes in the southern Levant were largely controlled by the effective moisture availability and the LIG optimum is inferred to be moister than the glacials. In contrast, it is argued that lake-level changes can gauge regional precipitation rates (Enzel et al., 2003) and the glacials are suggested to be wetter than the interglacials due to higher lake stands (Torfstein et al., 2015). However, the Dead Sea lake level is a balance between water input from the drainage area and evaporation (Alpert et al., 1997). Despite the climate model simulations highlight the role of evaporation in lake-level fluctuations of the Dead Sea since 80 ka (Stockhecke et al., 2016), the conditions concerning the investigated interval in this study remain unclear. In this case, the observations regarding moisture balance in the major headwater area of the Dead Sea, i.e., the northern drainage area surrounding the Sea of Galilee, might provide insights into the potential cause of Dead Sea lake-level variations.

The strong evapotranspiration effect of trees and shrubs, which grow in the most humid areas but transpire much more than herbs, probably consumed a large part of the rainfall that was the main source of the Dead Sea water. For instance, in the Lower Galilee, even taking no account of the rainfall consumed by soil evaporation, deciduous and evergreen oaks transpire 51% and 44% of the annual precipitation, respectively (Schiller et al., 2010). The sclerophyll *Phillyrea latifolia* in northern Israel is estimated to transpire 30–61% of the annual

precipitation (Schiller et al., 2002). Additionally, in drier years the trees make use of a higher proportion of the annual rainfall than in wetter years (Schiller et al., 2003).

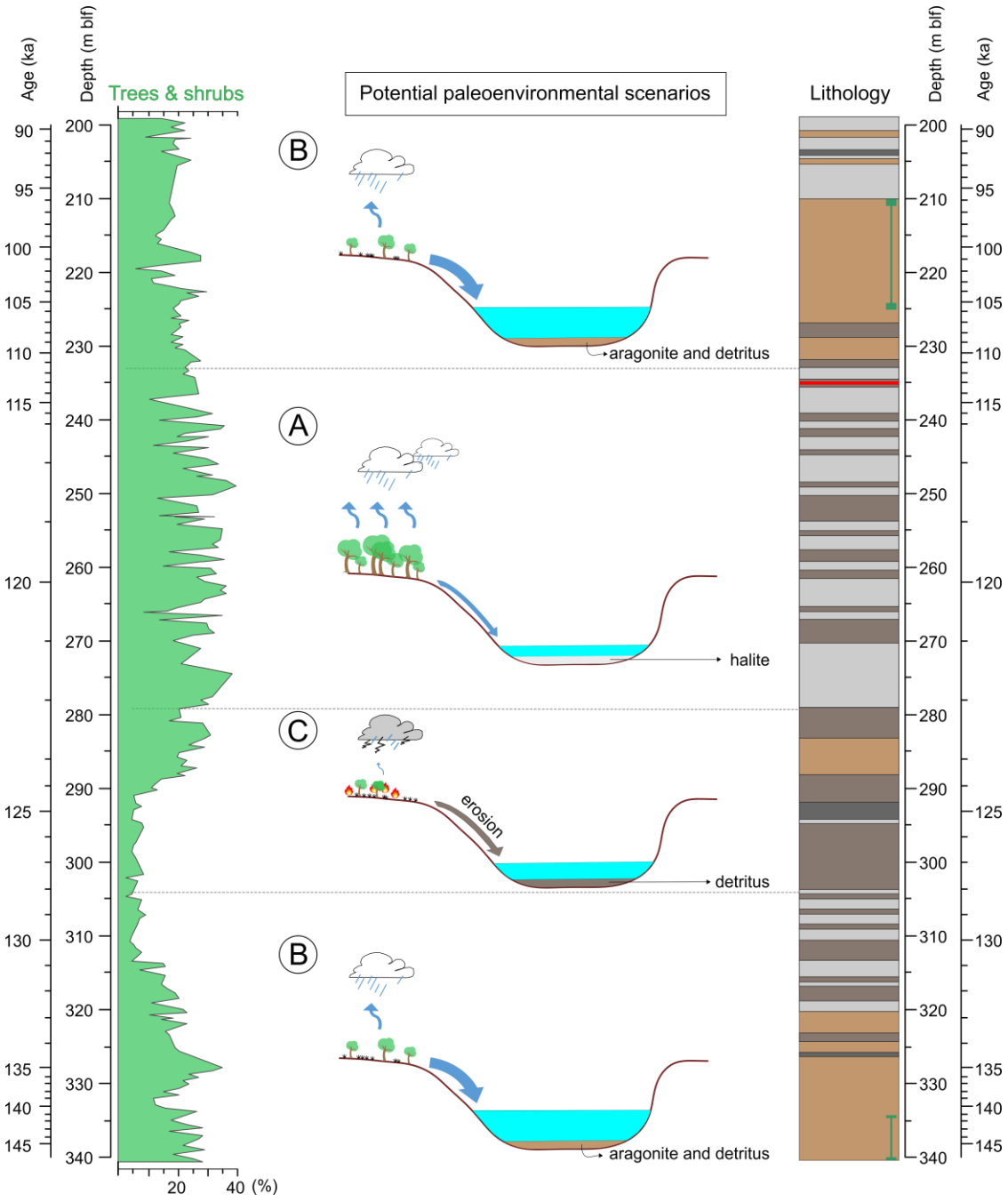

Figure 16: Potential paleoenvironmental scenarios of the southern Levant (middle) inferred based on tree and shrub pollen percentages (left, this study) and lithological profile (right, adapted after Neugebauer et al. (2014)) of the Dead Sea core 5017-1A sediments.

As discussed above, the Dead Sea pollen record alone is inadequate for reconstructing the woodland coverage and actual amplitude of arboreal changes in places such as the Galilee Mountains. In these areas, especially during the LIG optimum, the proportions of trees and shrubs might be underestimated by the low AP percentages in the Dead Sea 5017-1A record due to the significant influence of herbaceous pollen from the surroundings of the Dead Sea. Nevertheless, combining the observations of evapotranspiration effect and available paleorecords, potential scenarios concerning the paleoenvironmental setting in the southern Levant can be proposed (Figure 16).

Scenario A. After the LIG optimum onset, the occurrence of a relatively high abundance of trees and shrubs in the southern Levant was nearly coeval with the massive halite deposition in the Dead Sea. As evidence from the Dead Sea pollen spectra and speleothem records both suggest an enhanced rainfall during most of the LIG optimum, the lake lowering was probably caused by an increased evaporation and/or a reduced water input. The strong evapotranspiration of abundant trees and shrubs in the northern headwater area presumably consumed a significant part of the rainfall. As a result, only minor water volumes in the drainage basin were supplied to the Dead Sea, leading to the concomitant massive halite deposition in the Dead Sea. Similar conditions have been registered at Lake Zeribar (Iran) during the early Holocene when lake-level declines coincided with an enhanced evapotranspiration induced by regional vegetation development (Stevens et al., 2001).

Scenario B. The woodland contractions in the southern Levant suggest relatively drier conditions during glacials, which contradicts the implications of concurrent *aad* deposition in the Dead Sea. This phenomenon might be attributed to the reduced temperatures and a weaker evapotranspiration effect, which led to less water loss in the drainage area. As a consequence, the discharge into the Dead Sea was increased resulting in a lake-level rise and *aad* deposition.

Scenario C. The transition from the initial warming to the LIG optimum represents an interval of unstable climate conditions. Analyses of pollen assemblages, lithologic characters, and speleothem carbon isotope suggest this period was marked by increased fire activities and flood-induced erosions. In particular, when desert components prevailed in the southern Levant during the initial warming, the sub-tropical climate systems might have sporadically reached the southern part of the Dead Sea drainage area. Short-lived rainstorms were characteristic of the rainfall regime, resulting in the delivery of numerous coarse detritus to the Dead Sea via flash floods.

These scenarios potentially explain the paleoenvironmental inconsistencies inferred by different records and need to be tested with further investigations. For instance, modern observations show that about 1/3 of the precipitation in the Soreq cave area is lost to the

unsaturated zone (Ayalon et al., 1998). Therefore, rainwater drained to the karst caves should be taken into consideration for estimating water balance in the southern Levant.

6.2 Paleoenvironmental implications for the early modern human dispersal

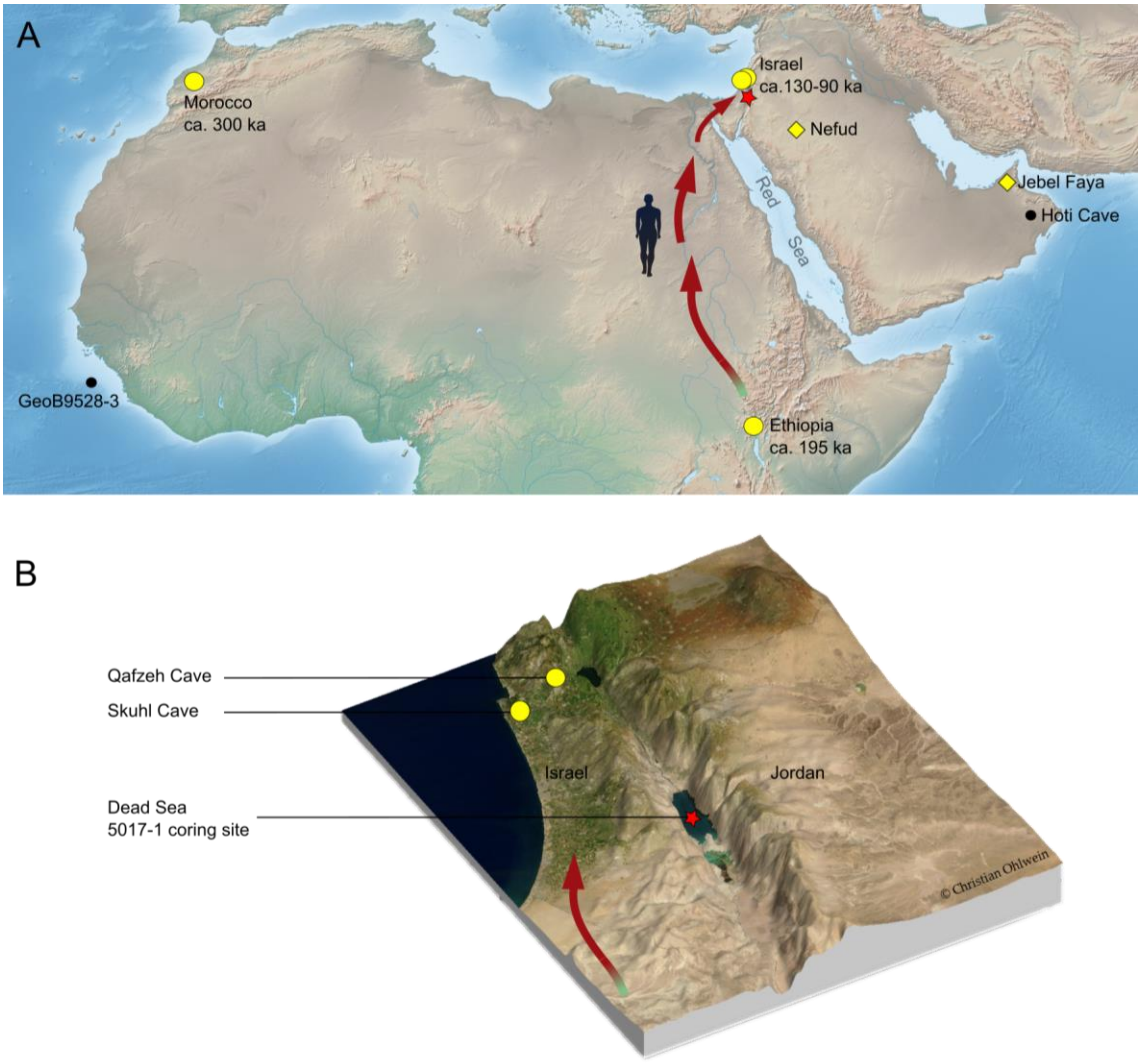

Figure 17: A) One of the dispersal routes for early modern human migrating out of Africa to the southern Levant. The yellow dots indicate archaeological sites of early modern human burials. The diamonds denote the Arabian archaeological sites with findings of MIS 5 artifacts associated with the early modern human. The black dots indicate the geological archives of the marine core GeoB9528-3 in the northwestern African margin and the Hoti Cave in Oman, respectively. The red star is the location of the Dead Sea 5017-1 cores, this study; B) Sites of early modern human burials in the southern Levant. For references please see the text.

The anatomically modern human (AMH) *Homo sapiens* first appeared in Africa (Figure 17A; Gibbons, 2017). Evidence for the earliest dispersal of modern human out of Africa comes from the archaeological findings in Israel. Since the 1930s, excavations in the Israeli caves Qafzeh and Skhul have yielded a number of archaeological remains including abundant

hominin burials (Figure 17B; Shea and Bar-Yosef, 2005). Dating techniques of thermoluminescence, ESR, and U-series are performed on burnt flints (Mercier et al., 1993; Valladas et al., 1988), teeth and bones of animals (Grün et al., 2005; McDermott et al., 1993; Schwarcz et al., 1988; Stringer et al., 1989), and humans (Grün et al., 2005; Yokoyama et al., 1997). Despite the abundance of ages obtained, the wide range of dating uncertainties and variance of these dates result in ambiguities timing human occupation in these two caves. Millard (2008) evaluates the available dates and applies a Bayesian stratigraphical model to them. The result shows the Qafzeh hominins could be ascribed to the time range of 87–97 ka, whereas the ages of Skuhl hominins are rather poorly constraint. A comprehensive chronological investigation by Grün et al. (2005) suggests the Skuhl burials are dated to 130–100 ka, most likely contemporaneous with the Qafzeh burials in a broad sense.

It is widely agreed that the early modern human dispersal has been triggered by climatic ameliorations during MIS 5 (Breeze et al., 2016; Frumkin et al., 2011; Petraglia et al., 2010; Vaks et al., 2007). In Africa, the intensification of ITCZ-controlled African summer monsoon led to pluvial conditions in the Sahara during summer insolation maxima. These pluvial intervals are termed as the Green Sahara Periods. As one of these periods, the MIS 5e is characterized by fluvio-lacustrine formations throughout the Sahara as a result of activated hydrological systems (Coulthard et al., 2013; Larrasoaña et al., 2013). For instance, permanent waterbodies such as the paleolake Megachad sustained in the Sahara Desert (Drake et al., 2011; Larrasoaña et al., 2013). The wetter-than-present conditions allowed the dispersal of Savannah plants into the Sahara Desert, as well as the occurrence of hominins and large faunas across most of the Sahara (Drake et al., 2011; Scerri et al., 2014). This conclusion is consolidated by the marine record (core GeoB9528-3) from northwestern African margin (Figure 17A), which shows C3 plants notably increased and the climate at 120–110 ka was much wetter than present in the Sahara (Figure 18A; Castañeda et al., 2009). These lines of fossil evidence agree with the biome modeling result that indicates the inhospitable area in northern Africa was substantially declined (Larrasoaña et al., 2013; Scerri et al., 2014). As a result, the connected watercourses drained northwards to the Mediterranean Sea and probably developed into viable routes that enabled colonization and migration of floras and faunas. In particular, there is a strong indication that the narrowed desert barrier between Africa and the Levant opened up a short gateway for further hominin dispersal into Eurasia (Breeze et al., 2016).

The southern Levant links northeastern Africa with southeastern Asia. A major part of this land bridge, i.e., the Sinai-Negev Desert, is nowadays hyper-arid and un-inhabitable. As concluded by Vaks et al. (2007) earlier, the Negev Desert was wetter than present especially during MIS 5e based on speleothem deposition in the area (Figure 18B). Moreover, freshwater activity in the northern Red Sea shore and in the southern Dead Sea drainage area

greatly enhanced approximately at the same time (Lazar and Stein, 2011; Waldmann et al., 2010). The increased wetness led to a significant reduction of desert components in plant communities, as suggested by the Dead Sea 5017-1A pollen record (Figure 18D). The vegetation cover correspondingly increased and the resultant biomass enhancement probably contributed to the occurrence of larger animals as food resources for the hunter-gatherers. These favorable conditions turned the desert barrier into a migrational corridor for the early modern human.

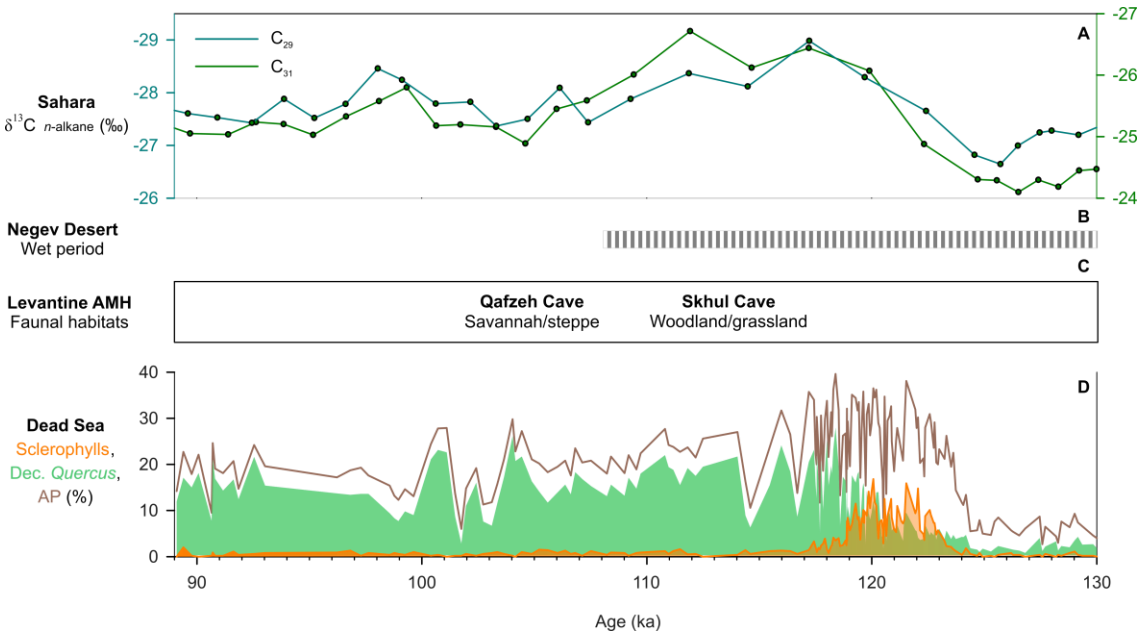

Figure 18: Compilation of MIS 5 vegetation records from the Sahara and southern Levant, as well as anatomically modern human (AMH) findings from the Levantine caves. A) *n*-alkane $\delta^{13}C$ records from marine core GeoB9528-3, northwest African margin (Castañeda et al., 2009); B) Timing of the Negev Humid Period 1 represented by speleothem deposition in the present central and southern Negev Desert (Vaks et al., 2007); C) Levantine AMH occupation during MIS 5 and inferred habitats of the faunas found in the caves (Marín-Arroyo, 2013); D) Dead Sea pollen record, this study.

Excavation of the Skuhl Cave, located at the foot of Mount Carmel near the coast, discovered abundant remains of aurochs, fallow deer, and gazelle, which were important components of the early modern human diet. This hominin site, compared with adjacent Paleolithic sites of different ages, is distinctive by an expanded diet breadth of animals inhabiting grasslands or woodlands with greater water availability. This fact demonstrates a high biodiversity and prominently ameliorated climatic conditions in northern Israel during the early modern human occupation (Marín-Arroyo, 2013). In contrast, the early modern humans in the Qafzeh Cave were notably associated with the African-Arabian faunal assemblages such as camel, ostrich, and Savannah rodents. The occurrence of these animals indicates that open lands

predominated by steppe or Savannah patches were close to the Qafzeh Cave that is situated on the presently sub-humid Galilee mountains (Rabinovich and Tchernov, 1995; Tchernov, 1998). This might be explained by the expansion of steppe or Savannah under relatively dry conditions. Nevertheless, the Qafzeh Cave area has an advantaged setting for hominins concerning its location. Provided that climate deteriorated in the southern Levant, some woodlands could still sustain in the surrounding mountains of the Qafzeh Cave. Besides, the cave is in the proximity of the warm low-lying Jordan Valley. Such a setting allowed a selective hunting in woodlands or in steppe/Savannah. It can be inferred that the strong topographic relief and the diverse ecosystems provided great potentials for the residence of early modern human in the southern Levant during MIS 5.

Regarding further AMH dispersal to southwestern Asia, the archaeological site in the Nefud Desert (northern Arabia; Figure 17A) yields a number of artifacts that share similarities with those associated with the AMH (Petragalia 2012). These remains were discovered along paleolake shores, which were indicated to be populated by grasses with some trees during MIS 5 according to carbon isotope analysis of sedimentary deposits (Petragalia 2011). Favorable conditions also occurred in the present deserts of Jordan, where paleolakes emerged and served as oases for hominin occupation (Cordova et al., 2013; Petit-Maire et al., 2002, 2010). The greening of these arid areas, especially during MIS 5e, complies with the modeling results suggesting an increased precipitation (Jennings et al., 2015) and active paleohydrological systems existed in the Levant and northern Arabia (Breeze et al., 2016).

Despite the enhanced biogeographical connectivity between Africa and Asia provided an ideal land bridge for hominin dispersal, the possibility of an alternative route via the southern end of the Red Sea should not be precluded. The discovery of AMH-related artifacts in Jebel Faya (the United Arab Emirates; Figure 17A), dated to ca. 125 ka, is indicative of a new out-of-Africa route across the Bab al-Mandab Strait (Armitage et al., 2011). It is suggested that the Red Sea level was considerably low prior to the onset of MIS 5e climatic optimum and thus a temporary land bridge was exposed for migration into Arabia. Subsequent hominin movements towards southeastern Arabia might be facilitated by increased moisture availability as indicated by the Hoti Cave speleothem records in Oman (Figure 17A; Burns et al., 2001; Fleitmann and Matter, 2009). According to Parton et al. (2015), the Arabian Peninsula was characterized by increased precipitation and freshwater availability, as well as vegetation development during MIS 5e.

Recently, AMH teeth are discovered in southern China and are dated to older than 80 ka (Liu et al., 2015). This finding provides preliminary evidence for a new dispersal route of early modern human into East Asia before the same species arrived in Europe at ca. 45 ka (Hershkovitz et al., 2015).

6.3 Response of the eastern Mediterranean vegetation to regional climatic variability

In this section, comparisons are applied to palynologically investigated sites in the EM region (Figure 19). The aim is to reveal similarities and unconformities of vegetation changes in the region and to address possible climatic mechanisms behind these changes.

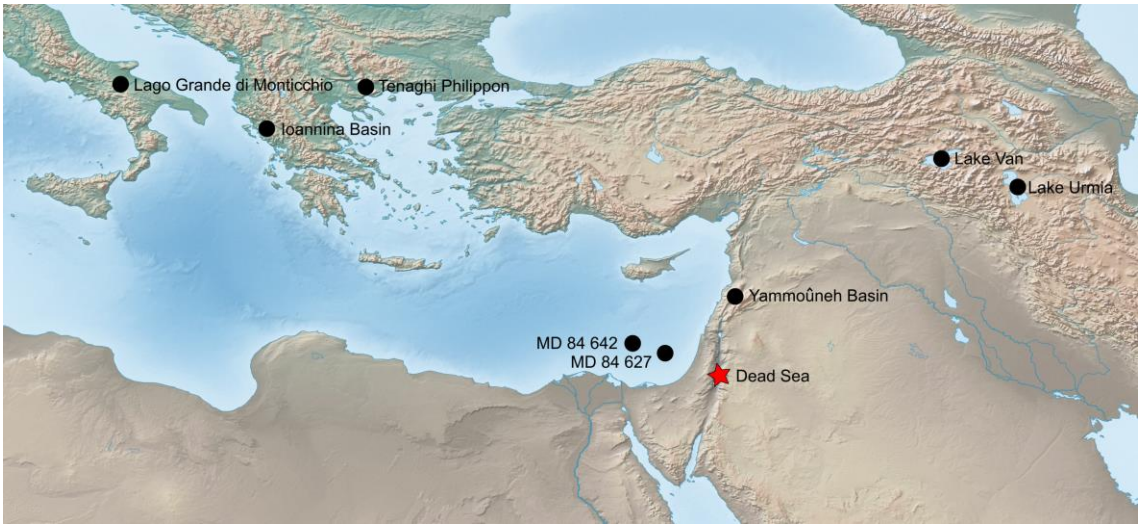

Figure 19: Palynologically studied sites in the Eastern Mediterranean region concerning the investigated interval in this study (black dots): Lago Grande di Monticchio (Allen et al., 1999; Brauer et al., 2007), Ioannina Basin (Tzedakis et al., 2002a, 2003a), Tenaghi Philippon (Milner et al., 2016; Tzedakis et al., 2006), Lake Van (Pickarski et al., 2015a, b), Lake Urmia (Djamali et al., 2008), Yammoûneh Basin (Gasse et al., 2011, 2015), and the marine cores MD 84 642 & MD 84 627 (Cheddadi and Rossignol-Strick, 1995a). The red star marks the Dead Sea 5017-1 drilling site in this study.

6.3.1 Eastern Mediterranean glacial-interglacial vegetation changes

In southern Europe and the Near East, palynologically investigated sites concerning the studied interval can be represented by the Tenaghi Philippon (Figure 20C; Milner et al., 2012, 2013, 2016; Tzedakis et al., 2006), Lake Van (Figure 20D; Pickarski et al., 2015a, 2015b), the Yammoûneh Basin (Figure 20E; Gasse et al., 2011, 2015), and the Dead Sea (Figure 20F; this study). Although these sites have differential environmental settings, the glacial-interglacial vegetation changes across the EM region basically share similarities.

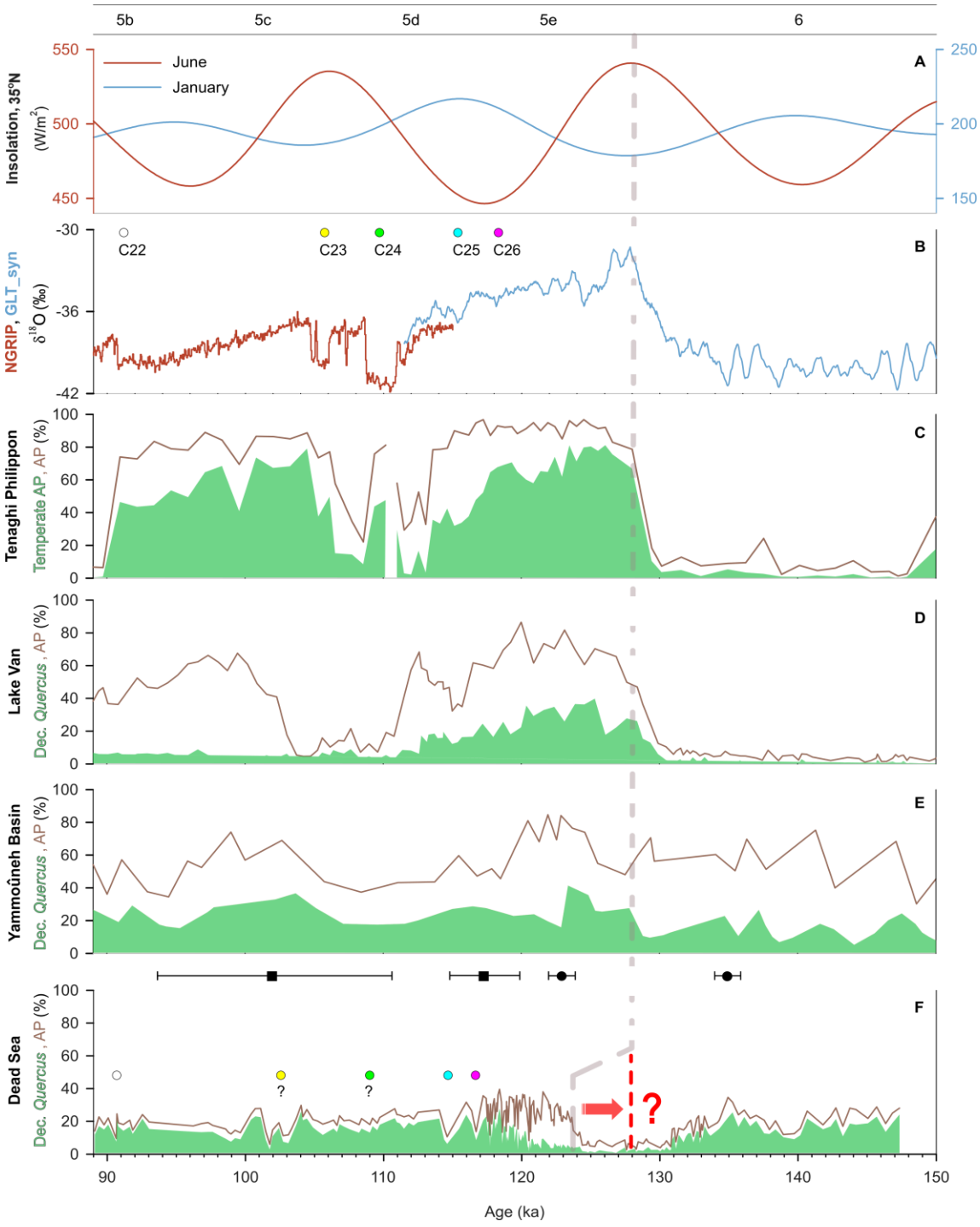

Figure 20: Comparison of Eastern Mediterranean pollen records and ice core $\delta^{18}O$ records. Arboreal pollen (AP) and deciduous *Quercus*/temperate AP data are used for correlation of pollen records. Deciduous *Quercus* accounts for the majority of temperate AP, except at Tenaghi Philippon. The dashed gray line correlates the onset of the LIG optimum in each record. Marine Isotope Stages (MIS) and Substages are after Lisiecki and Raymo (2005). A) June and January insolation at 35°N (Laskar et al., 2004); B) $\delta^{18}O$ record of NorthGRIP ice cores (Wolff et al., 2010) and synthetic ice core record GLT_syn (Barker et al., 2011). Colored dots indicate cooling events in the North Atlantic; C) Tenaghi Philippon pollen record (Tzedakis et al., 2006); D) Lake Van pollen record (Pickarski et al., 2015a, b); E) Yammoûneh Basin pollen record (Gasse et al., 2011); F) Dead Sea 5017-1A pollen record, this study. Colored dots indicate possible cooling events causing AP reductions. Black squares and dots mark the dated points. The red signs denote the possibility of a revised timing for the onset of the LIG optimum.

Generally uniform phases of vegetation successions during the last glacial-interglacial cycle, in response to the variations in orbital-driven summer insolation (Figure 21A), were characteristic of the whole EM region. That is, the MIS 5e interglacial and MIS 5c interstadial were characterized by woodland expansions, while the glacials were marked by herbaceous dispersal. This condition contradicts former paleohydrological studies that suggest pluvial conditions prevailed in the southern Levant during glacial periods, whereas the interglacials and interstadials were warm and dry (Stein, 2014 and references therein). Thus, the hypothesis that an anti-phase relationship existed between the southern Levant and the rest of the Mediterranean region in terms of glacial-interglacial climate is challenged (Stockhecke et al., 2016).

Closer comparisons of the EM pollen records show that the proportion and diversity of temperate trees were much lower in the Near East, as compared to southern Europe. This was partly a result of moisture deficit caused by a fade-out effect of the Mediterranean rains towards the continental interior. For instance, a strong continentality was implied by high contents of coniferous pollen at Lake Van. In the northern Levant, the Yammoûneh Basin is situated at high altitudes, and the growth of thermophilous plants was significantly influenced by snow and/or ice volume. Therefore, the pollen assemblages consisted of high proportions of cold-resistant conifers. In the southern Levant, it was the persistent close proximity of the Dead Sea to the steppe and desert vegetation that led to the low amounts of arboreal pollen in the Dead Sea 5017-1A record.

Moreover, the amplitude of vegetation changes in the Levant was less significant (Figure 20E, F), as compared to the other parts of the EM region. This was probably a result of buffered climatic changes in the Levant. On account of the varied topography and low-latitude setting, the Levantine mountains served as plant refugia during the glacials (Cheddadi and Khater, 2016). Glacial refugia were protected areas that were relatively warm, receiving a certain level of orographic rain supporting woody population survival. For instance, during MIS 2, scattered stands of deciduous oaks were distributed in the Sea of Galilee area where micro-climate was favorable (Miebach et al., 2017). On the Golan Height, however, a significant loss of tree population during MIS 2 was inevitable due to the high elevation and the impact of low temperatures (Schiebel, 2013). In southern Europe, glacial plant refugia were present at the Ioannina Basin, where arboreal changes had a lower amplitude than the adjacent Tenaghi Philippon area (Tzedakis et al., 2002b).

The LIG optimum is termed as the ‘Eemian’ by European pollen records, and its onset was marked by a rapid forest expansion. The varve-constraint chronology of the Lago Grande di Monticchio pollen record places the Eemian onset at 127.2 ka (Brauer et al., 2007). This timing is generally consistent with the Lake Van and southern European pollen records (Figure 20C, D). However, woodland dispersal in the southern Levant started later and the

onset of LIG optimum was dated to ca. 124 ka, based on the current age-depth model of the Dead Sea 5017-1A pollen record (Figure 20F). There seems to be a ca. 3 ka delay that cannot be explained by the migrational lag of thermophilous trees due to the existence of botanical refugia in the Levant. In this case, possible causes are discussed below.

Delayed arboreal expansion in the southern Levant. An enhanced moisture originating from the North Atlantic and the Mediterranean Sea and delivered to the Mediterranean region was the main factor driving woodland expansions (Shackleton et al., 2002). The southern Levant is located at the boundary between the Mediterranean and desert climate zones. Thus, the delayed arboreal expansion was likely a feedback to changes in southern climate systems. During summer insolation maxima, the remote effect of intensified Indian summer monsoon would lead to stronger air subsidence in the Levant and consequently to a reduced rainfall (Enzel et al., 2015). It is suggested that early Holocene woodland expansion in the Near East was delayed by the same effect (Djamali et al., 2010). An alternative explanation could be related to local conditions in the southern Levant such as fire activities. Micro-charcoal data from the Ioannina Basin show that the increase of fire activities was coeval with forest expansion during the last and present interglacial (Lawson et al., 2013). In contrast, in the southern Levant, C/T ratios of the Dead Sea 5017-1A record indicate that fires started to intensify at ca. 128 ka, prior to the spread of woodlands at ca. 124 ka. It is thus possible that intensified fire hazards potentially delayed woodland dispersal in the southern Levant.

Chronological uncertainties. In the Dead Sea 5017-1A pollen record, the timing of LIG optimum onset at ca. 124 ka highly depends on the isotope-correlated anchor ages at 123 ka and 135 ka. These two ages are subject to uncertainties due to the absence of absolute dates within a long time interval (Figure 20F). In biostratigraphical terms, however, interglacial woodland expansions in the EM region were expected to be broadly simultaneous (Litt et al., 2014). Further discussions in this respect continue in the next subsection.

6.3.2 Interglacial seasonality

Seasonal moisture deficit is characteristic of the Mediterranean region (Ziv et al., 2006). The Mediterranean sclerophylls, represented by *Olea*, *Pistacia*, *Phillyrea*, and evergreen *Quercus*, are well-adapted to summer heat and drought (Cheddadi and Rossignol-Strick, 1995a). During the LIG optimum, the prominent expansion of sclerophylls across the Mediterranean borderland pointed to a strong seasonal moisture deficit, as indicated by palynological studies from the Iberian margin in the northwest to the Levant in the southeast.

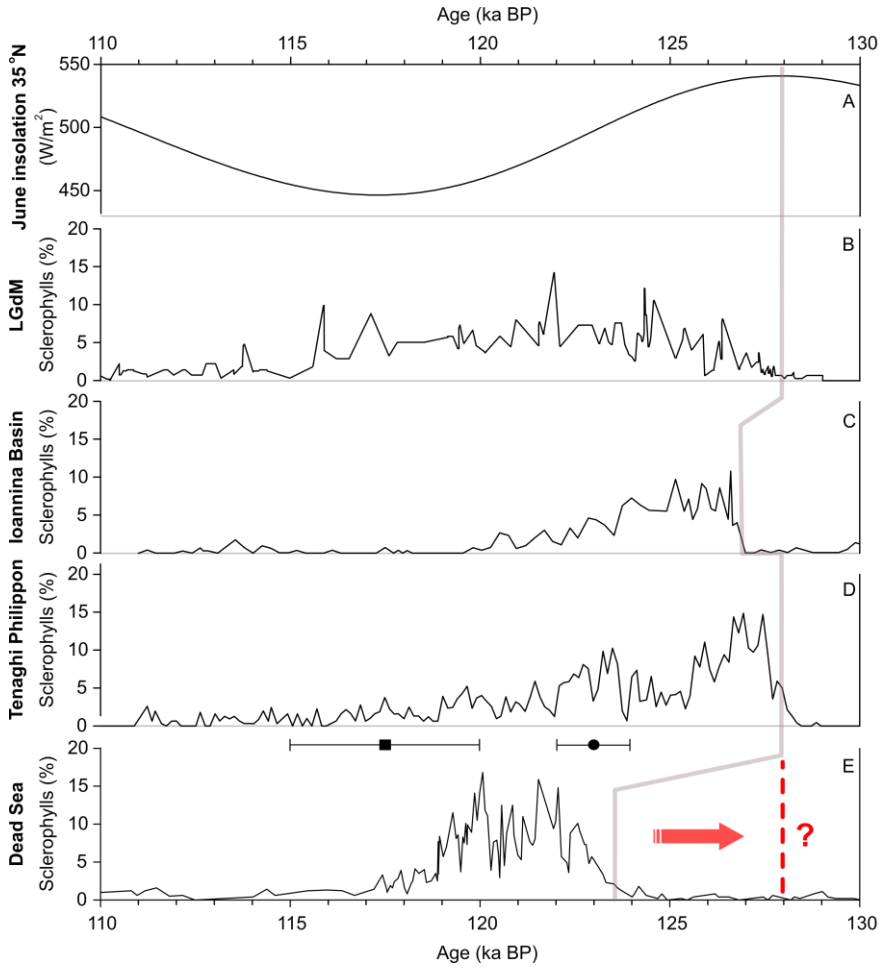

Figure 21: Eastern Mediterranean sclerophyllous pollen percentage (*Olea*, *Pistacia*, *Phillyrea*, and evergreen *Quercus*) during the LIG optimum. The verticle gray line correlates the onset of the LIG optimum in each record. A) June insolation at 35°N (Laskar et al., 2004); B) Lago Grande di Monticchio (LGdM) pollen record (Brauer et al., 2007); C) Ioannina Basin pollen record (Tzedakis, 2007); D) Tenaghi Philippon pollen record (Milner et al., 2012); E) Dead Sea pollen 5017-1A record, this study. Note that *Pistacia* is not included in the sclerophyllous pollen of this record. The red signs denote the possibility of a revised timing for the onset of the LIG optimum.

Multi-proxy analyses of the Tenaghi Philippon sediment cores highlight the role of seasonality in the northeastern Mediterranean region (Figure 21D; Milner et al., 2012). The summers between 128 and 122 ka were notably dry as indicated by peak values of sclerophyllous pollen and aragonite deposition. At the same time, the annual precipitation was high, because the sediments turned from the mire to lacustrine and numerous aquatic macrofossils were found. In Italy, similar conditions were inferred from the Lago Grande di Monticchio record (Figure 21B) that additionally suggests the enhanced seasonal drought led to active fires (Brauer et al., 2007). After this period of strong seasonality, the sclerophylls in southern Europe were reduced and were replaced by mesic woody taxa (e.g., deciduous oaks and hornbeams). It is thus concluded that the rainfall was better distributed seasonally during the later part of the LIG optimum (Tzedakis, 2007).

In the Near East, prominent increases of sclerophylls were also evident, suggesting the enhanced seasonality was Mediterranean-wide during the LIG optimum. Besides, local characteristics were obvious. For instance, olive trees accounted for the majority of sclerophylls in the southern Levant, while evergreen oaks were the most important sclerophyllous components in the northern Levant. The percentages of evergreen oak pollen never exceeded 8% in the Yammoûneh Basin record (Gasse et al., 2011), possibly a result of mitigated summer drought in the high altitudes. In the Lake Van (Pickarski et al., 2015a) and Lake Urmia (Djamali et al., 2008) records, sclerophyllous pollen were generally rare and were represented by deciduous pistachios (*Pistacia atlantica*).

In general, pistachio pollen increased synchronously with the *Olea*, *Phillyrea*, and evergreen *Quercus* pollen in the Mediterranean region during peak interglacials (Tzedakis, 2007). In this case, the Dead Sea 5017-1A pollen record is an exemption. The pistachio pollen remained relatively abundant before and after the peak LIG optimum, while other sclerophyllous taxa disappeared. The Dead Sea pistachio pollen can be attributed to evergreen (e.g., *P. lentiscus*) or deciduous species (e.g., *P. atlantica* and *P. palaestina*). During periods before and after the peak LIG optimum, it is possible that pistachio species relatively more resistant to winter frosts survived (e.g., *P. atlantica*; Freitag, 1977). Alternatively, pistachio pollen during these periods might represent an increase in populations of *P. palaestina* that tends to have a more reasonable pollen percentage as compared to other seriously underrepresented species (van Zeist and Bottema, 1977).

In terms of Holocene pollen records, early anthropogenic influences in the southern Levant make it difficult to identify to what extent the occurrence/disappearance of the olive-represented sclerophylls was caused by climate changes. Pollen records in Italy and Greece, where evergreen oaks constituted most of the Holocene sclerophylls and were less associated with human impact, provide insights into Holocene seasonality in the EM region (Peyron et al., 2011). The results show that the early to middle Holocene was characterized by sclerophyllous expansion, active fire events, and low lake levels. This phase was coeval with the increased rainfall recorded by Corchia cave isotopes in Italy (Zanchetta et al., 2007). These facts reveal a high annual precipitation superimposed by enhanced seasonality during the early to middle Holocene. Indeed, pollen-based climatic reconstruction suggests that the winter rainfall was three times higher than the summer rainfall during 9.5–7.8 ka in the northern Mediterranean region (Peyron et al., 2011).

Marine cores in the Nile Cone area (Figure 19) allow direct investigations of pollen grains incorporated in the organic-rich sapropel layers in the EM Sea (Cheddadi and Rossignol-Strick, 1995a; Rossignol-Strick and Paterne, 1999). Peak amounts of arboreal and sclerophyllous pollen characterized the sapropel event S5 and S1 dated to the time interval around 125 ka and 9–7 ka, respectively, according to the foraminiferal $\delta^{18}O$ correlated

chronology. This indicates that the circum-EM region was humid but seasonally arid during sapropel depositions. Sapropel events were recurrent (Rossignol-Strick and Paterne, 1999). They were closely related to substantially increased Nile influx triggered by intensification of African monsoons during summer insolation maxima in the Northern Hemisphere (Williams et al., 2015).

Magri and Tzedakis (2000) evaluate the link between independently-dated southern European pollen sequences with astronomical configurations, unraveling the close association between sclerophyllous expansion and perihelion in boreal summer. They found out that the sclerophylls became competitive against the mesic elements by adapting to the increased summer radiation and evaporation. During the past 200 ka, the highest mid-June insolation at 35°N occurred at ca. 128 ka (540 W/m^2; Berger et al., 2007), triggering the remarkable sclerophyllous expansion in the Mediterranean region (Figure 21A). This challenges the timing of ca. 124 ka for the initial sclerophyllous expansion inferred from the current age-depth model of the Dead Sea 5017-1A pollen record (Figure 21E). Therefore, chronological uncertainties are more probable as the cause for the assumed delay of arboreal expansion in the southern Levant.

It is interesting to note that the periods of summer insolation maxima were also marked by winter insolation minima. The low winter temperatures theoretically would have inhibited the survival of frost-intolerant sclerophylls. On the contrary, these plants disappeared when winter insolation increased and seasonal contrast was correspondingly declined during the ice-growth glacials. During the interstadials, a weakened seasonal cycle led these warm periods to be featured by the predominance of temperate trees in the woodlands.

6.3.3 Climatic instability

In the Northern Hemisphere, a number of paleorecords reflect long-term environmental changes in the mid-high latitudes. Among them, the $\delta^{18}O$ records of ice cores, e.g., the North Greenland ice cores (NGRIP members, 2004), document air temperature variations. The marine records in the North Atlantic provide information of changes in the SST and ice volume (e.g., Chapman and Shackleton, 1999). These changes were important drivers for shifts of thermohaline circulations in the North Atlantic, as well as atmospheric changes in Europe and the Near East (e.g., Shackleton et al., 2002).

The long-term variations were disrupted by a series of millennial-scale cold phases (Figure 20B; NGRIP members, 2004). The end of the LIG optimum was marked by cooling events C26 and C25 in the mid-latitude North Atlantic. The C26 event occurred at ca. 118 ka when

the ice volume initiated to increase (Sirocko et al., 2005). It is indicated to be a short aridity pulse characterized by a 2–3 °C SST reduction. Comparatively, the C25 event at ca. 115 ka was recorded by a substantial SST drop of ca. 6–7 °C during the initial course of continental ice-sheet build-up (Chapman and Shackleton, 1999; Cortijo et al., 1999). During the early last glacial, the ice volume progressively increased in the high latitudes but still allowed the thermohaline circulation to operate and transport heat to the subpolar North Atlantic (McManus et al., 2002). The C24 event at ca. 110 ka was associated with major ice-sheet collapses accompanied by a 6–7°C of SST drop. The C23 and C22 events were less prominent, as indicated by minor decreases in North Atlantic SST (Chapman and Shackleton, 1999).

During the cold phases, the reduced SST led to low sea-water evaporation and subsequently to a poor moisture content of the low-pressure atmospheric systems over the Mediterranean region (Tzedakis, 2005). As a consequence, the cooling events were registered as intervals of abrupt aridity in southern Europe and the Near East (Allen et al., 1999; Brauer et al., 2007; Milner et al., 2013; Pickarski et al., 2015b; Tzedakis et al., 2003a; Wolff et al., 2010).

These hydroclimatic shifts were expressed as various extents and durations of woodland contractions across the Mediterranean region (Brauer et al., 2007; Milner et al., 2013; Pickarski et al., 2015a; Tzedakis et al., 2003a). Moreover, the numbers and timing of the cooling events recorded might differ between the archives. In the Dead Sea 5017-1A pollen record, the millennial-scale aridities can be mirrored by rapid AP reductions, although the dating uncertainties and buffered AP changes restrict a precise correlation with the cooling events in the North Atlantic (Figure 20F). In the northern Levant, the low sampling resolution of the Yammoûneh Basin pollen record does not allow a reliable recognition of cooling events (Figure 20E). In the Tenaghi Philippon and Lake Van pollen records (Figure 20C, D), the cooling events are prominent as indicated by the abrupt and pronounced declines in woody cover.

Climatic instabilities were also registered by the lithological shifts of Dead Sea sediments. The lake-stand indicators (i.e., gypsum layer) from outcrops in the DSB marginal areas identified abrupt and extreme Dead Sea lake-level drops since MIS 4 (Torfstein et al., 2013b). The lake-level drops were attributed to catastrophic aridities caused by the decline of Mediterranean storm tracks that were further related to the cold North Atlantic sea surface. Such a sensitive response of hydrological variations since MIS 4 is also observed from the Soreq Cave $\delta^{18}O$ record (Bar-Matthews et al., 1999).

During the early last glacial, the massive halite deposition in Dead Sea 5017-1A sediment cores was suggested to be a feedback of lake-level drops to the cooling events C24 and C22+21 (Neugebauer et al., 2016). However, it is problematic to directly correlate the halite

intervals with the cooling events, because the halite deposition coincident with the C24 event is the uppermost part of the long halite interval deposited during MIS 5e. Hence, in addition to pollen and deposit facies, more proxies and archives are needed for better investigating climatic instabilities in the southern Levant during MIS 5.

7 Summary

This study analyzes pollen, non-pollen-palynomorphs, and charcoal from the deep-drilled Dead Sea 5017-1A sediment cores. It reconstructs a high-resolution vegetation and environment history of the southern Levant at 147–89 ka, encompassing the late penultimate glacial (147.3–130.9 ka), the initial warming (130.9–124.2 ka), the last interglacial optimum (124.2–115.5 ka), and the early last glacial (115.5–89.1 ka).

The result shows that the late penultimate glacial and early last glacial were cool and were characterized by steppe and desert expansions. Sub-humid conditions were confined to the mountains where moderate amounts of deciduous oaks were distributed. The initial warming was marked by a prevalence of desert components and a virtual absence of trees and shrubs. A concomitant increase in frost-sensitive pistachio trees suggests that the extensive aridity was accompanied by a prominent warming. The last interglacial optimum was initiated by an abrupt grass expansion replacing desert components and was followed by a fast spread of woodlands in the mountains. A remarkable sclerophyllous increase points to enhanced Mediterranean rains superimposed by strong seasonal drought.

The predominance of herbaceous pollen during the whole investigated interval suggests that steppe and desert vegetation was persistently close to the Dead Sea in the low latitudes. Due to the prominent vegetation gradient in the southern Levant, the relatively low arboreal pollen contents probably underestimate the actual density of trees and shrubs in the northern mountains (e.g., the Galilee Mountains). The major headwater area of the Dead Sea is located in these places, where a strong arboreal evapotranspiration effect is observed. During the last interglacial optimum, the abundant trees and shrubs possibly consumed a significant part of the precipitation. Consequently, small water volumes were supplied to the Dead Sea, resulting in extremely low lake levels and massive halite deposition. A reverse scenario might explain the contrast between the coeval occurrence of low woodland coverage and high lake stands during glacials.

A synthesis of regional records (pollen, lacustrine sediments, and speleothems) indicates that the environment of the southern Levant at 128–122 ka was unstable, marked by generally low vegetation cover, intensified fire activities, and extensive flood-induced erosions. There were signs of moisture contribution from the sub-tropics during this episode, despite the dominant control of the Mediterranean rains during the whole investigated interval. In the southern Dead Sea drainage area, the sub-tropical atmospheric systems brought short-lived rainstorms that led to the delivery of numerous coarse detritus to the Dead Sea.

Archaeological evidence from the Israeli caves proves the occupation of anatomically modern human during 130–90 ka. This period was characterized by activated hydrological systems in the Sahara and the Negev Desert, as well as increased vegetation cover in the Sahara and the southern Levant. Hence, the present desert barrier between Africa and Asia was probably turned into a migrational corridor. In the southern Levant, the diverse ecosystems provided shelters and potential food resources for the residence and further dispersal of the hominins.

In the whole eastern Mediterranean region, a comparatively high abundance of trees and shrubs was characteristic of the last interglacial and vice versa for the glacials. This condition disapproves former hypothesis that an anti-phase relationship existed between the southern Levant and the rest of the Mediterranean region in terms of glacial-interglacial climate. The Mediterranean-wide phenomenon of sclerophyllous expansion during the early phase of the last interglacial points to the boreal summer insolation maximum as the trigger. It further questions the possibility of delayed arboreal expansion in the southern Levant that is based on the current age-depth model of the Dead Sea 5017-1A pollen record.

This study fills the gap of vegetation history during 147–89 ka in the southern Levant. The independent paleobotanical reconstructions add information to the paleoenvironment and gain new insights into resolving the controversies indicated by existing paleorecords. It improves our understanding of the environmental setting for early modern human dispersal, as well as the close association between the Mediterranean vegetation changes and the Atlantic-Mediterranean atmospheric-oceanic circulations.

List of figures

List of tables

List of abbreviations

aad	Alternating aragonite and detritus
AMH	Anatomically modern human
amsl	Above mean sea level
AP	Arboreal pollen
blf	Below lake floor
bmsl	Below mean sea level
C/T ratio	Charcoal to terrestrial pollen ratio
ca.	*circa*, approximately
CONISS	Constrained incremental sums of squares cluster analysis
DLDS	Deep Lake Drilling System
DOSECC	Drilling, Observation and Sampling of the Earth's Continental Crust
DSB	Dead Sea Basin
DSDDP	Dead Sea Deep Drilling Project
DST	Dead Sea Transform
e.g.	*exempli gratia*, for example
EM	Eastern Mediterranean
FM.	Formation
hd	Halite and detrital marl
hh	Homogeneous halite
i.e.	*id est*, that is
ICDP	International Continental Scientific Drilling Program
IODP	Integrated Ocean Drilling Program
ITCZ	Intertropical Convergence Zone
ka	*kiloannum*, thousand of years ago
LB	Lower boundary
ld	Laminated detritus
lh	Layered halite
LIG	Last interglacial
MAP	Mean annual precipitation
MAT	Mean annual temperature
MIS	Marine isotope stage
NAP	Non-arboreal pollen
NGRIP	North Greenland Ice-core Project
NHP	Negev Humid Period
NPP	Non-pollen-palynomorph
PAS	Pollen assemblage superzone
PAZ	Pollen assemblage zone
SST	Sea-surface temperature

Appendix

Table A.1: List of analyzed pollen samples from DSDDP cores 5017-1A, including information of sample ID, core section, depth of sample in core section (cm), composite sample depth (m blf = meter below lake floor) and deposit type of the pollen sample.

Sample ID	Core section	Depth in section (cm)	Composite depth (m blf)	Deposit type
PO762	5017_1A_80A_1	95.0–102.0	199.245	halite
PO312	5017_1A_80A_1	143.0–150.0	199.725	halite
PO420	5017_1A_80A_2	51.5–60.0	200.318	halite
PO314	5017_1A_80A_2	100.0–109.0	200.805	halite
PO421	5017_1A_81A_1	39.5–46.0	201.738	halite
PO79	5017_1A_81A_1	49.0–51.0	201.810	laminae
PO422	5017_1A_81A_1	63.0–70.5	201.978	halite
PO315	5017_1A_81A_2	20.0–28.0	202.550	halite
PO80	5017_1A_81A_2	97.0–99.0	203.290	laminae
PO423	5017_1A_81A_3	31.0–35.5	203.643	halite
PO81	5017_1A_82A_1	39.0–41.0	204.760	laminae
PO316	5017_1A_82A_1	115.0–121.0	205.540	halite
PO82	5017_1A_84A_1	17.0–19.0	210.640	laminae
PO83	5017_1A_84A_2	20.0–22.0	211.600	laminae
PO424	5017_1A_84A_2	95.5–98.0	212.358	laminae
PO84	5017_1A_84A_3	29.0–31.0	212.890	laminae
PO426	5017_1A_85A_1	88.0–90.0	214.400	laminae
PO85	5017_1A_85A_2	29.0–31.0	214.735	laminae
PO427	5017_1A_85A_2	57.5–60.0	215.023	laminae
PO428	5017_1A_85A_2	104.5–106.5	215.490	laminae
PO86	5017_1A_85A_3	45.0–47.0	216.095	laminae
PO87	5017_1A_86A_1	76.0–78.0	217.330	laminae
PO429	5017_1A_86A_2	36.0–38.0	217.830	laminae
PO88	5017_1A_86A_2	98.0–100.0	218.450	laminae
PO430	5017_1A_86A_3	38.0–40.0	219.050	laminae
PO431	5017_1A_86A_3	82.5–84.5	219.495	laminae
PO89	5017_1A_86A_3	116.0–118.0	219.830	laminae
PO90	5017_1A_87A_1	86.0–88.0	220.480	laminae
PO432	5017_1A_87A_2	39.0–41.0	220.910	laminae
PO433	5017_1A_87A_2	91.0–93.0	221.430	laminae
PO434	5017_1A_87A_3	4.0–6.0	221.760	laminae
PO91	5017_1A_87A_3	45.0–47.0	222.170	laminae
PO435	5017_1A_87A_3	97.5–100.0	222.698	laminae
PO436	5017_1A_87A_3	115.0–117.0	222.870	laminae

Table A.1: continued from previous page

Sample ID	Core section	Depth in section (cm)	Composite depth (m)	Deposit type
PO92	5017_1A_88A_1	59.0–61.0	223.260	laminae
PO437	5017_1A_88A_2	28.5–30.5	223.870	laminae
PO93	5017_1A_88A_2	74.0–76.0	224.325	laminae
PO439	5017_1A_88A_3	6.5–8.5	224.850	laminae
PO94	5017_1A_88A_3	66.0–68.0	225.445	laminae
PO440	5017_1A_88A_3	113.0–115.5	225.918	laminae
PO442	5017_1A_89A_1	53.5–55.5	226.255	laminae
PO95	5017_1A_89A_1	80.0–82.0	226.520	laminae
PO443	5017_1A_89A_2	35.5–37.5	226.955	laminae
PO96	5017_1A_89A_2	89.0–91.0	227.490	laminae
PO97	5017_1A_89A_3	67.0–68.0	228.465	laminae
PO444	5017_1A_89A_3	91.0–93.0	228.710	laminae
PO98	5017_1A_90A_1	77.0–79.0	229.540	laminae
PO445	5017_1A_90A_2	13.0–15.0	229.790	laminae
PO446	5017_1A_90A_2	61.0–62.0	230.265	laminae
PO447	5017_1A_90A_2	86.5–87.5	230.520	laminae
PO99	5017_1A_91A_1	19.0–21.0	232.010	laminae
PO449	5017_1A_91A_1	41.0–43.0	232.230	laminae
PO448	5017_1A_91A_1	69.5–71.0	232.513	laminae
PO100	5017_1A_91A_1	111.0–113.0	232.930	laminae
PO317	5017_1A_91A_2	14.0–23.0	233.395	halite
PO800	5017_1A_91A_2	66.0–68.0	233.880	laminae
PO318	5017_1A_91A_2	109.5–113.5	234.325	halite
PO320	5017_1A_93A_1	26.0–33.0	236.435	halite
PO319	5017_1A_93A_1	75.0–81.0	236.920	halite
PO450	5017_1A_93A_1	105.0–111.0	237.220	halite
PO321	5017_1A_94A_1	18.0–26.0	238.410	halite
PO322	5017_1A_94A_1	89.0–96.0	239.115	halite
PO323	5017_1A_94A_1	146.0–148.0	239.660	laminae
PO451	5017_1A_94A_2	40.0–41.0	240.095	laminae
PO325	5017_1A_94A_3	10.0–12.0	240.800	laminae
PO326	5017_1A_94A_3	60.0–65.0	241.315	halite
PO328	5017_1A_95A_1	80.0–82.0	241.860	laminae
PO452	5017_1A_95A_1	117.0–124.0	242.255	halite
PO329	5017_1A_95A_1	124.0–126.0	242.300	laminae
PO330	5017_1A_95A_2	35.0–44.0	242.955	halite
PO454	5017_1A_95A_2	83.5–90.5	243.430	halite
PO331	5017_1A_95A_2	122.0–128.0	243.810	halite
PO332	5017_1A_96A_1	44.0–50.0	244.570	halite

Table A.1: continued from previous page

Sample ID	Core section	Depth in section (cm)	Composite depth (m)	Deposit type
PO333	5017_1A_96A_1	108.0–115.0	245.215	halite
PO334	5017_1A_96A_2	62.0–68.0	245.950	halite
PO335	5017_1A_96A_2	122.0–124.0	246.530	laminae
PO336	5017_1A_96A_2	138.0–141.0	246.695	halite
PO337	5017_1A_97A_1	26.0–36.0	247.450	halite
PO338	5017_1A_97A_2	13.0–15.0	247.710	laminae
PO339	5017_1A_97A_2	61.0–67.0	248.210	halite
PO340	5017_1A_97A_3	40.5–42.5	249.025	laminae
PO456	5017_1A_98A_1	8.5–14.5	250.155	halite
PO341	5017_1A_98A_1	55.0–60.0	250.615	halite
PO101	5017_1A_98A_2	81.5–83.5	251.645	laminae
PO102	5017_1A_98A_3	52.0–54.0	252.567	laminae
PO458	5017_1A_98A_3	88.0–90.5	252.930	laminae
PO343	5017_1A_98A_3	103.0–110.0	253.102	halite
PO460	5017_1A_98A_3	112.0–114.0	253.167	laminae
PO345	5017_1A_99A_1	28.0–34.0	253.400	halite
PO346/2	5017_1A_100A_1	0.0–10.0	254.180	halite
PO347	5017_1A_100A_2	47.0–53.0	254.855	halite
PO348	5017_1A_100A_3	61.0–68.0	256.230	halite
PO349	5017_1A_100A_4	26.0–37.0	256.895	halite
PO463	5017_1A_101A_1	10.0–19.0	257.325	halite
PO350	5017_1A_101A_1	66.0–73.0	257.875	halite
PO465	5017_1A_101A_2	14.5–16.0	258.348	laminae
PO103	5017_1A_102A_1	25.0–27.0	258.640	laminae
PO353	5017_1A_102A_1	57.0–59.0	258.960	laminae
PO466	5017_1A_102A_1	87.0–88.0	259.255	laminae
PO467	5017_1A_102A_1	88.0–97.0	259.305	halite
PO355	5017_1A_102A_2	17.0–20.0	259.775	halite
PO468	5017_1A_102A_2	56.5–64.0	260.193	halite
PO356	5017_1A_102A_3	23.0–25.0	260.830	laminae
PO104	5017_1A_102A_3	77.0–79.0	261.370	laminae
PO357	5017_1A_103A_1	45.0–51.0	261.900	halite
PO358	5017_1A_103A_2	15.0–23.0	262.530	halite
PO359	5017_1A_103A_2	68.0–74.0	263.050	halite
PO360	5017_1A_103A_3	24.0–30.0	263.578	halite
PO361	5017_1A_103A_3	97.0–103.0	264.308	halite
PO362	5017_1A_104A_1	32.0–37.0	264.815	halite
PO471	5017_1A_104A_1	103.0–105.0	265.510	laminae
PO363	5017_1A_104A_1	141.0–143.0	265.890	laminae

Table A.1: continued from previous page

Sample ID	Core section	Depth in section (cm)	Composite depth (m)	Deposit type
PO364	5017_1A_104A_2	12.0–18.0	266.120	halite
PO472	5017_1A_104A_2	52.5–60.0	266.533	halite
PO473	5017_1A_104A_2	114.0–120.0	267.140	halite
PO365	5017_1A_105A_1	7.0–13.0	267.610	halite
PO366	5017_1A_105A_1	80.5–82.5	268.325	laminae
PO367	5017_1A_105A_1	136.0–138.0	268.880	laminae
PO474	5017_1A_105A_2	13.0–14.0	269.145	laminae
PO368	5017_1A_105A_2	95.0–97.0	269.970	laminae
PO369	5017_1A_105A_3	67.0–72.0	270.705	halite
PO370	5017_1A_106A_1	47.0–53.0	271.060	halite
PO371	5017_1A_106A_2	45.0–51.0	272.530	halite
PO477	5017_1A_106A_2	103.0–110.0	273.115	halite
PO372	5017_1A_107A_1	0.0–5.0	273.635	halite
PO373	5017_1A_107A_1	70.0–75.0	274.335	halite
PO480	5017_1A_108A_1	85.5–92.0	277.548	halite
PO375	5017_1A_108A_1	129.0–134.0	277.975	halite
PO376	5017_1A_108A_2	33.0–38.0	278.519	halite
PO377	5017_1A_108A_2	105.0–107.0	279.224	laminae
PO481	5017_1A_109A_1	68.0–69.0	280.395	laminae
PO378	5017_1A_109A_1	103.0–105.0	280.750	laminae
PO105	5017_1A_109A_1	135.5–137.5	281.075	laminae
PO106	5017_1A_109A_3	132.0–134.0	282.703	laminae
PO482	5017_1A_110A_1	34.5–37.0	283.118	laminae
PO483	5017_1A_110A_1	136.5–137.5	284.130	laminae
PO107	5017_1A_110A_2	16.0–18.0	284.435	laminae
PO484	5017_1A_110A_2	76.5–78.5	285.040	laminae
PO108	5017_1A_110A_2	136.0–138.0	285.635	laminae
PO485	5017_1A_111A_1	28.0–30.0	286.090	laminae
PO486	5017_1A_111A_1	111.0–113.0	286.920	laminae
PO109	5017_1A_111A_1	140.0–142.0	287.210	laminae
PO487	5017_1A_111A_2	64.0–66.0	287.950	laminae
PO110	5017_1A_111A_2	97.0–99.0	288.280	laminae
PO488	5017_1A_111A_2	134.5–137.0	288.658	laminae
PO489	5017_1A_112A_1	75.5–77.5	289.615	laminae
PO111	5017_1A_112A_1	97.0–99.0	289.830	laminae
PO112	5017_1A_112A_2	27.0–29.0	290.230	laminae
PO490	5017_1A_112A_2	95.5–98.0	290.918	laminae
PO491	5017_1A_113A_1	9.0–10.0	291.985	laminae
PO380	5017_1A_113A_1	44.5–46.5	292.345	laminae

Table A.1: continued from previous page

Sample ID	Core section	Depth in section (cm)	Composite depth (m)	Deposit type
PO381	5017_1A_113A_1	94.0–96.0	292.840	laminae
PO382	5017_1A_114A_1	58.0–60.0	294.120	laminae
PO383	5017_1A_114A_1	114.5–116.5	294.685	laminae
PO384	5017_1A_115A_1	31.0–33.0	295.270	laminae
PO385	5017_1A_115A_3	19.0–21.0	297.240	laminae
PO494	5017_1A_115A_3	49.5–51.0	297.543	laminae
PO386	5017_1A_116A_1	49.5–51.5	298.505	laminae
PO387	5017_1A_116A_2	52.5–54.5	299.440	laminae
PO388	5017_1A_117A_1	61.5–63.5	301.675	laminae
PO496	5017_1A_117A_2	17.0–19.0	302.090	laminae
PO390	5017_1A_117A_2	62.5–64.5	302.545	laminae
PO391	5017_1A_118A_3	41.5–43.5	304.225	laminae
PO498	5017_1A_118A_3	72.0–76.0	304.540	halite
PO392	5017_1A_118A_3	123.5–125.5	305.045	laminae
PO393	5017_1A_119A_1	45.0–50.0	306.325	halite
PO394	5017_1A_119A_2	26.5–28.5	307.105	laminae
PO397	5017_1A_120A_1	45.0–51.0	307.620	halite
PO395	5017_1A_120A_1	116.0–118.0	308.310	laminae
PO499	5017_1A_121A_1	0.0–5.0	309.965	halite
PO398	5017_1A_121A_1	68.0–74.0	310.650	halite
PO113	5017_1A_121A_1	115.0–117.0	311.100	laminae
PO500	5017_1A_121A_2	31.0–33.0	311.640	laminae
PO114	5017_1A_121A_2	88.0–90.0	312.210	laminae
PO115	5017_1A_121A_3	52.0–54.0	312.860	laminae
PO502	5017_1A_122A_1	9.5–12.0	313.298	laminae
PO116	5017_1A_122A_1	48.0–50.0	313.680	laminae
PO503	5017_1A_122A_1	95.0–97.0	314.150	laminae
PO400	5017_1A_122A_2	2.0–8.0	314.590	halite
PO117	5017_1A_122A_2	75.0–77.0	315.300	laminae
PO118	5017_1A_123A_1	28.0–30.0	316.530	laminae
PO504	5017_1A_123A_1	87.5–89.5	317.125	laminae
PO505	5017_1A_123A_2	2.0–4.5	317.663	lamine
PO119	5017_1A_123A_2	70.0–72.0	318.340	laminae
PO120	5017_1A_124A_1	16.0–18.0	319.010	laminae
PO401	5017_1A_125A_1	47.0–52.0	319.835	halite
PO121	5017_1A_125A_1	98.0–100.0	320.330	laminae
PO784	5017_1A_125A_2	6.0–8.0	320.710	laminae
PO122	5017_1A_125A_2	40.0–42.0	321.050	laminae
PO786	5017_1A_125A_2	63.0–64.0	321.275	laminae

Table A.1: continued from previous page

Sample ID	Core section	Depth in section (cm)	Composite depth (m)	Deposit type
PO123	5017_1A_126A_1	8.0–10.0	321.800	laminae
PO124	5017_1A_126A_2	10.0–12.0	322.800	laminae
PO507	5017_1A_126A_2	65.0–66.0	323.345	laminae
PO125	5017_1A_127A_1	35.0–37.0	325.120	laminae
PO126	5017_1A_127A_2	3.0–5.0	325.550	laminae
PO127	5017_1A_128A_1	30.0–32.0	327.740	laminae
PO508	5017_1A_128A_1	82.0–84.5	328.263	laminae
PO128	5017_1A_128A_1	125.0–127.0	328.690	laminae
PO129	5017_1A_128A_2	24.0–26.0	329.130	laminae
PO509	5017_1A_128A_2	67.0–68.5	329.558	laminae
PO130	5017_1A_128A_2	112.0–114.0	330.010	laminae
PO510	5017_1A_129A_1	10.0–14.0	330.600	halite
PO131	5017_1A_129A_1	50.0–52.0	330.990	laminae
PO511	5017_1A_129A_1	94.5–95.5	331.430	laminae
PO132	5017_1A_130A_1	47.0–49.0	332.010	laminae
PO133	5017_1A_130A_2	45.0–47.0	332.820	laminae
PO512	5017_1A_130A_2	91.0–92.0	333.275	laminae
PO134	5017_1A_130A_3	31.0–33.0	333.780	laminae
PO135	5017_1A_131A_1	36.0–38.0	334.950	laminae
PO513	5017_1A_131A_1	91.0–93.0	335.500	laminae
PO136	5017_1A_131A_1	130.0–132.0	335.890	laminae
PO514	5017_1A_131A_2	48.0–50.5	336.413	laminae
PO137	5017_1A_131A_2	100.0–102.0	336.930	laminae
PO515	5017_1A_131A_2	145.0–147.0	337.380	laminae
PO138	5017_1A_132A_1	64.0–66.0	338.270	laminae
PO518	5017_1A_132A_2	11.0–12.5	338.908	laminae
PO139	5017_1A_132A_2	78.0–80.0	339.580	laminae
PO519	5017_1A_132A_3	28.0–30.0	340.080	laminae
PO140	5017_1A_132A_3	80.0–82.0	340.600	laminae

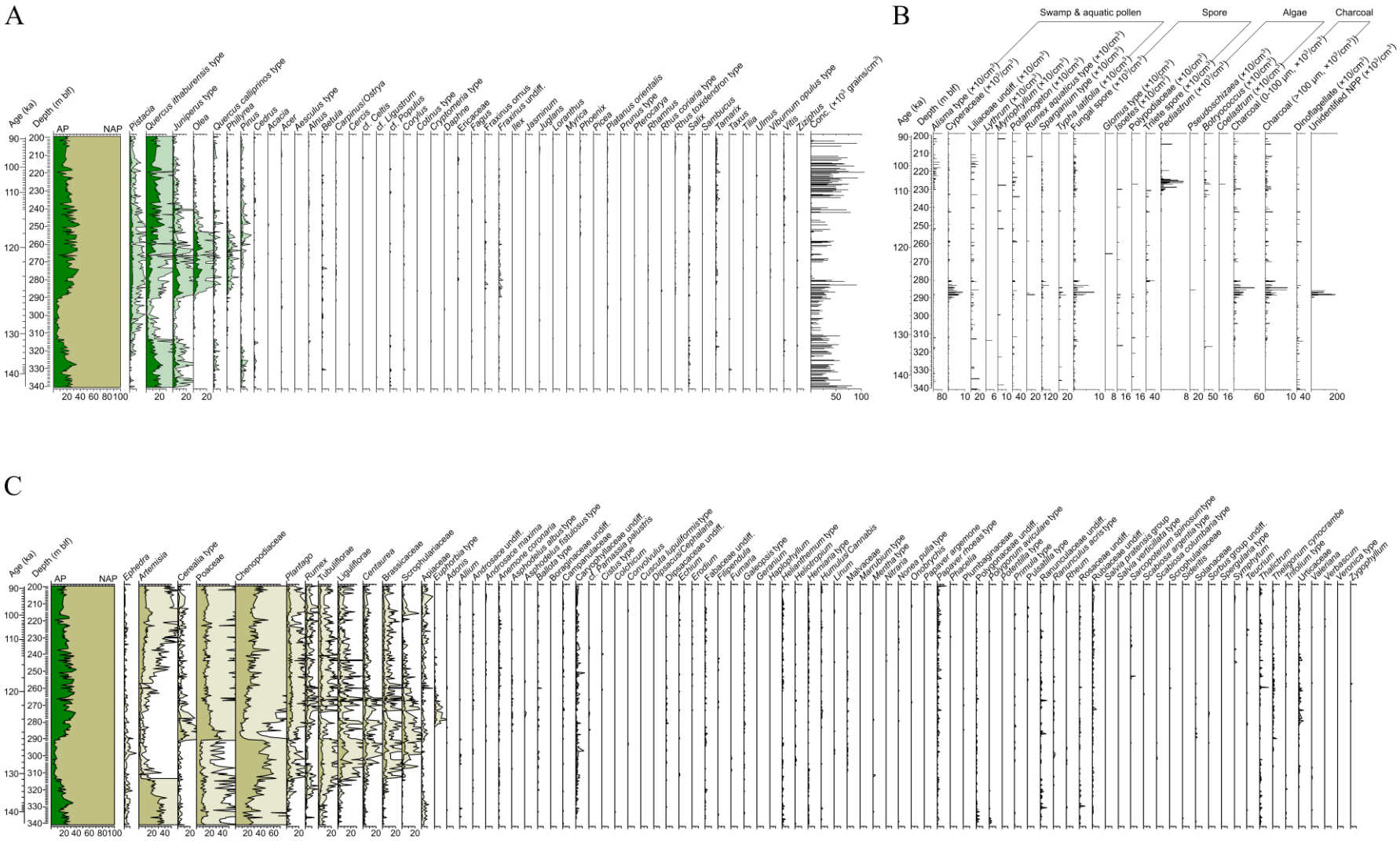

Figure A.1: Complete palynomorph diagram of the Dead Sea core 5017-1A sediments at the depth between 340.6 and 199.2 m blf. A) Arboreal pollen (AP) percentages (%) and terrestrial pollen concentration (grains/cm^3); B) Concentration of swamp and aquatic pollen (grains/cm^3), charcoal (particles/cm^3) and non-pollen-palynomorphs (NPPs) including spore, algae and other objects (specimens/cm^3); C) Non-arboreal pollen (NAP) percentages (%). A 5-fold exaggeration is applied to the pollen percentages.

References

Agnon, A., 2014. Pre-instrumental earthquakes along the Dead Sea Rift, in: Garfunkel, Z., Ben-Avraham, Z., Kagan, E. (Eds.), Dead Sea transform fault system: reviews. Springer, pp. 207-261.

Aharonovich, S., Sharon, G., Weinstein-Evron, M., 2014. Palynological investigations at the Middle Palaeolithic site of Nahal Mahanayeem Outlet, Israel. Quaternary International 331, 149-166.

Al-Eisawi, D., 1996. Vegetation of Jordan. UNESCO-Cairo Office, Egypt.

Al-Eisawi, D., Dajani, B., 1987. A study of airborne pollen grains in Amman, Jordan. Grana 26, 231-238.

Al-Eisawi, D., Dajani, B., 1988. Airborne pollen of Jordan. Grana 27, 219-227.

Al-Qura'n, S., 2008. Analysis of airborne pollen fall in Tafileh, Jordan, 2002-2003. World Applied Sciences Journal 4, 730-735.

Allen, J.R., Brandt, U., Brauer, A., Hubberten, H.-W., Huntley, B., Keller, J., Kraml, M., Mackensen, A., Mingram, J., Negendank, J.F., 1999. Rapid environmental changes in southern Europe during the last glacial period. Nature 400, 740-743.

Allen, J.R., Hickler, T., Singarayer, J.S., Sykes, M.T., Valdes, P.J., Huntley, B., 2010. Last glacial vegetation of northern Eurasia. Quaternary Science Reviews 29, 2604-2618.

Allen, J.R., Huntley, B., 2009. Last Interglacial palaeovegetation, palaeoenvironments and chronology: a new record from Lago Grande di Monticchio, southern Italy. Quaternary Science Reviews 28, 1521-1538.

Allen, J.R., Watts, W.A., Huntley, B., 2000. Weichselian palynostratigraphy, palaeovegetation and palaeoenvironment; the record from Lago Grande di Monticchio, southern Italy. Quaternary International 73, 91-110.

Almogi-Labin, A., Bar-Matthews, M., Shriki, D., Kolosovsky, E., Paterne, M., Schilman, B., Ayalon, A., Aizenshtat, Z., Matthews, A., 2009. Climatic variability during the last ~90 ka of the southern and northern Levantine Basin as evident from marine records and speleothems. Quaternary Science Reviews 28, 2882-2896.

Aloni, E., Eshel, A., Waisel, Y., 1997. The botanical conquest of the newly exposed shores of the Dead Sea, in: Niemi, T.M., Ben-Avraham, Z., Gat, J.R. (Eds.), The Dead Sea: The lake and its setting. Oxford University Press, New York, Oxford, pp. 277-281.

Alpert, P., Neeman, B., Shay-El, Y., 1990. Climatological analysis of Mediterranean cyclones using ECMWF data. Tellus A 42, 65-77.

Alpert, P., Shafir, H., Issahary, D., 1997. Recent changes in the climate of the Dead Sea Valley. Climatic Change 7, 1-25.

Alpert, P., Ziv, B., 1989. The Sharav cyclone: observations and some theoretical considerations. Journal of Geophysical Research: Atmospheres (1984–2012) 94, 18495-18514.

Anati, D.A., 1997. The hydrography of a hypersaline lake, in: Niemi, T.M., Ben-Avraham, Z., Gat, J.R. (Eds.), The Dead Sea: The Lake and Its Setting. Oxford University Press, New York, Oxford, pp. 89-103.

Andersen, S.T., 1970. The relative pollen productivity and pollen representation of north European trees, and correction factors for tree pollen spectra. Danmarks Geologiske Undersoegelse, Raekke 2 96, 1-99.

Andersen, S.T., 1974. Wind conditions and pollen deposition in a mixed deciduous forest: I. Wind conditions and pollen dispersal. Grana 14, 57-63.

Armitage, S.J., Jasim, S.A., Marks, A.E., Parker, A.G., Usik, V.I., Uerpmann, H.P., 2011. The Southern Route "Out of Africa": Evidence for an Early Expansion of Modern Humans into Arabia. Science 331, 453-456.

Atkinson, K., Beaumont, P., 1971. The forests of Jordan. Economic Botany 25, 305-311.

Ayalon, A., Bar-Matthews, M., Sass, E., 1998. Rainfall-recharge relationships within a karstic terrain in the Eastern Mediterranean semi-arid region, Israel: $\delta^{18}O$ and δD characteristics. Journal of Hydrology 207, 18-31.

Bar-Matthews, M., Ayalon, A., Gilmour, M., Matthews, A., Hawkesworth, C.J., 2003. Sea-land oxygen isotopic relationships from planktonic foraminifera and speleothems in the Eastern Mediterranean region and their implication for paleorainfall during interglacial intervals. Geochimica et Cosmochimica Acta 67, 3181-3199.

Bar-Matthews, M., Ayalon, A., Kaufman, A., 1997. Late quaternary paleoclimate in the eastern Mediterranean region from stable isotope analysis of speleothems at Soreq Cave, Israel. Quaternary Research 47, 155-168.

Bar-Matthews, M., Ayalon, A., Kaufman, A., 2000. Timing and hydrological conditions of Sapropel events in the Eastern Mediterranean, as evident from speleothems, Soreq cave, Israel. Chemical Geology 169, 145-156.

Bar-Matthews, M., Ayalon, A., Kaufman, A., Wasserburg, G.J., 1999. The Eastern Mediterranean paleoclimate as a reflection of regional events: Soreq cave, Israel. Earth and Planetary Science Letters 166, 85-95.

Bar-Matthews, M., Ayalon, A., Vaks, A., Frumkin, A., 2017. Climate and environment reconstructions based on speleothems from the Levant, in: Enzel, Y., Bar-Yosef, O. (Eds.), Quaternary of the Levant: environments, climate change, and humans. Cambridge University Press, Cambridge, New York, pp. 151-164.

Barkan, E., Luz, B., Lazar, B., 2001. Dynamics of the carbon dioxide system in the Dead Sea. Geochimica et Cosmochimica Acta 65, 355-368.

Barker, S., Knorr, G., Edwards, R.L., Parrenin, F., Putnam, A.E., Skinner, L.C., Wolff, E., Ziegler, M., 2011. 800,000 years of abrupt climate variability. science 334, 347-351.

Bartov, Y., Bookman, R., Enzel, Y., 2006. Current depositional environments at the Dead Sea margins as indicators of past lake levels. Geological Society of America Special Papers 401, 127-140.

Bartov, Y., Goldstein, S.L., Stein, M., Enzel, Y., 2003. Catastrophic arid episodes in the Eastern Mediterranean linked with the North Atlantic Heinrich events. Geology 31, 439-442.

Bartov, Y., Stein, M., Enzel, Y., Agnon, A., Reches, Z.e., 2002. Lake levels and sequence stratigraphy of Lake Lisan, the late Pleistocene precursor of the Dead Sea. Quaternary Research 57, 9-21.

Baruch, U., 1986. The Late Holocene Vegetational History of Lake Kinneret (Sea of Galilee), Israel. Paléorient 12, 37-48.

Baruch, U., 1990. Palynological evidence of human impact on the vegetation as recorded in Late Holocene lake sediments in Israel, in: Bottema, S., Entjes-Nieborg, G., van Zeist, W. (Eds.), Man's role in the shaping of the Eastern Mediterranean landscape. A. A. Balkema, Rotterdam, Brookfield, pp. 283-293.

Baruch, U., 1993. The palynology of Late Quaternary sediments of the Dead Sea (in Hebrew with English abstract). Unpublished Ph.D. dissertation. Hebrew University of Jerusalem, Jerusalem.

Baruch, U., Bottema, S., 1991. Palynological evidence for climatic changes in the Levant ca. 17,000-9,000 BP. The Natufian culture in the Levant, 11-20.

Baruch, U., Bottema, S., 1999. A new pollen diagram from Lake Hula: vegetational, climatic and anthropogenic implications, in: Kawanabe, H., Coulter, G.W., Roosevelt, A.C. (Eds.), Ancient lakes: their cultural and biological diversity. Kenobi Productions, Ghent, pp. 75-86.

Begin, Z., Ehrlich, A., Nathan, Y., 1974. Lake Lisan: the Pleistocene precursor of the Dead Sea. Geological survey of Israel Bulletin 63, 1-30.

Behre, K.-E., 1990. Some reflections on anthropogenic indicators and the record of prehistoric occupation phases in pollen diagrams from the Near East, in: Bottema, S., Entjes-Nieborg, G., van Zeist, W. (Eds.), Man's role in the shaping of the eastern Mediterranean landscape. . A. A. Balkema, Rotterdam, Brookfield, pp. 219-230.

Ben-Avraham, Z., 2014. Geophysical Studies of the Crustal Structure Along the Southern Dead Sea Fault, in: Garfunkel, Z., Ben-Avraham, Z., Kagan, E. (Eds.), Dead Sea Transform Fault System: Reviews. Springer, pp. 1-27.

Bentor, Y.K., 1961. Some geochemical aspects of the Dead Sea and the question of its age. Geochimica et Cosmochimica Acta 25, 239-260.

Berger, A., Loutre, M.-F., Kaspar, F., Lorenz, S.J., 2007. Insolation during interglacial. Developments in Quaternary Sciences 7, 13-27.

Berglund, B.E., Ralska-Jasiewiczowa, M., 1986. Pollen analysis and pollen diagrams, in: Berglund, B.E., Ralska-Jasiewiczowa, M. (Eds.), Handbook of Holocene palaeoecology and palaeohydrology. John Wiley and Sons, pp. 455-484.

Beug, H.-J., 2004. Pollenbestimmung für Mitteleuropa und angrenzende Gebiete. Verlag Dr. Friedrich Pfeil, München.

Birks, H.J.B., Birks, H.H., 1980. Quaternary palaeoecology. Edward Arnold, London.

Bitan, A., 1974. The wind regime in the north-west section of the Dead-Sea. Archiv für Meteorologie, Geophysik und Bioklimatologie, Serie B 22, 313-335.

Bookman (Ken-Tor), R., Enzel, Y., Agnon, A., Stein, M., 2004. Late Holocene lake levels of the Dead Sea. Geological Society of America Bulletin 116, 555-571.

Bookman, R., Bartov, Y., Enzel, Y., Stein, M., 2006. Quaternary lake levels in the Dead Sea basin: two centuries of research. Geological Society of America Special Papers 401, 155-170.

Bottema, S., Woldring, H., 1990. Anthropogenic indicators in the pollen record of the Eastern Mediterranean, in: Bottema, S., Entjes-Nieborg, G., van Zeist, W. (Eds.), Man's role in the shaping of the Eastern Mediterranean landscape. A. A. Balkema, Rotterdam, Brookfield, pp. 231-264.

Bowman, D., 1997. Geomorphology of the Dead Sea western margin, in: Niemi, T.M., Ben-Avraham, Z., Gat, J.R. (Eds.), The Dead Sea: The Lake and Its Setting. Oxford University Press, New York, Oxford, pp. 217-225.

Brauer, A., Allen, J.R., Mingram, J., Dulski, P., Wulf, S., Huntley, B., 2007. Evidence for last interglacial chronology and environmental change from Southern Europe. Proceedings of the National Academy of Sciences 104, 450-455.

Breeze, P.S., Groucutt, H.S., Drake, N.A., White, T.S., Jennings, R.P., Petraglia, M.D., 2016. Palaeohydrological corridors for hominin dispersals in the Middle East ~250–70,000 years ago. Quaternary Science Reviews 144, 155-185.

Brewer, S., Giesecke, T., Davis, B.A., Finsinger, W., Wolters, S., Binney, H., de Beaulieu, J.-L., Fyfe, R., Gil-Romera, G., Kühl, N., 2016. Late-glacial and Holocene European pollen data. Journal of Maps, 1-8.

Broecker, W.S., 1998. The end of the present interglacial: how and when? Quaternary Science Reviews 17, 689-694.

Bunting, M.J., Armitage, R., Binney, H.A., Waller, M., 2005. Estimates of 'relative pollen productivity' and 'relevant source area of pollen' for major tree taxa in two Norfolk (UK) woodlands. The Holocene 15, 459-465.

Burns, S.J., Fleitmann, D., Matter, A., Neff, U., Mangini, A., 2001. Speleothem evidence from Oman for continental pluvial events during interglacial periods. Geology 29, 623-626.

Calvo, R., 2002. Stratigraphy and petrology of the Hazeva Formation in the Arava and the Negev: Implications for the development of sedimentary basins and the morphotectonics of the Dead Sea Rift Valley (in Hebrew with English abstract). Ph.D. dissertation. Hebrew University of Jerusalem, Jerusalem, p. 264.

Campbell, I.D., 1991. Experimental mechanical destruction of pollen grains. Palynology 15, 29-33.

Campbell, I.D., 1999. Quaternary pollen taphonomy: examples of differential redeposition and differential preservation. Palaeogeography, Palaeoclimatology, Palaeoecology 149, 245-256.

Campbell, I.D., Campbell, C., 1994. Pollen preservation: Experimental wet-dry cycles in saline and desalinated sediments. Palynology 18, 5-10.

Castañeda, I.S., Mulitza, S., Schefuß, E., dos Santos, R.A.L., Damsté, J.S.S., Schouten, S., 2009. Wet phases in the Sahara/Sahel region and human migration patterns in North Africa. Proceedings of the National Academy of Sciences 106, 20159-20163.

Chapman, M.R., Shackleton, N.J., 1999. Global ice-volume fluctuations, North Atlantic ice-rafting events, and deep-ocean circulation changes between 130 and 70 ka. Geology 27, 795-798.

Chapman, M.R., Shackleton, N.J., Duplessy, J.-C., 2000. Sea surface temperature variability during the last glacial–interglacial cycle: assessing the magnitude and pattern of climate change in the North Atlantic. Palaeogeography, Palaeoclimatology, Palaeoecology 157, 1-25.

Cheddadi, R., Khater, C., 2016. Climate change since the last glacial period in Lebanon and the persistence of Mediterranean species. Quaternary Science Reviews 150, 146-157.

Cheddadi, R., Rossignol-Strick, M., 1995a. Eastern Mediterranean Quaternary Paleoclimates from Pollen and Isotope Records of Marine Cores in the Nile Cone Area. Paleoceanography 10, 291-300.

Cheddadi, R., Rossignol-Strick, M., 1995b. Improved preservation of organic matter and pollen in eastern Mediterranean sapropels. Paleoceanography 10, 301-309.

Cordova, C.E., Nowell, A., Bisson, M., Ames, C.J.H., Pokines, J., Chang, M., al-Nahar, M., 2013. Interglacial and glacial desert refugia and the Middle Paleolithic of the Azraq Oasis, Jordan. Quaternary International 300, 94-110.

Cortijo, E., Lehman, S., Keigwin, L., Chapman, M., Paillard, D., Labeyrie, L., 1999. Changes in meridional temperature and salinity gradients in the North Atlantic Ocean (30-72°N) during the last interglacial period. Paleoceanography 14, 23-33.

Coulthard, T.J., Ramirez, J.A., Barton, N., Rogerson, M., Brücher, T., 2013. Were Rivers Flowing across the Sahara During the Last Interglacial? Implications for Human Migration through Africa. PloS one 8, e74834.

Cushing, E.J., 1967. Evidence for differential pollen preservation in late Quaternary sediments in Minnesota. Review of Palaeobotany and Palynology 4, 87-101.

Danin, A., 1992. Flora and vegetation of Israel and adjacent areas. The zoogeography of Israel, 129-158.

Danin, A., Plitmann, U., 1987. Revision of the plant geographical territories of Israel and Sinai. Plant Systematics and Evolution 156, 43-53.

Davies, C.P., Fall, P.L., 2001. Modern pollen precipitation from an elevational transect in central Jordan and its relationship to vegetation. Journal of Biogeography 28, 1195-1210.

Davis, B.A.S., Brewer, S., Stevenson, A., Guiot, J., 2003. The temperature of Europe during the Holocene reconstructed from pollen data. Quaternary Science Reviews 22, 1701-1716.

Davis, B.A.S., Zanon, M., Collins, P., Mauri, A., Bakker, J., Barboni, D., Barthelmes, A., Beaudouin, C., Bjune, A.E., Bozilova, E., Bradshaw, R.H.W., Brayshay, B.A., Brewer, S., Brugiapaglia, E., Bunting, J., Connor, S.E., Beaulieu, J.-L., Edwards, K., Ejarque, A., Fall, P., Florenzano, A., Fyfe, R., Galop, D., Giardini, M., Giesecke, T., Grant, M.J., Guiot, J., Jahns, S., Jankovská, V., Juggins, S., Kahrmann, M., Karpińska-Kołaczek, M., Kołaczek, P., Kühl, N., Kuneš, P., Lapteva, E.G., Leroy, S.A.G., Leydet, M., Guiot, J., Jahns, S., Jankovská, V., Juggins, S., Kahrmann, M., Karpińska-Kołaczek, M., Kołaczek, P., Kühl, N., Kuneš, P., Lapteva, E.G., Leroy, S.A.G., Leydet, M., López Sáez, J.A., Masi, A., Matthias, I., Mazier, F., Meltsov, V., Mercuri, A.M., Miras, Y., Mitchell, F.J.G., Morris, J.L., Naughton, F., Nielsen, A.B., Novenko, E., Odgaard, B., Ortu, E., Overballe-Petersen, M.V., Pardoe, H.S., Peglar, S.M., Pidek, I.A., Sadori, L., Seppä, H., Severova, E., Shaw, H., Święta-Musznicka, J., Theuerkauf, M., Tonkov, S., Veski, S., Knaap, W.O., Leeuwen, J.F.N., Woodbridge, J., Zimny, M., Kaplan, J.O., 2013. The European Modern Pollen Database (EMPD) project. Vegetation History and Archaeobotany 22, 521-530.

Davis, M.B., 1963. On the theory of pollen analysis. American Journal of Science 261, 897-912.

Davis, M.B., Brubaker, L.B., 1973. Differential Sedimentation of Pollen Grains in Lakes. Limnology and Oceanography 18, 635-646.

Dayan, U., Morin, E., 2006. Flash flood-producing rainstorms over the Dead Sea: A review. Geological Society of America Special Papers 401, 53-62.

Djamali, M., Akhani, H., Andrieu-Ponel, V., Braconnot, P., Brewer, S., de Beaulieu, J.-L., Fleitmann, D., Fleury, J., Gasse, F., Guibal, F., 2010. Indian Summer Monsoon variations could have affected the early-Holocene woodland expansion in the Near East. The Holocene 20, 813-820.

Djamali, M., de Beaulieu, J.-L., Shah-hosseini, M., Andrieu-Ponel, V., Ponel, P., Amini, A., Akhani, H., Leroy, S.A., Stevens, L., Lahijani, H., 2008. A late Pleistocene long pollen record from Lake Urmia, NW Iran. Quaternary Research 69, 413-420.

Donders, T.H., Hagemans, K., Dekker, S.C., de Weger, L.A., de Klerk, P., Wagner-Cremer, F., 2014. Region-Specific Sensitivity of Anemophilous Pollen Deposition to Temperature and Precipitation. PloS one 9, e104774.

Drake, N.A., Blench, R.M., Armitage, S.J., Bristow, C.S., White, K.H., 2011. Ancient watercourses and biogeography of the Sahara explain the peopling of the desert. Proceedings of the National Academy of Sciences 108, 458-462.

Dutton, A., Carlson, A.E., Long, A.J., Milne, G.A., Clark, P.U., DeConto, R., Horton, B.P., Rahmstorf, S., Raymo, M.E., 2015. Sea-level rise due to polar ice-sheet mass loss during past warm periods. Science 349, aaa4019.

Eig, A., Zohary, M., Feinbrun-Dothan, N., 1931. The plants of Palestine: an analytical key. University Press, Jerusalem.

El-Moslimany, A.P., 1990. Ecological significance of common nonarboreal pollen - examples from drylands of the Middle-East. Review of Palaeobotany and Palynology 64, 343-350.

Elazari-Volcani, B.E., 1940a. Algae in the bed of the Dead Sea. Nature 145, 975.

Elazari-Volcani, B.E., 1940b. Studies on the microflora of the Dead Sea. Ph.D. disseration. The Hebrew University of Jerusalem, Jerusalem.

Emeis, K.C., Schulz, H., Struck, U., Rossignol-Strick, M., Erlenkeuser, H., Howell, M., Kroon, D., Mackensen, A., Ishizuka, S., Oba, T., 2003. Eastern Mediterranean surface water temperatures and $\delta^{18}O$ composition during deposition of sapropels in the late Quaternary. Paleoceanography 18, 5 (1-18).

Enzel, Y., Agnon, A., Stein, M.E., 2006. New frontiers in Dead Sea paleoenvironmental research. Geological Society of America, Colorado.

Enzel, Y., Amit, R., Dayan, U., Crouvi, O., Kahana, R., Ziv, B., Sharon, D., 2008. The climatic and physiographic controls of the eastern Mediterranean over the late Pleistocene climates in the southern Levant and its neighboring deserts. Global and Planetary Change 60, 165-192.

Enzel, Y., Amit, R., Grodek, T., Ayalon, A., Lekach, J., Porat, N., Bierman, P., Blum, J.D., Erel, Y., 2012. Late Quaternary weathering, erosion, and deposition in Nahal Yael, Israel: An "impact of climatic change on an arid watershed"? Geological Society of America Bulletin 124, 705-722.

Enzel, Y., Kushnir, Y., Quade, J., 2015. The middle Holocene climatic records from Arabia: Reassessing lacustrine environments, shift of ITCZ in Arabian Sea, and impacts of the southwest Indian and African monsoons. Global and Planetary Change 129, 69-91.

Enzel, Y., Sharon, D., Gvirtzman, H., Dayan, U., Ziv, B., Stein, M., 2003. Late Holocene climates of the Near East deduced from Dead Sea level variations and modern regional winter rainfall. Quaternary Research 60, 263-273.

Faegri, K., Iversen, J., 1989. Textbook of Pollen Analysis, 4ed. John Wiley &. Sons, Chichester, New York, Brisbane, Toronto, Singapore.

Fagerlind, F., 1952. The real signification of pollen diagrams. Botaniska Notiser 105, 185-224.

Fairbridge, R.W., 1972. Climatology of a glacial cycle. Quaternary Research 2, 283-302.

Fleitmann, D., Matter, A., 2009. The speleothem record of climate variability in Southern Arabia. Comptes Rendus Geoscience 341, 633-642.

Ford, D., Williams, P.D., 2007. Karst hydrogeology and geomorphology. John Wiley & Sons, Chichester.

Freitag, H., 1977. The Pleniglacial, Late-Glacial and Early Postglacial vegetations of Zeribar and their present-day counterparts. Palaeohistoria Bussum 19, 87-95.

Frogley, M., Tzedakis, P., 1999. Climate variability in northwest Greece during the last interglacial. Science 285, 1886-1889.

Frumkin, A., Bar-Yosef, O., Schwarcz, H.P., 2011. Possible paleohydrologic and paleoclimatic effects on hominin migration and occupation of the Levantine Middle Paleolithic. Journal of Human Evolution 60, 437-451.

Frumkin, A., Ford, D.C., Schwarcz, H.P., 1999. Continental oxygen isotopic record of the last 170,000 years in Jerusalem. Quaternary Research 51, 317-327.

Frumkin, A., Ford, D.C., Schwarcz, H.P., 2000. Paleoclimate and vegetation of the Last Glacial Cycles in Jerusalem from a Speleothem Record. Global Biogeochemical Cycles 14, 863-870.

Frumkin, A., Stein, M., 2004. The Sahara–East Mediterranean dust and climate connection revealed by strontium and uranium isotopes in a Jerusalem speleothem. Earth and Planetary Science Letters 217, 451-464.

Ganopolski, A., Winkelmann, R., Schellnhuber, H.J., 2016. Critical insolation-CO_2 relation for diagnosing past and future glacial inception. Nature 529, 200-203.

Gardosh, M., Kashai, E., Salhov, S., Shulman, H., Tannenbaum, E., 1997. Hydrocarbon exploration in the southern Dead Sea area, in: Niemi, T.M., Ben-Avraham, Z., Gat, J.R. (Eds.), The Dead Sea: The lake and its setting. Oxford University Press, New York, Oxford, pp. 57-72.

Garfunkel, Z., 1997. The history and formation of the Dead Sea Basin, in: Niemi, T.M., Ben-Avraham, Z., Gat, J.R. (Eds.), The Dead Sea: The lake and its setting. Oxford University Press, New York, Oxford, pp. 36-56.

Garfunkel, Z., Ben-Avraham, Z., 1996. The structure of the Dead Sea basin. Tectonophysics 266, 155-176.

Gasse, F., Vidal, L., Develle, A.-L., Campo, E.V., 2011. Hydrological variability in the Northern Levant: a 250 ka multiproxy record from the Yammoûneh (Lebanon) sedimentary sequence. Climate of the Past 7, 1261-1284.

Gasse, F., Vidal, L., Van Campo, E., Demory, F., Develle, A.-L., Tachikawa, K., Elias, A., Bard, E., Garcia, M., Sonzogni, C., 2015. Hydroclimatic changes in northern Levant over the past 400,000 years. Quaternary Science Reviews 111, 1-8.

Gat, J.R., 1984. The stable isotope composition of Dead Sea waters. Earth and Planetary Science Letters 71, 361-376.

Gavrieli, I., Stein, M., 2006. On the origin and fate of the brines in the Dead Sea basin. Geological Society of America Special Papers 401, 183-194.

Gibbard, P.L., Van Kolfschoten, T., 2004. The Pleistocene and Holocene epochs, in: Gradstein, F.M., Ogg, J.G., Smith, A.G. (Eds.), A geologic timescale. Cambridge University Press, Cambridge, pp. 441-452.

Gibbons, A., 2017. Oldest members of our species discovered in Morocco. Science 356, 993-994.

Giesecke, T., Fontana, S.L., van der Knaap, W.O., Pardoe, H.S., Pidek, I.A., 2010. From early pollen trapping experiments to the Pollen Monitoring Programme. Vegetation history and archaeobotany 19, 247-258.

Goldreich, Y., 2003. The climate of Israel: observation, research and application. Springer Science & Business Media, New York.

Goudie, A.S., Middleton, N.J., 2001. Saharan dust storms: nature and consequences. Earth-Science Reviews 56, 179-204.

Govin, A., Capron, E., Tzedakis, P., Verheyden, S., Ghaleb, B., Hillaire-Marcel, C., St-Onge, G., Stoner, J., Bassinot, F., Bazin, L., 2015. Sequence of events from the onset to the demise of the Last Interglacial: Evaluating strengths and limitations of chronologies used in climatic archives. Quaternary Science Reviews 129, 1-36.

Grant, K., Rohling, E., Bar-Matthews, M., Ayalon, A., Medina-Elizalde, M., Ramsey, C.B., Satow, C., Roberts, A., 2012. Rapid coupling between ice volume and polar temperature over the past 150,000 years. Nature 491, 744-747.

Greenbaum, N., Ben-Zvi, A., Haviv, I., Enzel, Y., 2006a. The hydrology and paleohydrology of the Dead Sea tributaries. Geological Society of America Special Papers 401, 63-93.

Greenbaum, N., Porat, N., Rhodes, E., Enzel, Y., 2006b. Large floods during late Oxygen Isotope Stage 3, southern Negev desert, Israel. Quaternary Science Reviews 25, 704-719.

Grimm, E.C., 1987. CONISS: a Fortran 77 program for stratigraphically constrained cluster-analysis by the method of incremental sum of squares. Computers & Geosciences 13, 13-35.

Grün, R., Stringer, C., McDermott, F., Nathan, R., Porat, N., Robertson, S., Taylor, L., Mortimer, G., Eggins, S., McCulloch, M., 2005. U-series and ESR analyses of bones and teeth relating to the human burials from Skhul. Journal of Human Evolution 49, 316-334.

Guiot, J., Pons, A., de Beaulieu, J.L., Reille, M., 1989. A 140,000-year continental climate reconstruction from two European pollen records. Nature 338, 309-313.

Haase-Schramm, A., Goldstein, S.L., Stein, M., 2004. U-Th dating of Lake Lisan (late Pleistocene Dead Sea) aragonite and implications for glacial East Mediterranean climate change. Geochimica et Cosmochimica Acta 68, 985-1005.

Haliva-Cohen, A., Stein, M., Goldstein, S.L., Sandler, A., Starinsky, A., 2012. Sources and transport routes of fine detritus material to the Late Quaternary Dead Sea basin. Quaternary Science Reviews 50, 55-70.

Hall, J.K., 1997. Topography and bathymetry of the Dead Sea depression, in: Niemi, T.M., Ben-Avraham, Z., Gat, J.R. (Eds.), The Dead Sea: The Lake and Its Setting. Oxford University Press, New York, Oxford, pp. 11-21.

Harting, P., 1874. De bodem van het Eemdal. Verslagen en Mededelingen van de Koninklijke Academie van Wetenschappen afdeling Natuurkunde II 8, 282-290.

Havinga, A.J., 1964. Investigation into the differential corrosion susceptibility of pollen and spores. Pollen et Spores 6, 621-635.

Havinga, A.J., 1984. A 20-year experimental investigation into the differential corrosion susceptibility of pollen and spores in various soil types. Pollen et spores 26, 541-558.

Hazan, N., Stein, M., Agnon, A., Marco, S., Nadel, D., Negendank, J.F.W., Schwab, M.J., Neev, D., 2005. The late Quaternary limnological history of Lake Kinneret (Sea of Galilee), Israel. Quaternary Research 63, 60-77.

Heim, C., Nowaczyk, N.R., Negendank, J.F., Leroy, S.A., Ben-Avraham, Z., 1997. Near East desertification: evidence from the Dead Sea. Naturwissenschaften 84, 398-401.

Hershkovitz, I., Marder, O., Ayalon, A., Bar-Matthews, M., Yasur, G., Boaretto, E., Caracuta, V., Alex, B., Frumkin, A., Goder-Goldberger, M., 2015. Levantine cranium from Manot Cave (Israel) foreshadows the first European modern humans. Nature 520, 216-219.

Hofstetter, A., Dorbath, C., Dorbath, L., 2014. Instrumental data on the seismic activity along the Dead Sea Transform, in: Garfunkel, Z., Ben-Avraham, Z., Kagan, E. (Eds.), Dead Sea Transform Fault System: Reviews. Springer, pp. 263-278.

Horowitz, A., 1966. Tropical and northern pollen and spores in recent sediments from the Bay of Elat (Aqaba). Israel Journal of Earthscience 15, 125-130.

Horowitz, A., 1969. Recent pollen sedimentation in Lake Kinneret, Israel. Pollen et spores 9, 353-384.

Horowitz, A., 1971. Climatic and vegetational developments in northeastern Israel during Upper Pleistocene-Holocene times. Pollen et Spores 13, 255-278.

Horowitz, A., 1979. The quaternary of Israel. Academic Press, New York, London, Toronto, Sydney, San Francisco.

Horowitz, A., 1989. Continuous Pollen Diagrams for the Last 3.5 My from Israel-Vegetation, Climate and Correlation with the Oxygen Isotope Record. Palaeogeography Palaeoclimatology Palaeoecology 72, 63-78.

Horowitz, A., 1992. Palynology of arid lands. Elsevier, New York.

Horowitz, A., Baum, B., 1967. The arboreal pollen flora of Israel. Pollen et Spores 9, 71-93.

Horowitz, A., Weinstein, M., Ganor, E., 1975. Palynological determination of dust storms provenances in Israel. Pollen et spores 17, 223-231.

Ionescu, D., Siebert, C., Polerecky, L., Munwes, Y.Y., Lott, C., Häusler, S., Bižić-Ionescu, M., Quast, C., Peplies, J., Glöckner, F.O., 2012. Microbial and chemical characterization of underwater fresh water springs in the Dead Sea. PloS one 7, e38319.

Iversen, J., 1944. Viscum, Hedera and Ilex as Climate Indicators. Geologiska Foereningan i Stockholm. Foerhandlingar 66, 463-483.

Jankovská, V., Komárek, J., 2000. Indicative value of Pediastrum and other coccal green algae in palaeoecology. Folia Geobotanica 35, 59-82.

Jennings, R.P., Singarayer, J., Stone, E.J., Krebs-Kanzow, U., Khon, V., Nisancioglu, K.H., Pfeiffer, M., Zhang, X., Parker, A., Parton, A., Groucutt, H.S., White, T.S., Drake, N.A., Petraglia, M.D., 2015. The greening of Arabia: Multiple opportunities for human occupation of the Arabian Peninsula during the Late Pleistocene inferred from an ensemble of climate model simulations. Quaternary International 382, 181-199.

Jessen, K., Milthers, V., 1928. Stratigraphical and paleontological studies of interglacial fresh-water deposits in Jutland and Northwest Germany. Danmarks Geologiske Undersøgelse 48, 1-379.

Keynan, N., Waisel, Y., Shomer-Ilan, A., Goren, A., Brener, S., 1991. Annual variations of air-borne pollen in the coastal plain of Israel. Grana 30, 477-480.

Kiro, Y., Goldstein, S.L., Garcia-Veigas, J., Levy, E., Kushnir, Y., Stein, M., Lazar, B., 2017. Relationships between lake-level changes and water and salt budgets in the Dead Sea during extreme aridities in the Eastern Mediterranean. Earth and Planetary Science Letters 464, 211-226.

Kiro, Y., Goldstein, S.L., Lazar, B., Stein, M., 2015. Environmental implications of salt facies in the Dead Sea. Geological Society of America Bulletin 128, 824-841.

Kitagawa, H., Stein, M., Goldstein, S.L., Nakamura, T., Lazar, B., 2017. Radiocarbon Chronology of the DSDDP Core at the Deepest Floor of the Dead Sea. Radiocarbon 59, 383-394.

Kühl, N., Gebhardt, C., Litt, T., Hense, A., 2002. Probability Density Functions as Botanical-Climatological Transfer Functions for Climate Reconstruction. Quaternary Research 58, 381-392.

Kukla, G.J., Bender, M.L., de Beaulieu, J.-L., Bond, G., Broecker, W.S., Cleveringa, P., Gavin, J.E., Herbert, T.D., Imbrie, J., Jouzel, J., Keigwin, L.D., Knudsen, K.-L., McManus, J.F., Merkt, J., Muhs, D.R., Müller, H., Poore, R.Z., Porter, S.C., Seret, G., Shackleton, N.J., Turner, C., Tzedakis, P.C., Winograd, I.J., 2002. Last Interglacial Climates. Quaternary Research 58, 2-13.

Kushnir, Y., Stein, M., 2010. North Atlantic influence on 19th–20th century rainfall in the Dead Sea watershed, teleconnections with the Sahel, and implication for Holocene climate fluctuations. Quaternary Science Reviews 29, 3843-3860.

Lamb, H.F., Gasse, F., Benkaddour, A., El Hamouti, N., van der Kaars, S., Perkins, W.T., Pearce, N.J., Roberts, C.N., 1995. Relation between century-scale Holocene arid intervals in tropical and temperate zones. Nature 373, 134-137.

Langgut, D., 2017. Late Quaternary Nile flows as recorded in the Levantine Basin: The palynological evidence. Quaternary International, in press.

Langgut, D., Adams, M.J., Finkelstein, I., 2016. Climate, settlement patterns and olive horticulture in the southern Levant during the Early Bronze and Intermediate Bronze Ages (c. 3600-1950 BC). Levant 48, 117-134.

Langgut, D., Almogi-Labin, A., Bar-Matthews, M., Weinstein-Evron, M., 2011. Vegetation and climate changes in the South Eastern Mediterranean during the Last Glacial-Interglacial cycle (86 ka): new marine pollen record. Quaternary Science Reviews 30, 3960-3972.

Langgut, D., Finkelstein, I., Litt, T., 2013a. Climate and the Late Bronze Collapse: new evidence from the Southern Levant. Tel Aviv 40, 149-175.

Langgut, D., Finkelstein, I., Litt, T., Neumann, F.H., Stein, M., 2015a. Vegetation and climate changes during the Bronze and Iron Ages (~3600-600 BCE) in the Southern Levant based on palynological records. Radiocarbon 57, 217-235.

Langgut, D., Gadot, Y., Porat, N., Lipschits, O., 2013b. Fossil pollen reveals the secrets of the Royal Persian Garden at Ramat Rahel, Jerusalem. Palynology 37, 115-129.

Langgut, D., Neumann, F.H., Stein, M., Wagner, A., Kagan, E.J., Boaretto, E., Finkelstein, I., 2014. Dead Sea pollen record and history of human activity in the Judean Highlands (Israel) from the Intermediate Bronze into the Iron Ages (~2500-500 BCE). Palynology, 1-23.

Langgut, D., Yannai, E., Taxel, I., Agnon, A., Marco, S., 2015b. Resolving a historical earthquake date at Tel Yavneh (central Israel) using pollen seasonality. Palynology, 1-16.

Larrasoaña, J.C., Roberts, A.P., Rohling, E.J., 2013. Dynamics of green Sahara periods and their role in hominin evolution. PloS one 8, e76514.

Laskar, J., Robutel, P., Joutel, F., Gastineau, M., Correia, A.C.M., Levrard, B., 2004. A long-term numerical solution for the insolation quantities of the Earth. Astron Astrophys 428, 261-285.

Lawson, I., Tzedakis, P., Roucoux, K., Galanidou, N., 2013. The anthropogenic influence on wildfire regimes: charcoal records from the Holocene and Last Interglacial at Ioannina, Greece. Journal of Biogeography 40, 2324-2334.

Lazar, B., Sivan, O., Yechieli, Y., Levy, E., Antler, G., Gavrieli, I., Stein, M., 2014. Long-term freshening of the Dead Sea brine revealed by porewater Cl^- and $\delta^{18}O$ in ICDP Dead Sea deep-drill. Earth and Planetary Science Letters 400, 94-101.

Lazar, B., Stein, M., 2011. Freshwater on the route of hominids out of Africa revealed by U-Th in Red Sea corals. Geology 39, 1067-1070.

Lebreton, V., Messager, E., Marquer, L., Renault-Miskovsky, J., 2010. A neotaphonomic experiment in pollen oxidation and its implications for archaeopalynology. Review of Palaeobotany and Palynology 162, 29-38.

Leroy, S.A.G., 1992. Palynological evidence of Azolla nilotica Dec. in recent Holocene of the eastern Nile Delta and palaeoenvironment. Vegetation History and Archaeobotany 1, 43-52.

Leroy, S.A.G., 2010. Pollen analysis of core DS7-1SC (Dead Sea) showing intertwined effects of climatic change and human activities in the Late Holocene. Journal of Archaeological Science 37, 306-316.

Leroy, S.A.G., Marco, S., Bookman, R., Miller, C.S., 2010. Impact of earthquakes on agriculture during the Roman-Byzantine period from pollen records of the Dead Sea laminated sediment. Quaternary Research 73, 191-200.

Lézine, A.-M., Von Grafenstein, U., Andersen, N., Belmecheri, S., Bordon, A., Caron, B., Cazet, J.-P., Erlenkeuser, H., Fouache, E., Grenier, C., 2010. Lake Ohrid, Albania, provides an exceptional multi-proxy record of environmental changes during the last glacial-interglacial cycle. Palaeogeography, Palaeoclimatology, Palaeoecology 287, 116-127.

Limaye, R.B., Kumaran, K., Nair, K., Padmalal, D., 2007. Non-pollen palynomorphs as potential palaeoenvironmental indicators in the Late Quaternary sediments of the west coast of India. Current Science 92, 1370-1382.

Lisiecki, L.E., Raymo, M.E., 2005. A Pliocene-Pleistocene stack of 57 globally distributed benthic $\delta^{18}O$ records. Paleoceanography 20, PA1003.

Lisker, S., Vaks, A., Bar-Matthews, M., Porat, R., Frumkin, A., 2009. Stromatolites in caves of the Dead Sea Fault Escarpment: implications to latest Pleistocene lake levels and tectonic subsidence. Quaternary Science Reviews 28, 80-92.

Lisker, S., Vaks, A., Bar-Matthews, M., Porat, R., Frumkin, A., 2010. Late Pleistocene palaeoclimatic and palaeoenvironmental reconstruction of the Dead Sea area (Israel), based on speleothems and cave stromatolites. Quaternary Science Reviews 29, 1201-1211.

Litt, T., Ohlwein, C., Neumann, F.H., Hense, A., Stein, M., 2012. Holocene climate variability in the Levant from the Dead Sea pollen record. Quaternary Science Reviews 49, 95-105.

Litt, T., Pickarski, N., Heumann, G., Stockhecke, M., Tzedakis, P.C., 2014. A 600,000 year long continental pollen record from Lake Van, eastern Anatolia (Turkey). Quaternary Science Reviews 104, 30-41.

Liu, W., Martinon-Torres, M., Cai, Y.-j., Xing, S., Tong, H.-w., Pei, S.-w., Sier, M.J., Wu, X.-h., Edwards, R.L., Cheng, H., Li, Y.-y., Yang, X.-x., de Castro, J.M.B., Wu, X.-j., 2015. The earliest unequivocally modern humans in southern China. Nature 526, 696-699.

Livnat, A., Kronfeld, J., 1985. Paleoclimatic implications of U-series dates for lake sediments and travertines in the Arava Rift Valley, Israel. Quaternary Research 24, 164-172.

López-Merino, L., Leroy, S.A.G., Eshel, A., Epshtein, V., Belmaker, R., Bookman, R., 2016. Using palynology to re-assess the Dead Sea laminated sediments - Indeed varves? Quaternary Science Reviews 140, 49-66.

MacDonald, G.M., Larsen, C.P., Szeicz, J., Moser, K., 1991. The reconstruction of boreal forest fire history from lake sediments: a comparison of charcoal, pollen, sedimentological, and geochemical indices. Quaternary Science Reviews 10, 53-71.

Machlus, M., Enzel, Y., Goldstein, S.L., Marco, S., Stein, M., 2000. Reconstructing low levels of Lake Lisan by correlating fan-delta and lacustrine deposits. Quaternary International 73, 137-144.

Magri, D., Tzedakis, P., 2000. Orbital signatures and long-term vegetation patterns in the Mediterranean. Quaternary International 73, 69-78.

Marder, O., Yeshurun, R., Lupu, R., Bar‐Oz, G., Belmaker, M., Porat, N., Ron, H., Frumkin, A., 2011. Mammal remains at Rantis Cave, Israel, and Middle–Late Pleistocene human subsistence and ecology in the Southern Levant. Journal of Quaternary Science 26, 769-780.

Marín-Arroyo, A.B., 2013. Palaeolithic Human Subsistence in Mount Carmel (Israel). A Taphonomic Assessment of Middle and Early Upper Palaeolithic Faunal Remains from Tabun, Skhul and el-Wad. International Journal of Osteoarchaeology 23, 254-273.

Martinson, D.G., Pisias, N.G., Hays, J.D., Imbrie, J., Moore Jr, T.C., Shackleton, N.J., 1987. Age dating and the orbital theory of the ice ages: development of a high-resolution 0 to 300,000-year chronostratigraphy. Quaternary Research 27, 1-29.

Masson-Delmotte, V., Stenni, B., Pol, K., Braconnot, P., Cattani, O., Falourd, S., Kageyama, M., Jouzel, J., Landais, A., Minster, B., Barnola, J.M., Chappellaz, J., Krinner, G., Johnsen, S., Röthlisberger, R., Hansen, J., Mikolajewicz, U., Otto-Bliesner, B., 2010. EPICA Dome C record of glacial and interglacial intensities. Quaternary Science Reviews 29, 113-128.

McDermott, F., 2004. Palaeo-climate reconstruction from stable isotope variations in speleothems: a review. Quaternary Science Reviews 23, 901-918.

McDermott, F., Grün, R., Stringer, C., Hawkesworth, C., 1993. Mass-spectrometric U-series dates for Israeli Neanderthal/early modern hominid sites. Nature 363, 252-255.

McGarry, S., Bar-Matthews, M., Matthews, A., Vaks, A., Schilman, B., Ayalon, A., 2004. Constraints on hydrological and paleotemperature variations in the Eastern Mediterranean region in the last 140ka given by the δD values of speleothem fluid inclusions. Quaternary Science Reviews 23, 919-934.

McManus, J.F., Bond, G.C., Broecker, W.S., Johnsen, S., Labeyrie, L., Higgins, S., 1994. High-Resolution Climate Records from the North-Atlantic during the Last Interglacial. Nature 371, 326-329.

McManus, J.F., Oppo, D.W., Keigwin, L.D., Cullen, J.L., Bond, G.C., 2002. Thermohaline circulation and prolonged interglacial warmth in the North Atlantic. Quaternary Research 58, 17-21.

Mellars, P., 2006a. Going east: new genetic and archaeological perspectives on the modern human colonization of Eurasia. Science 313, 796-800.

Mellars, P., 2006b. Why did modern human populations disperse from Africa ca. 60,000 years ago? A new model. Proceedings of the National Academy of Sciences 103, 9381-9386.

members, 2004. High-resolution record of Northern Hemisphere climate extending into the last interglacial period. Nature 431, 147-151.

Mercier, N., Valladas, H., Bar-Yosef, O., Vandermeersch, B., Stringer, C., Joron, J.-L., 1993. Thermoluminescence date for the Mousterian burial site of Es-Skhul, Mt. Carmel. Journal of Archaeological Science 20, 169-174.

Miebach, A., 2017. Climate- and Human-Induced Vegetation Changes in Northwestern Turkey and the Southern Levant since the Last Glacial. Ph.D. dissertation. Rheinische Friedrich-Wilhelms-Universität Bonn, Bonn, p. 132.

Miebach, A., Chen, C., Schwab, M.J., Stein, M., Litt, T., 2017. Vegetation and climate during the Last Glacial high stand (ca. 28-22 ka BP) of the Sea of Galilee, northern Israel. Quaternary Science Reviews 156, 47-56.

Migowski, C., Agnon, A., Bookman, R., Negendank, J.F., Stein, M., 2004. Recurrence pattern of Holocene earthquakes along the Dead Sea transform revealed by varve-counting and radiocarbon dating of lacustrine sediments. Earth and Planetary Science Letters 222, 301-314.

Migowski, C., Stein, M., Prasad, S., Negendank, J.F., Agnon, A., 2006. Holocene climate variability and cultural evolution in the Near East from the Dead Sea sedimentary record. Quaternary Research 66, 421-431.

Milano, M., Ruelland, D., Fernandez, S., Dezetter, A., Fabre, J., Servat, E., 2012. Facing climatic and anthropogenic changes in the Mediterranean basin: What will be the medium-term impact on water stress? Comptes Rendus Geoscience 344, 432-440.

Millard, A.R., 2008. A critique of the chronometric evidence for hominid fossils: I. Africa and the Near East 500–50 ka. Journal of Human Evolution 54, 848-874.

Milner, A.M., Collier, R.E.L., Roucoux, K.H., Müller, U.C., Pross, J., Kalaitzidis, S., Christanis, K., Tzedakis, P.C., 2012. Enhanced seasonality of precipitation in the Mediterranean during the early part of the Last Interglacial. Geology 40, 919-922.

Milner, A.M., Müller, U.C., Roucoux, K.H., Collier, R.E., Pross, J., Kalaitzidis, S., Christanis, K., Tzedakis, P.C., 2013. Environmental variability during the Last Interglacial: a new high‐resolution pollen record from Tenaghi Philippon, Greece. Journal of Quaternary Science 28, 113-117.

Milner, A.M., Roucoux, K.H., Collier, R.E.L., Müller, U.C., Pross, J., Tzedakis, P.C., 2016. Vegetation responses to abrupt climatic changes during the Last Interglacial Complex (Marine Isotope Stage 5) at Tenaghi Philippon, NE Greece. Quaternary Science Reviews 154, 169-181.

Moshe, L.B., Haviv, I., Enzel, Y., Zilberman, E., Matmon, A., 2008. Incision of alluvial channels in response to a continuous base level fall: field characterization, modeling, and validation along the Dead Sea. Geomorphology 93, 524-536.

Mudie, P., Leroy, S., Marret, F., Gerasimenko, N., Kholeif, S., Sapelko, T., Filipova-Marinova, M., 2011. Nonpollen palynomorphs: indicators of salinity and environmental change in the Caspian–Black Sea–Mediterranean corridor. Geological Society of America Special Papers 473, 89-115.

Müller, U.C., Kukla, G.J., 2004. North Atlantic Current and European environments during the declining stage of the last interglacial. Geology 32, 1009-1012.

Nadel, D., Grinberg, U., Boaretto, E., Werker, E., 2006. Wooden objects from Ohalo II (23,000 cal BP), Jordan Valley, Israel. J Hum Evol 50, 644-662.

NEEM community members, 2013. Eemian interglacial reconstructed from a Greenland folded ice core. Nature 493, 489-494.

Neev, D., Emery, K., 1967. The Dead Sea. Geological Survey of Israel Bulletin 41, 1-147.

Neev, D., Hall, J.K., 1979. New Aspects of Sedimentation in Small Ocean Basins Geophysical investigations in the Dead Sea. Sedimentary Geology 23, 209-238.

Neugebauer, I., Brauer, A., Schwab, M.J., Waldmann, N.D., Enzel, Y., Kitagawa, H., Torfstein, A., Frank, U., Dulski, P., Agnon, A., 2014. Lithology of the long sediment record recovered by the ICDP Dead Sea Deep Drilling Project (DSDDP). Quaternary Science Reviews 102, 149-165.

Neugebauer, I., Schwab, M., Waldmann, N., Tjallingii, R., Frank, U., Hadzhiivanova, E., Naumann, R., Taha, N., Agnon, A., Enzel, Y., 2016. Hydroclimatic variability in the Levant during the early last glacial (∼ 117–75 ka) derived from micro-facies analyses of deep Dead Sea sediments. Climate of the Past 12, 75-90.

Neumann, F.H., Kagan, E.J., Schwab, M.J., Stein, M., 2007. Palynology, sedimentology and palaeoecology of the late Holocene Dead Sea. Quaternary Science Reviews 26, 1476-1498.

Neumann, F.H., Kagan, E.J., Stein, M., Agnon, A., 2009. Assessment of the effect of earthquake activity on regional vegetation--high-resolution pollen study of the Ein Feshka section, Holocene Dead Sea. Review of Palaeobotany and Palynology 155, 42-51.

Neumann, F.H., Schölzel, C., Litt, T., Hense, A., Stein, M., 2006. Holocene vegetation and climate history of the northern Golan heights (Near East). Vegetation History and Archaeobotany 16, 329-346.

Niemi, T.M., 1997a. Dead Sea research-an introduction, in: Niemi, T.M., Ben-Avraham, Z., Gat, J.R. (Eds.), The Dead Sea: The lake and its setting. Oxford University Press, New York, Oxford, pp. 3-7.

Niemi, T.M., 1997b. Fluctuations of the late Pleistocene Lake Lisan in the Dead Sea Rift, in: Niemi, T.M., Ben-Avraham, Z., Gat, J.R. (Eds.), The Dead Sea: The lake and its setting. Oxford University Press, New York, Oxford, pp. 226-236.

Oren, A., 1997. Microbiological studies in the Dead Sea: 1892-1992, in: Niemi, T.M., Ben-Avraham, Z., Gat, J.R. (Eds.), The Dead Sea: The Lake and Its Setting. Oxford University Press, New York, Oxford, pp. 205-213.

Oren, A., Ben-Yosef, N., 1997. Development and spatial distribution of an algal bloom in the Dead Sea: A remote sensing study. Aquatic microbial ecology 13, 219-223.

Oren, A., Ionescu, D., Hindiyeh, M., Malkawi, H., 2008. Microalgae and cyanobacteria of the Dead Sea and its surrounding springs. Israel Journal of Plant Sciences 56, 1-13.

Orland, I.J., Bar-Matthews, M., Ayalon, A., Matthews, A., Kozdon, R., Ushikubo, T., Valley, J.W., 2012. Seasonal resolution of Eastern Mediterranean climate change since 34ka from a Soreq Cave speleothem. Geochimica et Cosmochimica Acta 89, 240-255.

Orland, I.J., Bar-Matthews, M., Kita, N.T., Ayalon, A., Matthews, A., Valley, J.W., 2009. Climate deterioration in the Eastern Mediterranean as revealed by ion microprobe analysis of a speleothem that grew from 2.2 to 0.9 ka in Soreq Cave, Israel. Quaternary Research 71, 27-35.

Orland, I.J., Burstyn, Y., Bar-Matthews, M., Kozdon, R., Ayalon, A., Matthews, A., Valley, J.W., 2014. Seasonal climate signals (1990-2008) in a modern Soreq Cave stalagmite as revealed by high-resolution geochemical analysis. Chemical Geology 363, 322-333.

Overpeck, J.T., Webb, T., Prentice, I.C., 1985. Quantitative Interpretation of Fossil Pollen Spectra - Dissimilarity Coefficients and the Method of Modern Analogs. Quaternary Research 23, 87-108.

Parton, A., Farrant, A.R., Leng, M.J., Telfer, M.W., Groucutt, H.S., Petraglia, M.D., Parker, A.G., 2015. Alluvial fan records from southeast Arabia reveal multiple windows for human dispersal. Geology 43, 295-298.

Penck, A., Brückner, E., 1909. Die alpen im Eiszeitalter. Tauchnitz, Leipzig.

Petit-Maire, N., Carbonel, P., Reyss, J.-L., Sanlaville, P., Abed, A., Bourrouilh, R., Fontugne, M., Yasin, S., 2010. A vast Eemian palaeolake in Southern Jordan (29°N). Global and Planetary Change 72, 368-373.

Petit-Maire, N., Sanlaville, P., Abed, A., Yasin, S., Bourrouith, R., Carbonel, P., Fontugne, M., Reyss, J., 2002. New data for an Eemian lacustrine phase in southern Jordan. Episodes 25, 279-280.

Petraglia, M.D., Alsharekh, A., Breeze, P., Clarkson, C., Crassard, R., Drake, N.A., Groucutt, H.S., Jennings, R., Parker, A.G., Parton, A., Roberts, R.G., Shipton, C., Matheson, C., al-Omari, A., Veall, M.-A., 2012. Hominin Dispersal into the Nefud Desert and Middle Palaeolithic Settlement along the Jubbah Palaeolake, Northern Arabia. PLoS ONE 7, e49840.

Petraglia, M.D., Alsharekh, A.M., Crassard, R., Drake, N.A., Groucutt, H., Parker, A.G., Roberts, R.G., 2011. Middle Paleolithic occupation on a Marine Isotope Stage 5 lakeshore in the Nefud Desert, Saudi Arabia. Quaternary Science Reviews 30, 1555-1559.

Petraglia, M.D., Haslam, M., Fuller, D.Q., Boivin, N., Clarkson, C., 2010. Out of Africa: new hypotheses and evidence for the dispersal of Homo sapiens along the Indian Ocean rim. Annals of Human Biology 37, 288-311.

Peyron, O., Goring, S., Dormoy, I., Kotthoff, U., Pross, J., De Beaulieu, J.-L., Drescher-Schneider, R., Vannière, B., Magny, M., 2011. Holocene seasonality changes in the central Mediterranean region reconstructed from the pollen sequences of Lake Accesa (Italy) and Tenaghi Philippon (Greece). The Holocene 21, 131-146.

Picard, J.L., 1952. The Pleistocene peat of lake Hula. Bulletin of the Research Council of Israel 62, 147-156.

Pickarski, N., Kwiecien, O., Djamali, M., Litt, T., 2015a. Vegetation and environmental changes during the last interglacial in eastern Anatolia (Turkey): a new high-resolution pollen record from Lake Van. Palaeogeography, Palaeoclimatology, Palaeoecology 435, 145-158.

Pickarski, N., Kwiecien, O., Langgut, D., Litt, T., 2015b. Abrupt climate and vegetation variability of eastern Anatolia during the last glacial. Clim. Past 11, 1491-1505.

Prentice, I.C., 1985. Pollen Representation, Source Area, and Basin Size-toward a Unified Theory of Pollen Analysis. Quaternary Research 23, 76-86.

Prentice, I.C., Guiot, J., Huntley, B., Jolly, D., Cheddadi, R., 1996. Reconstructing biomes from palaeoecological data: A general method and its application to European pollen data at 0 and 6 ka. Climate Dynamics 12, 185-194.

Punt, W., 1976-1991. The northwest European pollen flora. Elsevier, Amsterdam.

Rabinovich, R., Tchernov, E., 1995. Chronological, paleoecological and taphonomical aspects of the Middle Paleolithic site of Qafzeh, Israel. Archaeozoology of the near East 2, 5-44.

Reille, M., 1995. Pollen et spores d'Europe et d'Afrique du Nord: supplement 1. Laboratoire de Botanique Historique et Palynologie, Marseille.

Reille, M., 1998. Pollen et spores d'Europe et d'Afrique du Nord: supplement 2. Laboratoire de Botanique Historique et Palynologie, Marseille.

Reille, M., 1999. Pollen et spores d'Europe et d'Afrique du Nord, 2nd ed. Laboratoire de botanique historique et de palynologie, Marseille.

Rodwell, M.J., Hoskins, B.J., 1996. Monsoons and the dynamics of deserts. Quarterly Journal of the Royal Meteorological Society 122, 1385-1404.

Rohling, E.J., Grant, K., Hemleben, C., Siddall, M., Hoogakker, B.A.A., Bolshaw, M., Kucera, M., 2007. High rates of sea-level rise during the last interglacial period. Nature Geoscience 1, 38-42.

Rohling, E.J., Hayes, A., Mayewski, P.A., Kucera, M., 2009. Holocene climate variability in the eastern Mediterranean, and the End of the Bronze Age, in: Bachhuber, C., Roberts, R.G. (Eds.), Forces of Transformation: The end of the Bronze Age in the Mediterranean, BANEA Publication Series 1. Oxbow Books, Oxford, pp. 2-5.

Rossignol-Strick, M., 1969. Sedimentation palynologique recente dans la Mer Morte. Pollen Spores 11, 17-38.

Rossignol-Strick, M., 1995. Sea-land correlation of pollen records in the Eastern Mediterranean for the glacial-interglacial transition: Biostratigraphy versus radiometric time-scale. Quaternary Science Reviews 14, 893-915.

Rossignol-Strick, M., Dubertret, L., André, C., Gayet, M., 1969. Sédimentation palynologique dans le domaine marin quaternaire de Palestine, in: Dubertret, L. (Ed.), Notes et Mémoires sur le Moyen-Orient. Muséum national d'histoire naturelle, bibliothèque centrale, Paris, pp. 1-269.

Rossignol-Strick, M., Paterne, M., 1999. A synthetic pollen record of the eastern Mediterranean sapropels of the last 1 Ma: implications for the time-scale and formation of sapropels. Marine Geology 153, 221-237.

Saaroni, H., Ziv, B., Bitan, A., Alpert, P., 1998. Easterly wind storms over Israel. Theoretical and Applied Climatology 59, 61-77.

Sadori, L., Koutsodendris, A., Panagiotopoulos, K., Masi, A., Bertini, A., Combourieu-Nebout, N., Francke, A., Kouli, K., Joannin, S., Mercuri, A.M., 2016. Pollen-based paleoenvironmental and paleoclimatic change at Lake Ohrid (south-eastern Europe) during the past 500 ka. Biogeosciences 13, 1423-1437.

Sánchez Goñi, M.F., Eynaud, F., Turon, J.L., Shackleton, N.J., 1999. High resolution palynological record off the Iberian margin: direct land-sea correlation for the Last Interglacial complex. Earth and Planetary Science Letters 171, 123-137.

Scerri, E.M., Drake, N.A., Jennings, R., Groucutt, H.S., 2014. Earliest evidence for the structure of Homo sapiens populations in Africa. Quaternary Science Reviews 101, 207-216.

Schiebel, V., 2013. Vegetation and climate history of the southern levant during the last 30,000 years based on palynological investigation. Ph.D. dissertation. Rheinische Friedrich-Wilhelms-Universität Bonn, Bonn, p. 104.

Schiller, G., Ungar, E.D., Cohen, S., Herr, N., 2010. Water use by Tabor and Kermes oaks growing in their respective habitats in the Lower Galilee region of Israel. Forest ecology and management 259, 1018-1024.

Schiller, G., Ungar, E.D., Cohen, Y., 2002. Estimating the water use of a sclerophyllous species under an East-Mediterranean climate: I. Response of transpiration of Phillyrea latifolia L. to site factors. Forest ecology and management 170, 117-126.

Schiller, G., Unger, E.D., Moshe, Y., Cohen, S., Cohen, Y., 2003. Estimating water use by sclerophyllous species under east Mediterranean climate: II. The transpiration of Quercus calliprinos Webb. in response to silvicultural treatments. Forest Ecology and Management 179, 483-495.

Schramm, A., Stein, M., Goldstein, S.L., 2000. Calibration of the ^{14}C time scale to >40 ka by ^{234}U-^{230}Th dating of Lake Lisan sediments (last glacial Dead Sea). Earth and Planetary Science Letters 175, 27-40.

Schwarcz, H.P., Blackwell, B., Goldberg, P., Marks, A.E., 1979. Uranium series dating of travertine from archaeological sites, Nahal Zin, Israel. Nature 277, 558-560.

Schwarcz, H.P., Grün, R., Vandermeersch, B., Bar-Yosef, O., Valladas, H., Tchernov, E., 1988. ESR dates for the hominid burial site of Qafzeh in Israel. Journal of Human Evolution 17, 733-737.

Seppä, H., Birks, H., Odland, A., Poska, A., Veski, S., 2004. A modern pollen–climate calibration set from northern Europe: developing and testing a tool for palaeoclimatological reconstructions. Journal of Biogeography 31, 251-267.

Shackleton, N.J., Chapman, M., Sánchez-Goñi, M.F., Pailler, D., Lancelot, Y., 2002. The classic marine isotope substage 5e. Quaternary Research 58, 14-16.

Shackleton, N.J., Sánchez-Goñi, M.F., Pailler, D., Lancelot, Y., 2003. Marine Isotope Substage 5e and the Eemian Interglacial. Global and Planetary Change 36, 151-155.

Shaliv, G., 1991. Stages in the tectonic and volcanic history of the Neogene basin in the Lower Galilee and the valleys (in Hebrew with English abstract). Ph.D. dissertation, Geological Survey of Israel Report GSI/11/91, Jerusalem, p. 94.

Sharon, D., Kutiel, H., 1986. The distribution of rainfall intensity in Israel, its regional and seasonal variations and its climatological evaluation. Journal of Climatology 6, 277-291.

Shea, J.J., 2003. The middle paleolithic of the east Mediterranean Levant. Journal of World Prehistory 17, 313-394.

Shea, J.J., Bar-Yosef, O., 2005. Who Were The Skhul/Qafzeh People? An Archaeological Perspective on Eurasia's Oldest Modern Humans. Journal of The Israel Prehistoric Society 35, 451-468.

Shumilovskikh, L.S., Arz, H.W., Wegwerth, A., Fleitmann, D., Marret, F., Nowaczyk, N., Tarasov, P., Behling, H., 2013. Vegetation and environmental changes in Northern Anatolia between 134 and 119 ka recorded in Black Sea sediments. Quaternary Research 80, 349-360.

Sirocko, F., Seelos, K., Schaber, K., Rein, B., Dreher, F., Diehl, M., Lehne, R., Jäger, K., Krbetschek, M., Degering, D., 2005. A late Eemian aridity pulse in central Europe during the last glacial inception. Nature 436, 833-836.

Starinsky, A., Katz, A., 2014. The Story of Saline Water in the Dead Sea Rift–The Role of Runoff and Relative Humidity, in: Garfunkel, Z., Ben-Avraham, Z., Kagan, E. (Eds.), Dead Sea Transform Fault System: Reviews. Springer, pp. 317-353.

Stein, M., 2001. The sedimentary and geochemical record of Neogene-Quaternary water bodies in the Dead Sea Basin-inferences for the regional paleoclimatic history. Journal of Paleolimnology 26, 271-282.

Stein, M., 2014. The evolution of Neogene-Quaternary water-bodies in the Dead Sea rift valley, in: Garfunkel, Z., Ben-Avraham, Z., Kagan, E. (Eds.), Dead Sea Transform Fault System: Reviews. Springer, pp. 279-316.

Stein, M., Agnon, A., Katz, A., Starinsky, A., 2002. Strontium isotopes in discordant dolomite bodies of the Judea Group, Dead Sea basin. Israel Journal of Earth Sciences 51, 219-224.

Stein, M., Ben-Avraham, Z., Goldstein, S., Agnon, A., Ariztegui, D., Brauer, A., Haug, G., Ito, E., Yasuda, Y., 2011a. Deep Drilling at the Dead Sea. Scientific Drilling, 46-47.

Stein, M., Ben‐Avraham, Z., Goldstein, S.L., 2011b. Dead Sea deep cores: A window into past climate and seismicity. EOS 92, 453-454.

Stein, M., Starinsky, A., Agnon, A., Katz, A., Raab, M., Spiro, B., Zak, I., 2000. The impact of brine-rock interaction during marine evaporite formation on the isotopic Sr record in the oceans: Evidence from Mt. Sedom, Israel. Geochimica et Cosmochimica Acta 64, 2039-2053.

Stein, M., Starinsky, A., Katz, A., Goldstein, S.L., Machlus, M., Schramm, A., 1997. Strontium isotopic, chemical, and sedimentological evidence for the evolution of Lake Lisan and the Dead Sea. Geochimica et Cosmochimica Acta 61, 3975-3992.

Stein, M., Torfstein, A., Gavrieli, I., Yechieli, Y., 2010. Abrupt aridities and salt deposition in the post-glacial Dead Sea and their North Atlantic connection. Quaternary Science Reviews 29, 567-575.

Steiner, M.L., Killebrew, A.E., 2014. The Oxford Handbook of the Archaeology of the Levant: c. 8000-332 BCE. Oxford University Press, Oxford.

Steinhorn, I., 1997. Evaporation estimate for the Dead Sea: essential considerations for the saline lakes, in: Niemi, T.M., Ben-Avraham, Z., Gat, J.R. (Eds.), The Dead Sea: The Lake and Its Setting. Oxford University Press, New York, Oxford, pp. 122-132.

Stevens, L.R., Wright Jr, H., Ito, E., 2001. Proposed changes in seasonality of climate during the Lateglacial and Holocene at Lake Zeribar, Iran. The Holocene 11, 747-755.

Stockhecke, M., Timmermann, A., Kipfer, R., Haug, G.H., Kwiecien, O., Friedrich, T., Menviel, L., Litt, T., Pickarski, N., Anselmetti, F.S., 2016. Millennial to orbital-scale variations of drought intensity in the Eastern Mediterranean. Quaternary Science Reviews 133, 77-95.

Stockmarr, J., 1971. Tablets with spores used in absolute pollen analysis. Pollen et spores 13, 615-621.

Stolzenberger, S., 2017. Probabilistische Evaluierung von dekadischen und paläoklimatischen Modellvorhersagen. Ph.D. dissertation. Rheinische Friedrich-Wilhelms-Universität Bonn, Bonn, p. 122.

Stringer, C.B., Grün, R., Schwarcz, H., Goldberg, P., 1989. ESR dates for the hominid burial site of Es Skhul in Israel. Nature 338, 756-758.

Sugita, S., 1993. A model of pollen source area for an entire lake surface. Quaternary research 39, 239-244.

Swain, A.M., 1973. A history of fire and vegetation in northeastern Minnesota as recorded in lake sediments. Quaternary Research 3, 383-396.

Tchernov, E., 1998. The faunal sequence of the southwest Asian Middle Paleolithic in relation to hominid dispersal events, in: Akazawa, T., Aoki, K., Bar-yosef, O. (Eds.), Neandertals and modern humans in western Asia. Kluwer Academic Publishers, New York, Boston, Dordrecht, London, Moscow, pp. 77-94.

Thomas, C., 2015. Investigating the subsurface biosphere of a hypersaline environment-the Dead Sea (Levant). Ph.D dissertation. University of Geneva, Geneva, p. 181.

Torfstein, A., Goldstein, S.L., Kagan, E.J., Stein, M., 2013a. Integrated multi-site U–Th chronology of the last glacial Lake Lisan. Geochimica et Cosmochimica Acta 104, 210-231.

Torfstein, A., Goldstein, S.L., Kushnir, Y., Enzel, Y., Haug, G., Stein, M., 2015. Dead Sea drawdown and monsoonal impacts in the Levant during the Last Interglacial. Earth and Planetary Science Letters 412, 235-244.

Torfstein, A., Goldstein, S.L., Stein, M., Enzel, Y., 2013b. Impacts of abrupt climate changes in the Levant from Last Glacial Dead Sea levels. Quaternary Science Reviews 69, 1-7.

Torfstein, A., Haase-Schramm, A., Waldmann, N., Kolodny, Y., Stein, M., 2009. U-series and oxygen isotope chronology of the mid-Pleistocene Lake Amora (Dead Sea basin). Geochimica et Cosmochimica Acta 73, 2603-2630.

Turner, R., Roberts, N., Eastwood, W.J., Jenkins, E., Rosen, A., 2010. Fire, climate and the origins of agriculture: micro-charcoal records of biomass burning during the last glacial–interglacial transition in Southwest Asia. Journal of Quaternary Science 25, 371-386.

Tzedakis, P.C., 1994a. Hierarchical biostratigraphical classification of long pollen sequences. Journal of Quaternary Science 9, 257-259.

Tzedakis, P.C., 1994b. Vegetation change through glacial-interglacial cycles: a long pollen sequence perspective. Philosophical Transactions of the Royal Society of London, Series B: Biological Sciences 345, 403-432.

Tzedakis, P.C., 1999. The last climatic cycle at Kopais, central Greece. Journal of the Geological Society 156, 425-434.

Tzedakis, P.C., 2003. Timing and duration of Last Interglacial conditions in Europe: a chronicle of a changing chronology. Quaternary Science Reviews 22, 763-768.

Tzedakis, P.C., 2007. Seven ambiguities in the Mediterranean palaeoenvironmental narrative. Quaternary Science Reviews 26, 2042-2066.

Tzedakis, P.C., Frogley, M., Heaton, T., 2003a. Last Interglacial conditions in southern Europe: evidence from Ioannina, northwest Greece. Global and Planetary Change 36, 157-170.

Tzedakis, P.C., Frogley, M.R., Heaton, T.H., 2002a. Duration of last interglacial conditions in northwestern Greece. Quaternary Research 58, 53-55.

Tzedakis, P.C., Hooghiemstra, H., Pälike, H., 2006. The last 1.35 million years at Tenaghi Philippon: revised chronostratigraphy and long-term vegetation trends. Quaternary Science Reviews 25, 3416-3430.

Tzedakis, P.C., Lawson, I.T., Frogley, M.R., Hewitt, G.M., Preece, R.C., 2002b. Buffered Tree Population Changes in a Quaternary Refugium: Evolutionary Implications. Science 297, 2044-2047.

Tzedakis, P.C., McManus, J., Hooghiemstra, H., Oppo, D., Wijmstra, T., 2003b. Comparison of changes in vegetation in northeast Greece with records of climate variability on orbital and suborbital frequencies over the last 450 000 years. Earth and Planetary Science Letters 212, 197-212.

Vaks, A., 2008. Quaternary paleoclimate of north-eastern boundary of the Saharan Desert: reconstruction from speleothems of Negev Desert, Israel. Ph.D. dissertation. Hebrew University of Jerusalem, Jerusalem, p. 205.

Vaks, A., Bar-Matthews, M., Ayalon, A., Matthews, A., Frumkin, A., Dayan, U., Halicz, L., Almogi-Labin, A., Schilman, B., 2006. Paleoclimate and location of the border between Mediterranean climate region and the Saharo–Arabian Desert as revealed by speleothems from the northern Negev Desert, Israel. Earth and Planetary Science Letters 249, 384-399.

Vaks, A., Bar-Matthews, M., Ayalon, A., Matthews, A., Halicz, L., Frumkin, A., 2007. Desert speleothems reveal climatic window for African exodus of early modern humans. Geology 35, 831-834.

Vaks, A., Bar-Matthews, M., Ayalon, A., Schilman, B., Gilmour, M., Hawkesworth, C.J., Frumkin, A., Kaufman, A., Matthews, A., 2003. Paleoclimate reconstruction based on the timing of speleothem growth and oxygen and carbon isotope composition in a cave located in the rain shadow in Israel. Quaternary research 59, 182-193.

Vaks, A., Bar-Matthews, M., Matthews, A., Ayalon, A., Frumkin, A., 2010. Middle-Late Quaternary paleoclimate of northern margins of the Saharan-Arabian Desert: reconstruction from speleothems of Negev Desert, Israel. Quaternary Science Reviews 29, 2647-2662.

Valladas, H., Reyss, J.L., Joron, J.L., Valladas, G., Bar-Yosef, O., Vandermeersch, B., 1988. Thermoluminescence dating of Mousterian Troto-Cro-Magnon' remains from Israel and the origin of modern man. Nature 331, 614-616.

van Zeist, W., Baruch, U., Bottema, S., 2009. Holocene palaeoecology of the Hula area, northeastern Israel, in: Lucas, P., Kaptijn, W. (Eds.), A timeless vale. Archaeological and related essays on the Jordan Valley in honour of Gerrit van der Kooij on the occasion of his sixty-fifth birthday, Archaeological Studies Leiden University. Leiden University Press, pp. 29-64.

van Zeist, W., Bottema, S., 1977. Palynological investigations in western Iran. Palaeohistoria Bussum 19, 19-85.

van Zeist, W., Bottema, S., 1991. Late Quaternary Vegetation of the Near East. Ludwig Reichert, Wiesbaden.

van Zeist, W., Bottema, S., 2009. A palynological study of the Acheulian site of Gesher Benot Ya'aqov, Israel. Vegetation History and Archaeobotany 18, 105-121.

van Zeist, W., Woldring, H., Stapert, D., 1975. Late Quaternary vegetation and climate of southwestern Turkey. Palaeohistoria 17, 53-143.

Waisel, Y., Ganor, E., Glikman, M., Epstein, V., Brenner, S., 1997. Seasonal distribution of airborne pollen in the coastal plain of Israel. Aerobiologia 13, 127-134.

Waldmann, N., Starinsky, A., Stein, M., 2007. Primary carbonates and Ca-chloride brines as monitors of a paleo-hydrological regime in the Dead Sea basin. Quaternary Science Reviews 26, 2219-2228.

Waldmann, N., Stein, M., Ariztegui, D., Starinsky, A., 2009. Stratigraphy, depositional environments and level reconstruction of the last interglacial Lake Samra in the Dead Sea basin. Quaternary Research 72, 1-15.

Waldmann, N., Torfstein, A., Stein, M., 2010. Northward intrusions of low-and mid-latitude storms across the Saharo-Arabian belt during past interglacials. Geology 38, 567-570.

Weinstein-Evron, M., 1976. Late Quaternary vegetation of the northern Golan. Pollen et spores 18, 553–562.

Weinstein-Evron, M., 1979. Airborne pollen, in: Horowitz, A. (Ed.), The Quaternary of Israel. Academic press, New York, London, Toronto, Sydney, San Francisco, pp. 180-210.

Weinstein-Evron, M., 1983. The paleoecology of the early Wurm in the Hula basin, Israel. Paléorient, 5-19.

Weinstein-Evron, M., 1987. Palynology of Pleistocene travertines from the Arava Valley, Israel. Quaternary Research 27, 82-88.

Weinstein-Evron, M., Horowitz, A., 1986. The late Pleistocene climate of Israël/Le climat au Pléistocene récent en Israël. Bulletin de l'Association française pour l'étude du quaternaire, 84-90.

Weinstein-Evron, M., Langgut, D., Chaim, S., Tsatskin, A., Nadel, D., 2015. Late Pleistocene palynological sequence from Ohalo II, Sea of Galilee, Israel. Transactions of the Royal Society of South Africa 70, 219-231.

Weinstein-Evron, M., Vogel, J., Kronfeld, J., 2001. Further attempts at dating the palynological sequence of the Hula Lo7 core, upper Jordan Valley, Israel. Radiocarbon 43, 561–570.

Weinstein, Y., Garfunkel, Z., 2014. The Dead Sea Transform and the Volcanism in Northwestern Arabia, in: Garfunkel, Z., Ben-Avraham, Z., Kagan, E. (Eds.), Dead Sea Transform Fault System: Reviews. Springer, pp. 91-108.

Williams, M.A.J., Duller, G.A.T., Williams, F.M., Woodward, J.C., Macklin, M.G., El Tom, O.A.M., Munro, R.N., El Hajaz, Y., Barrows, T.T., 2015. Causal links between Nile floods and eastern Mediterranean sapropel formation during the past 125 kyr confirmed by OSL and radiocarbon dating of Blue and White Nile sediments. Quaternary Science Reviews 130, 89-108.

Wolff, E.W., Chappellaz, J., Blunier, T., Rasmussen, S.O., Svensson, A., 2010. Millennial-scale variability during the last glacial: The ice core record. Quaternary Science Reviews 29, 2828-2838.

Yechieli, Y., 2006. Response of the groundwater system to changes in the Dead Sea level. Geological Society of America Special Papers 401, 113-126.

Yechieli, Y., Magaritz, M., Levy, Y., Weber, U., Kafri, U., Woelfli, W., Bonani, G., 1993. Late Quaternary geological history of the Dead Sea area, Israel. Quaternary Research 39, 59-67.

Yokoyama, Y., Falgueres, C., Lumley, M., 1997. Direct dating of a Qafzeh proto-cro magnon skull by non destructive gamma-ray spectrometry. Comptes Rendus de l'Academie des Sciences. Serie 2, Sciences de la Terre et des Planetes, 773-779.

Zak, I., 1967. The geology of Mount Sedom (in Hebrew with English abstract). Ph.D. dissertation. The Hebrew University of Jerusalem Jerusalem, p. 208.

Zanchetta, G., Drysdale, R.N., Hellstrom, J.C., Fallick, A.E., Isola, I., Gagan, M.K., Pareschi, M.T., 2007. Enhanced rainfall in the Western Mediterranean during deposition of sapropel S1: stalagmite evidence from Corchia cave (Central Italy). Quaternary Science Reviews 26, 279-286.

Zhao, Y., Liu, H., Li, F., Huang, X., Sun, J., Zhao, W., Herzschuh, U., Tang, Y., 2012. Application and limitations of the Artemisia/Chenopodiaceae pollen ratio in arid and semi-arid China. The Holocene 22, 1385-1392.

Ziv, B., Dayan, U., Kushnir, Y., Roth, C., Enzel, Y., 2006. Regional and global atmospheric patterns governing rainfall in the southern Levant. International Journal of Climatology 26, 55-73.

Zohary, M., 1962. Plant Life of Palestine: Israel and Jordan. Ronald Press, New York.

Zohary, M., Feinbrun-Dothan, N., 1966. Flora palaestina. The Israel Academy of Sciences and Humanities, Jerusalem.